TU Delft

Selective transport between monovalent and divalent ions in electrodialysis

The effect of current density and ionic species concentration

By Tobias A.P. Opschoor

Analysing selective transport between monovalent and divalent ions in electrodialysis

The effect of current density and ionic species concentration

by

Tobias Arie Pieter Opschoor

In partial fulfillment of the requirements for the degree of

Master of Science
in Civil Engineering

at the Delft University of Technology,
to be defended publicly on February 22nd 2021 at 15:00

Student number:	4224345	
Thesis committee:	Dr. Ir. Henri Spanjers,	TU Delft, supervisor
	Prof. Dr. Ir. Jules van Lier,	TU Delft
	Dr. Ir. David Vermaas,	TU Delft
Daily supervisor:	Ir. Dhavissen Narayen	TU Delft

TU Delft

Acknowledgement

Working on this topic has been very rewarding and would not have been possible without the contribution of some wonderful people.

Firstly, I would like to thank Ir. Niels van Linden for supplying me with this research topic, helping me get started with my experiments and giving valuable tips for analysing my results. Your expertise on this subject really sparked my enthusiasm for a further career in the industry. A very big thanks to my daily supervisor, Ir Dhavissen Narayen and Ir. Giacomo Bandinu. Both of you helped establish a bit of order in my somewhat chaotic mind when needed. Both of you were very helpful in helping me analyse results and giving suggestions for experiments. I would also like to thank the chair of my committee Dr. Ir. HenRi Spanjers, for guiding me through the graduation process. You were always there when I needed help with something, so thanks for that!

A big thank you to all other members of my committee, Prof. Dr. Ir. Jules van Lier and Dr. Ir David Vermaas. Your critical comments and useful suggestions during all stages of my graduation were extremely useful. A big shout out to Armand Middeldorp and Patricia van den Bos for helping me analyse a near infinite amount of samples in the IC.

Thanks to my mother Andrie and father René who have been my greatest supporters throughout my entire life. Without them I would not have been able to study at all. I hope I made them proud. Last but definitely not least, thanks to my girlfriend Shelley who always puts a smile on my face.

Executive summary

Industrial and municipal wastewaters often contain a high concentration of NH_4^+. To prevent excessive discharge into the environment, these wastewaters need to be treated. Electrodialysis has been shown to be a suitable technique for the removal and recovery of NH_4^+ from both synthetic and real wastewaters such as digestate rejection water and industrial condensate. These wastewaters can contain varying concentrations of Mg^{2+}, Ca^{2+} and CO_3^{2-}. Treating these waters with ED for NH_4^+ recovery also causes recovery of these divalent ions. The recovery of these ions can potentially cause scaling. Scaling is undesired and needs to be prevented.

The main objective of this research was to analyse what the applied current density, Mg^{2+}/NH_4^+ ratio and total ion concentration had on the the selective transport between NH_4^+ and Mg^{2+}. This was done by using a lab scale electrodialysis setup with synthetic water consisting of NH_4HCO_3 and $MgCl_2$. A fixed NH_4 concentration of 1.5 g/L was used with varying initial molar Mg^{2+}/NH_4^+ ratios of 1:20, 1:10 and 1:4. Electrodialysis was operated at three different fixed current densities of 32, 64 and 96 A/m^2 and a constant voltage of $10V$. Also, experiments were done without an externally applied potential difference to quantify the transport caused by uphill transport and back-diffusion. All experiments were done with a standard ion exchange membrane stack and monovalent selective ion exchange membrane stack.

A NH_4^+ removal efficiency of 68-92 % was achieved for both ion exchange membrane (IEM) types. The Mg^{2+} removal efficiency ranged from 78-100 % for standard IEMs and from 28-71 % for monovalent selective IEMs. Monovalent selective IEMs removed $\sim$ 1.5-2.5 times less Mg^{2+} from the diluate compared to standard IEMs. ED operated with monovalent selective IEMs resulted in a higher energy consumption compared to standard IEMs. This was caused by monovalent selective IEMs having a greater area resistance.

For standard IEMs, both Mg^{2+} NH_4^+ were transported from the diluate at a constant rate. A direct relationship was found between the Mg^{2+}/NH_4^+ ratio in the diluate solution and the current efficiencies of both ionic species. If the ratio of Mg^{2+}/NH_4^+ increased, the selective transport of NH_4^+ over Mg^{2+} decreased. Doubling the Mg^{2+}/NH_4^+ ratio, increased the current efficiency of Mg^{2+} by $\sim$ 10%. Tripling the Mg^{2+}/NH_4^+ ratio, increased the current efficiency of Mg^{2+} by $\sim$ 15-16% (vice versa for NH_4^+).

For standard IEMs, increasing the current density, increased the selective transport of NH_4^+ over Mg^{2+}. Higher current densities, increased the salinity gradient in the diffusive boundary layer (DBL) between the diluate bulk solution and IEM interface. A higher current density therefore caused more concentration polarization in the DBL. Mg^{2+} has a lower diffusion rate than NH_4^+. Therefore, concentration polarization in the DBL became more predominant for Mg^{2+} at higher current densities. Operating at 64 A/m^2 increased the current efficiency of Mg^{2+} by $\sim$ 4-5% compared to operating at 32 A/m^2. Operating at 96 A/m^2 increased the current efficiency of Mg^{2+} by $\sim$ 10% compared to operating at 32 A/m^2 (vice versa for NH_4^+) .

For monovalent selective IEMs, a clear ion transport order was present. Firstly, a large part of the NH_4^+ was transported from the diluate before Mg^{2+} transport started to exponentially increase. If the ratio of Mg^{2+}/NH_4^+ increased, the selective transport of NH_4^+ over Mg^{2+} decreased, just as with standard IEMs. It was found that concentration polarization in the DBL was dependent on the total NH_4^+ concentration in the diluate bulk solution. As more NH_4^+ was removed from the diluate, concentration polarization of NH_4^+ in the DBL increased. This subsequently increased Mg^{2+} transport from the diluate. Especially, when the limiting current density was reached, concentration polarization became so predominant for NH_4^+ that Mg^{2+} transport exponentially increased. Therefore, if the NH_4^+ concentration in the diluate decreased, the selective transport of NH_4^+ over Mg^{2+} decreased.

For monovalent selective IEMs it was found that at increasing current density, the current efficiency of Mg^{2+} only marginally increased. However, the differences in the current efficiency of Mg^{2+} were so little for the different current densities, that it was concluded that the current density had a negligible impact on the selective transport of NH_4^+ over Mg^{2+}. At increasing current density, the current efficiency of NH_4^+ increased. Operating at a higher current density lowered the run-time of an experiment. Therefore, less NH_4^+ back-diffusion took place at higher current densities.

Theoretically, $\sim$ 30% of the initial Mg^{2+} concentration in the diluate could be transported to the concentrate solution via uphill transport at infinite run time without an externally applied potential difference. For standard IEMs operated at 32, 64 and 96 A/m^2, uphill transport was calculated to be responsible for 11, 8 and 4 % of the total transported Mg^{2+}, respectively. For monovalent selective IEMs operated at 32, 64 and 96 A/m^2 uphill transport was calculated to be responsible for 24, 14 and 8 % of the total transported Mg^{2+}, respectively. These values were lower than the theoretical transport, but not insignificant. At equal operational conditions, less uphill transport took place for monovalent selective IEMs. It was therefore concluded that monovalent selective IEMs reduced uphill transport compared to standard IEMs.

The use of monovalent selective IEMs gave a noticeable increase in selective transport of NH_4^+ over Mg^{2+} compared to standard IEMs. However, the effectiveness in which NH_4^+ is removed over Mg^{2+} decreases exponentially at increasing NH_4^+ removal when operating ED with monovalent selective IEMs.

Contents

Acknowledgement iii

Executive summary v

Nomenclature ix

1 Introduction 1
- 1.1 The Nitrogen cycle and why it is unbalanced . . . 1
- 1.2 Global ammonia market and applications . . . 2
  - 1.2.1 Global ammonia production . . . 2
  - 1.2.2 Global ammonia consumption . . . 3
  - 1.2.3 Ammonia as Energy . . . 4
- 1.3 Ammonium-nitrogen rich wastewater streams . . . 4
- 1.4 Electrodialysis for ammonium recovery . . . 5
- 1.5 Problem statement . . . 5
  - 1.5.1 Scaling in electrodialysis . . . 5
  - 1.5.2 Feed water types . . . 6
  - 1.5.3 Selective ion transport in ED . . . 6
  - 1.5.4 Knowledge gap . . . 6
- 1.6 Research Plan . . . 6
  - 1.6.1 Objectives . . . 6
  - 1.6.2 Approach and (sub-)research questions . . . 7

2 Background theory 9
- 2.1 Electrodialysis . . . 9
- 2.2 Ion exchange membrane types . . . 11
- 2.3 Electrochemical and thermodynamic processes . . . 11
  - 2.3.1 Electrochemical potential . . . 11
  - 2.3.2 Ion transport in electrodialysis . . . 12
  - 2.3.3 Uphill transport . . . 12
  - 2.3.4 Back-diffusion . . . 14
  - 2.3.5 Electro-osmosis and osmosis . . . 14
- 2.4 Chemical and electrical potential distribution . . . 15
  - 2.4.1 Chemical potential distribution . . . 15
  - 2.4.2 Electrical potential distribution . . . 16
- 2.5 Limiting current density . . . 17
- 2.6 Scaling in Electrodialysis . . . 17
- 2.7 Current density, current efficiency and permselectivity . . . 18
- 2.8 Energy consumption and resistance . . . 19
- 2.9 Removal efficiency . . . 20

3 Materials and Methods 21
- 3.1 Material . . . 21
  - 3.1.1 Electrodialysis setup . . . 21
  - 3.1.2 Analytical equipment . . . 22

3.2 Experimental methodology . . . 22
3.2.1 Constant current selectivity experiments . . . 23
3.2.2 Constant voltage selectivity experiments . . . 24
3.2.3 Limiting current density determination . . . 25
3.2.4 Uphill transport experiments (1/2) . . . 25
3.2.5 Uphill transport and back-diffusion experiments (2/2) . . . 25

4 Results and discussion **27**
4.1 Limiting current density for different IEMs . . . 27
4.2 Overall performance . . . 28
4.2.1 Removal efficiencies . . . 28
4.2.2 Transport efficiencies . . . 30
4.2.3 Energy consumption . . . 31
4.3 Selective transport for standard ion exchange membranes . . . 32
4.3.1 Ion transport and current efficiency for standard IEMs . . . 32
4.3.2 Influence of ion ratio on current efficiency for standard IEMs . . . 33
4.3.3 Influence of current density on current efficiency for standard IEMs . . . 34
4.4 Selective transport for monovalent selective IEMs . . . 35
4.4.1 Ion transport and current efficiency for monovalent selective IEMs . . . 35
4.4.2 Influence of ion ratio on current efficiency for monovalent selective IEMs 36
4.4.3 Influence of current density on current efficiency for monovalent selective IEMs . . . 38
4.5 Constant voltage . . . 39
4.5.1 Current efficiency for standard IEMs at constant voltage . . . 40
4.5.2 Current efficiency for monovalent selective IEMs at constant voltage . . . 41
4.6 Uphill transport and back-diffusion . . . 42
4.6.1 Theoretical uphill transport . . . 42
4.6.2 Uphill transport and back-diffusion for standard IEMs . . . 43
4.6.3 Uphill transport and back-diffusion for monovalent selective IEMs . . . 45

5 Conclusions **47**

6 Recommendations **51**

Bibliography **52**

A Constant current standard IEMs **63**

B Constant current monovalent IEMs **67**

C Model constant current monovalent IEMs **71**
C.1 Model monovalent selective IEMs 32 A/m^2 . . . 72
C.2 Model monovalent selective IEMs 64 A/m^2 . . . 73
C.3 Model monovalent selective IEMs 96 A/m^2 . . . 74

Nomenclature

α	Membrane permselectivity
a	Activity
A	Effective membrane surface area
AEM	Anion exchange membrane
$AEEM$	Anion exchange end membrane
$BPMED$	Bipolar membrane electrodialysis
C	Concentration [mol/L]
Ca^{2+}	Calcium
$Ca(OH)_2$	Calcium hydroxide
$CaCO_3$	Calcium carbonate
CEM	Cation exchange membrane
$CEEM$	Cation exchange end membrane
CH_4	Methane
CO_2	Carbon dioxide
CO_3^{2-}	Carbonate
EC	Electrical conductivity [$\mu S/cm$]
D	Diffusion coefficient [m^2/s]
DBL	Diffusive boundary layer
η	Current efficiency [%]
E	Energy consumption [kWh]
ED	Electrodialysis
F	Faraday constant [C/mol]
γ	Activity coefficient [-]
H_2	Hydrogen
i	Current density [A/m^2]
I	Current [A]
IEM	Ion exchange membrane
J	Ion flux [$mmol/m^2 \cdot min$]
LCD	Limiting current density [A/m^2]
M	Mass [kg]
Mg^{2+}	Magnesium
$MgCl_2$	Magnesium chloride
$MgCO_3$	Magnesium carbonate
N	Number of cell pairs

NH_3	Ammonia
NH_4^+	Ammonium
$NH4HCO_3$	Ammonium bicarbonate
$(NH_4)_2SO_4$	Sulfuric acid
NO_x	Nitrogen oxides
NO_3^-	Nitrate
N_2O	Nitrous oxide
ϕ	Potential [V]
P	Permselectvity
R	Universal gas constant [$J/K \cdot mol$]
R	Resistance [Ω]
R	Area Resistance [$\Omega \cdot cm^2$]
$SOFC$	Solid oxide fuel cell
t	Time [min]
T	Temperature [K]
μ	Electrochemical potential [J/mol]
U	Potential [V]
V	Volume [L]
VMS	Vacuum membrane stripping
$WWTP$	Wastewater treatment plant
x	Distance [m]
z	Ion valence

1

Introduction

1.1. The Nitrogen cycle and why it is unbalanced

Nitrogen is one of the essential nutrients for all life forms. Organisms require nitrogen to form nucleic acids, amino acids, vitamins, cofactors and hormones [1]. The nitrogen cycle is the biogeochemical cycle which describes the main species and interconversions of nitrogen. This cycle is shown in figure 1.1. Nitrogen is present in the environment in a variety of organic and inorganic forms. Many of the nitrogen transformation reactions seen in figure 1.1 are conducted by various micro-organisms [2].

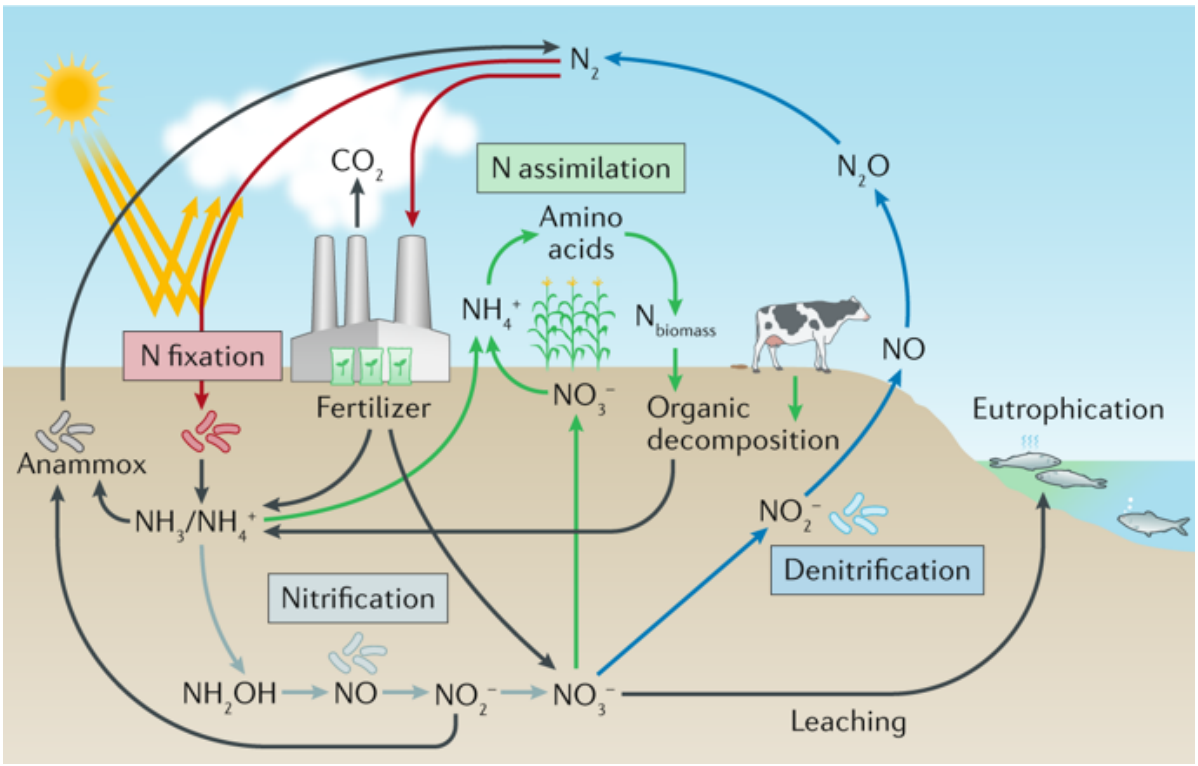

Figure 1.1: The nitrogen cycle with the the main species and interconversions [3].

Over the past centuries, increased anthropogenic discharge of nitrogen has greatly impacted the nitrogen cycle [4]. Fossil fuel burning causes NO_X and N_2O to be released. NO_X is toxic for humans and can cause breathing problems, headaches and chronically reduced lung

function [5]. N_2O is a powerful greenhouse gas that is ~ 250 times stronger than CO_2 . It is the third largest contributor to the enhanced greenhouse effect [6]. Synthetic fertilizer and manure used in agriculture add large quantities of NH_4^+ into the environment as N-source for crop growth. However, only ~ 50% of the N taken up by the plants [7]. Nitrification/denitrification performed by microorganisms in the soil transform the remaining NH_4^+ to form NO_3^- and N_2O. The N_2O gas is released into the atmosphere. NO_3^- and NH_4^+ leach into surrounding water bodies causing significant disturbance in the aquatic ecosystems. Fresh water sources and marine systems suffer from eutrophication and acidification. This is causing large decreases in biodiversity [8–10]. Volatile NH_3 gasses are also formed as a result of fertilization which evaporates and settles in downwind areas [11]. This causes increased N-inputs which has detrimental effect on the plant species richness, thus putting stress on the entire biodiversity [12].

1.2. Global ammonia market and applications

NH_3 is one of the most common inorganic chemical in the world. It is used in a wide variety of industrial applications. Besides these existing applications, NH_3 is becoming increasingly interesting as an energy carrier. This section gives an overview of the production and consumption of NH_3 on a global scale and the potential as energy carrier.

1.2.1. Global ammonia production

In 2018, the global industrial NH_3 production equaled 175 million tonnes [13]. This puts it in the top 5 of most produced chemicals worldwide [14, 15]. The most common way of producing NH_3 is by combining hydrogen with nitrogen via the so called Haber-Bosch process [16, 17]. Gaseous hydrogen is produced from hydrocarbons such as methane, LPG or Naphtha. This is done via a process called steam reforming [18]. After the steam reforming, air reforming takes place to produce more hydrogen from the remaining hydrocarbon source. Successive steps convert and remove carbon mono-/dioxide as well as water water from the process. After this ammonia synthesis is established [16, 19]. A schematic of the entire process is given in figure 1.2.

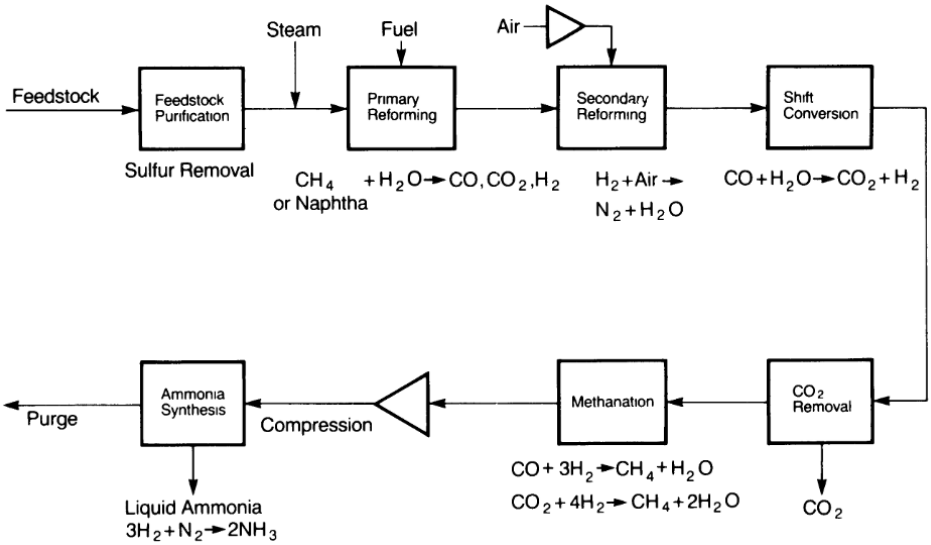

Figure 1.2: Schematic of the steam reforming route to ammonia synthesis [19].

Because of this process, the global NH_3 production requires an estimated 3-5% of global methane production and an estimated 1-3% of the worlds energy demand [20–23]. Because of this large footprint, green alternatives for ammonia production are much sought after. Especially hydrogen production from electrolysis as alternative to steam reforming of hydrocarbons seems promising. It requires only water and nitrogen gas as feedstock, nullifying the need for hydrocarbons and cutting CO_2 emissions [24]. However, this technique is not yet economically feasable as a purely industrial chemical producing technology from both a cost and overall efficiency viewpoint [24–27]. This alternative is likely to become more viable as technology improves and renewable energy becomes more widely available [27].

1.2.2. Global ammonia consumption

NH_3 is the basic building block of the worlds nitrogen industry. It can be used for a variety of applications in both its pure form or as feedstock for downstream products [28]. By far the largest application of NH_3 is as fertilizer. It accounts for roughly 80% of the global NH_3 consumption [28]. Although pure NH_3 fertilization is not uncommon, it is often processed into products such as urea, ammonium nitrates, ammonium sulfate and ammonium phosphates [29, 30]. It is estimated that around 48% of the world population is being fed by food grown with use of synthetic nitrogen fertilizers [31]. Over the past century, 42% of human population growth is directly related to the usage of synthetic nitrogen. Without it, about 3.5 billion(!) people would not have been born or have died from starvation [31, 32]. Roughly half of the fixed nitrogen required for DNA and protein synthesis in human bodies find their origin as synthetic nitrogen fertilizer [33, 34].

The second largest application of NH_3 is for the production of synthetic fibres such as nylon and acrylics. This uses about 10% of the global NH_3. About 5% of NH_3 is used for the production of explosives such as trinitrotoluene (TNT) and nitroglycerine. Other applications are for cleaning purposes, refrigerants, plastics, pharmaceuticals and metallurgy [29, 35]. A schematic of NH_3 applications is given in figure 1.4. The global NH_3 market is estimated to grow over the next years, due to increased food demand by an ever growing population and increased industrial demand [35, 36].

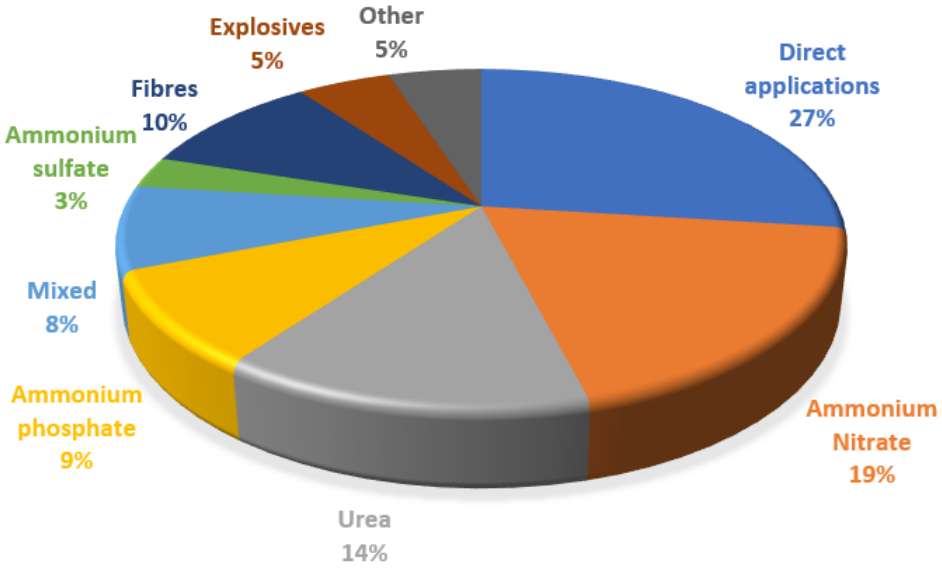

Figure 1.3: The different utilization of ammonia by percentage [29]. Fertilizer applications add up to 80%.

1.2.3. Ammonia as Energy

Anthropogenically enhanced global warming pushes countries to transition to a low carbon output economy. One such solution in achieving this is the transition towards a (green) hydrogen production [37]. However, there are issues associated to the storage and distribution of hydrogen [38]. These are currently large barriers for large scale implementations. NH_3 is increasingly mentioned as a viable solution for green hydrogen storage. NH_3 has an excellent energy density and is predicted to have the highest energy efficiency in direct energy applications [39, 40]. It is also considered easier to store, transport and handle compared to H_2 because of the stability in water, lower leaking potential and well established transport and handling networks already available [38, 40, 41]. NH_3 can be directly applied for energy production via solid oxide fuel cells (SOFC) [42]. Also NH_3 fueled engines are set to be developed for future airplane and marine engines [43, 44].

1.3. Ammonium-nitrogen rich wastewater streams

Many carbon rich biodegradable streams are treated by anaerobic digestion. These organic waste streams usually consist of livestock waste such as manure, agricultural and municipal waste and sewage sludge coming from wastewater treatment plants (WWTP) or any given combination as such. Microorganisms break down biodegradable material which leads to the production of biogas. This biogas consists of CH_4 and CO_2 [45]. Figure gives a schematic overview of the anaerobic digestion flow scheme.

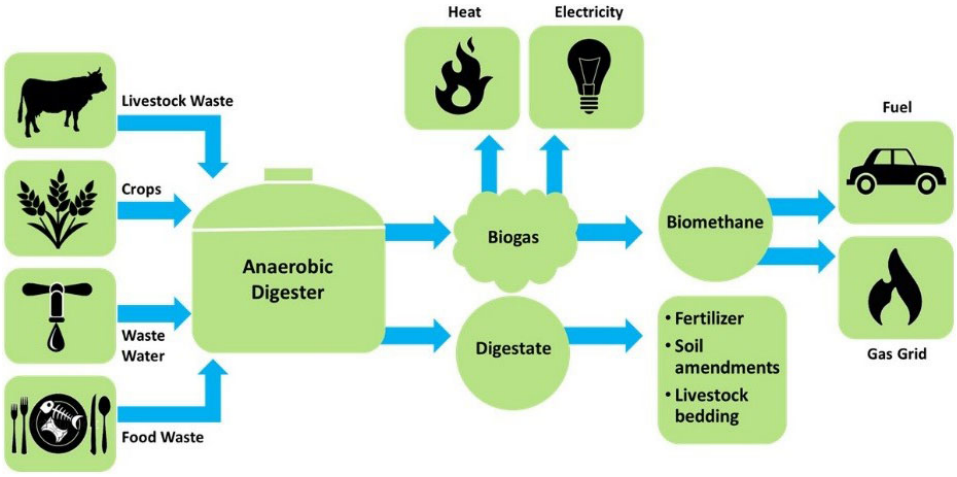

Figure 1.4: Flow scheme of anaerobic digestion process [46].

The left-over product of anaerobic digestion is called digestate. The thin fraction of the digestate is characterised by having a relatively low carbon and high inorganic nitrogen (NH_4^+) concentration. Besides the digestate reject water, other waste streams of interest that hold high quantities of NH_4^+ are industrial condensate and raw animal manure/urine [47, 48]. Before this streams can be discharged into the environment, a large part of the NH_4^+ needs to be removed or recovered. NH_4^+ is commonly removed via activated sludge and anammox processes. NH_4^+ components are degraded into atmospheric N_2 gas. NH_4^+ can is also recovered as $(NH_4)_2SO_4$ via stripping and scrubbing [49]. Chemicals are added to rise the pH of the solution such that NH_4^+ becomes volatile NH_3. The volatile NH_3 is stripped from the solution and subsequently scrubbed with acid to form $(NH_4)_2SO_4$. These techniques are energy/chemically intensive and require large spatial footprints and require centralized treatment facilities [49–51].

1.4. Electrodialysis for ammonium recovery

Contrary to the above mentioned application in NH_4^+ removal, electrodialysis (ED) has the potential to become an energy efficient efficient small spatial footprint alternative to biological treatment or stripping/scrubbing. ED is a membrane separation process where ions are transported through ion exchange membranes (IEMs) by application of an external electrical potential difference [52]. Ionic species from the feed water (diluate) are exchanged through the membranes and collected in a concentrated stream (concentrate).

ED was primarily designed as large scale brackish/seawater desalination technique for the production of potable water [53, 54]. However, ED is starting to be used for more applications of concentrating and separating ions from varying waste streams [55, 56]. Many cases of successful NH_4^+ removal is documented. *Wang et al.* were able to recover 95.8–100% of the NH_4^+ coming from sidestreams of anaerobic digesting excess sludge with ED [57]. *Ward et al.* were able to recover and concentrate NH_4^+ by a factor of 8.77 up to 9.1 g/L by using a pilot plant ED to treat domestic anaerobic digester supernatant [55]. *Mondor et al.* were able to recover and concentrate NH_4^+ by a factor 2.77 to 14.25 g/L by using a lab scale ED setup to treat liquid swine manure [58]. *Ippersiel et al.* were able to achieve a 21.35 g/L NH_4^+ concentration by treating a comparible liquid swine manure fraction as *Mondor et al.* They were also able to strip part of the volatile NH_3 by stripping under a vacuum [59].

Combined research under the *N2kWh* project has shown that it was able to concentrate NH_4^+ from synthetic wastewater up to 10 g/L of NH_4^+ by conducting sequencing batch experiments with an initial 1.5 g/L of NH_4^+ in the diluate. Also a $\sim$ 90% NH_4^+ removal efficiency was achieved for the batch experiments. Bipolar membrane electrodialysis (BPMED) was subsequently used to create a base solution which volatilized the majority of the NH_4^+ fraction to NH_3. Part of this fraction was successfully stripped via vacuum membrane stripping (VMS) and successfully fed to a SOFC to produce electricity [60–65]. The same sequence of experiments were successfully conducted with industrial condensate from NH_3 production [66].

1.5. Problem statement

ED is very suitable for the recovery and concentration of various nutrients from various wastewater types. The waste streams coming from the thin fractions of digestate and manure often contain a multitude of different ion species. Conventional ED is limited in steering selective transport of different ion species present in these solutions. Therefore, when aiming for recovery of just NH_4^+ for re-use purposes, other ions will be co-transported as well. Transport of non-targeted ionic species reduces the current utilization for the targeted species of the system as unwanted ions are transported. This increases the overall energy requirement and leads to the transport of species which can potentially significantly hamper the ED performance.

1.5.1. Scaling in electrodialysis

Ca^{2+}, Mg^{2+} and CO_3^{2-} are commonly present in anaerobic digester rejection waters and livestock manure [48, 67]. When feeding ED with these wastewaters, these ion species are also removed from the feedwater and concentrated. If saturation indexes are reached, uncontrolled precipitation known as scaling occurs in the ED compartments. This causes membrane fouling. Scaling is highly unwanted as it restricts long term ED operation [56]. *Zhang et al.* estimated the scaling potential of Ca^{2+}, Mg^{2+} and CO_3^{2-} in ED by estimating the critical scaling concentrations [68]. *Thompson-Brewster et al.* and *van Linden* observed $MgCO_3$ scaling in the concentrate compartment after recovering nutrients with ED from anaerobic digestate

reject water [69, 70]. *Casademont et al.* observed $Ca(OH)_2$ and $CaCO_3$ scaling on the cation exchange membrane (CEM) of the concentrate compartment when concentrating synthetic water containing both Mg^{2+} and Ca^{2+} [71].

1.5.2. Feed water types

The synthetic water compositions used for this research are based on real water compositions. Mg^{2+}, Ca^{2+} and NH_4^+ concentrations of the feed waters vary. Co-digested pig manure and sludge reject water has Mg^{2+} and Ca^{2+} concentrations ranging from 10-20 mg Mg^{2+}/L and 20-40 mg Ca^{2+}/L, respectively. Raw cow manure and sludge reject water after struvite precipitation has a Mg^{2+} concentrations ranging from 310-470 mg Mg^{2+}/L and a Ca^{2+} concentration of up $\sim$ 840 mg Ca^{2+}/L, respectively [48, 70]. NH_4^+ concentrations vary from 840 mg/L for sludge reject water to 4550 mg/L for co-digested pig manure, respectively [48, 70].

1.5.3. Selective ion transport in ED

There are ways to enhance the selective transport of monovalent ions over divalent ions. The most common method is by application of monovalent selective ion exchange membranes [72]. The use of monovalent selective IEMs has shown to increase preferential removal of monovalent ions over divalent ions [73, 74]. The applied current density and both relative and total concentration of ions in the feed water has been reported to have an effect on the selective transport of monovalent and divalent ions [75–77]. However, this was only documented for standard IEMs. The selective transport of mono- and divalent ions is potentially limited by divalent ion transport through the IEMs against the concentration gradient. This has been reported in reverse electrodialysis [78]. This phenomena is known as uphill transport [79]. Uphill transport has not yet been quantified for regular ED.

1.5.4. Knowledge gap

Little information is found in literature that describes how the selective transport of monovalent and divalent ions takes place as a function of the initial feed water conditions, operational conditions and different IEM types. This information is especially limited for ED operated with monovalent selective IEMs. The studies that did describe the selective ion transport as a function of operational conditions and for different IEM types, used feed water types that are not representative to the water types described in section 1.5.2 [73–77]. It is therefore required to gain knowledge on how to achieve high removal of NH_4^+ ions over scaling inducing divalent ions, what the limitations of selective transport are and how to optimise ED for selective NH_4^+ recovery.

1.6. Research Plan

1.6.1. Objectives

The main objective of this research was to analyse how selective transport of NH_4^+ and Mg^{2+} takes place when recovering NH_4^+ from synthetic wastewaters. ED was operated at different current densities and with different synthetic make-up waters. Both standard IEMs and monovalent selective IEMs were used. In order to fulfill the main goal, the following main research question was derived:

"What is the influence of applied current density, ion ratio and total ion concentration on the selective transport of NH_4^+ and Mg^{2+} when operating ED with standard and monovalent selective ion exchange membranes".

1.6.2. Approach and (sub-)research questions

The following (sub)-research questions were derived from knowledge gap found in literature:

1. How do standard IEMs and monovalent selective IEMs compare in terms of removal efficiency and energy consumption.
2. What is the influence of the molar Mg^{2+}/NH_4^+ ratio and total NH_4^+ and Mg^{2+} concentration in the diluate solution on the selective transport of NH_4^+ and Mg^{2+}.
3. What is the influence of the applied current density on the selective transport of NH_4^+ and Mg^{2+}.
4. What is the influence of the applied voltage on the selective transport of NH_4^+ and Mg^{2+}.
5. How much Mg^{2+} is transported by uphill transport.

All of the above mentioned research questions are applicable to ED operation with standard IEMs as well as with monovalent selective IEMs.

To answer these research questions, theoretical concepts are firstly explained by analysing literature. This is given in chapter 2. The theoretical concepts are used to conduct experiments that are designed to answer the various (sub-)research questions. A detailed methodology for these experiments is given in chapter 3. The results from the experiments are given in chapter 4. The results are thoroughly discussed and compared with representative literature. Chapter 5 concludes the results found in the experiments. Chapter 6 presents recommendations for further research, a framework for extension into other water types and potential process optimisation.

2

Background theory

This chapter describes the theoretical background of how electrodialysis works and what different processes are going on while operating electrodialysis. Also the methods of analysing the selective transport between ions and performance parameters are described.

2.1. Electrodialysis

Electrodialysis is a membrane separation process where ions are transported through ion exchange membranes (IEM) by application of an external electrical potential difference. Solution streams are separated via these IEM which consist of a polymer matrix that are combined with either positively or negatively charged fixed groups [53]. Membranes fixed with positive charged groups are called anion exchange membranes (AEM) and membranes fixed with negative charged groups are called cation exchange membranes (CEM). Ideally, an AEM is only permeable to anions and a CEM to cations (or so called counter-ions). The IEM membranes are separated by a spacer. The electrolyte solutions are pumped through these spacers [54]. The spacers also function as flow dispensers.

Membranes can be arranged in several ways, but for conventional ED the common arrangement is an alternating sequence of CEMs and AEMs stacked between an anode and a cathode. The combination of a CEM, AEM and the appurtenant spacers are called a cell pair. The amount of cell pairs per ED system can be varied from just 1-10 pairs (lab scale) to 200 pairs (full size scale) [52, 80]. At the electrode interfaces, an electrode rinse solution is recirculated. This rinse solution has a high salinity and is used to interconnect current transfer between the electrodes and the ED cells. The rinse solutions are separated from the ED electrolyte feed waters via an anion exchange end membrane (AEEM) or a cation exchange end membranes (CEEM). A visual representation of the different components in an ED stack are presented in figure 2.1.

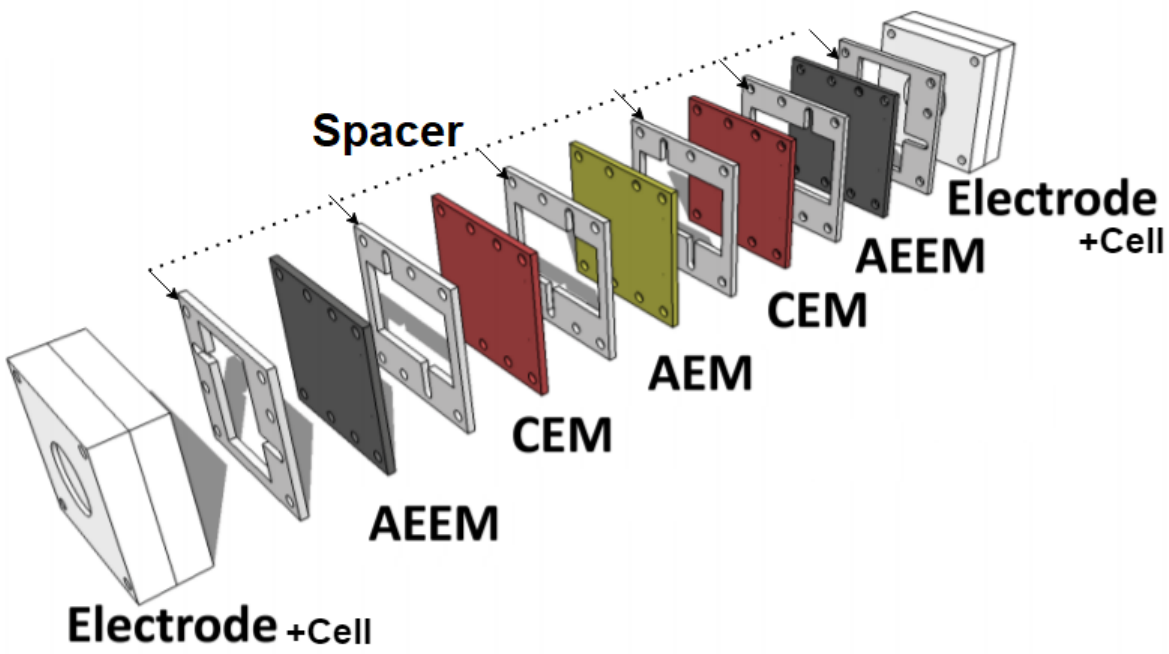

Figure 2.1: Visual representation of different components in an ED stack. Image retrieved from *Deckers* and adapted [61].

When ED is operated, an external potential difference is established by the electrodes. This results in migration of cations towards the cathode and anions towards the anode. Cations easily permeate the negatively charged cation exchange membranes. This is schematically visualised in figure 2.2. Once the cation permeated, it continues to migrate towards the cathode side. However the cation is maintained in the solution by the following up positively charged anion exchange membrane. The same occurs for anions in the exact opposite fashion. The net result when operating is that the concentration of one electrolyte solution decreases during operation while the concentration of the other solution increases. The decreasing solution is referred to as the diluate and the increasing solution as the concentrate [52, 54]. This is essentially the principle of electrodialysis. Figure 2.3 presents a graphical summary of the above described processes that happen when ED is operated.

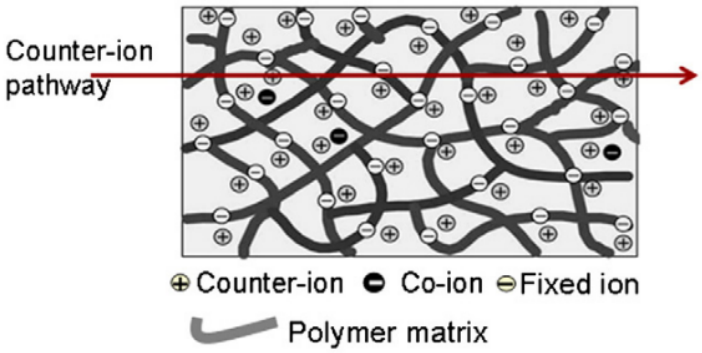

Figure 2.2: Visual representation of counter-ion transfer through a homogeneous IEM. Image retrieved from *Strathmann* [54]. Species with an opposite charge in regard to the fixed ionic charges within the IEM are also referred to as counter-ions. Species with the same charge as the fixed membrane charges are referred to as co-ions.

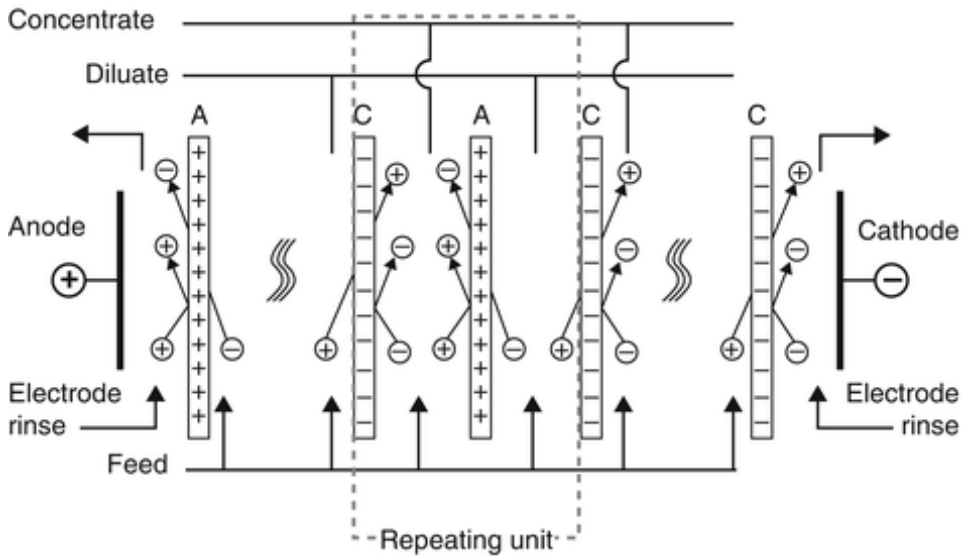

Figure 2.3: Schematic overview of the different streams and ion transport which are present during ED operation. Image retrieved from *Strathmann* and adapted [54].

2.2. Ion exchange membrane types

Standard IEMs show a high permselectivity towards counter-ions and a low permselectivity towards co-ions. Standard membranes are not primarily designed to achieve a form of selective transport between counter-ions. This can lead to difficulties when the water matrix consist of mono and divalent ions as explained in section 1.5.1. However, there are methods to improve ion selectivity of counter-ions for IEMs. This is mainly done by applying surface modification during the preparation of IEMs [72].

There are many surface modification types. The most common method is applying an oppositely charged surface layer to the IEM [72, 81, 82]. These membranes are designed and proven to have a higher permselectivity towards monovalent ions and are therefore called monovalent selective ion exchange membranes. Applying an oppositely charged surface layer is considered the most effective surface modification method as it increases selectivity of monovalent ions without substantially increasing the electrical resistance of the membrane [83]. What happens is that the transport of di-/multivalent ions is hindered by the surface layers of the membrane because of the same fixed charge as the counter-ions. Di-/multivalent ions have a stronger electrostatic repulsion compared to monovalent ions because of their higher charge [84]. Figure 2.4 schematically shows the difference between a standard CEM and a monovalent selective CEM.

2.3. Electrochemical and thermodynamic processes

Many different electrochemical and thermodynamic processes occur simultaneously during ED operation. These processes are the driving forces which act on the components in solution and are used to describe the performance of an electrodialysis system.

2.3.1. Electrochemical potential

In order for an ionic flux to be established for a certain species in solution, a difference in electrochemical potential needs to be present [85]. For electrodialysis this means that due to an electrochemical potential difference, ionic transport from the diluate solution through the adjacent ion exchange membrane to the concentrate solution takes place [52, 79].

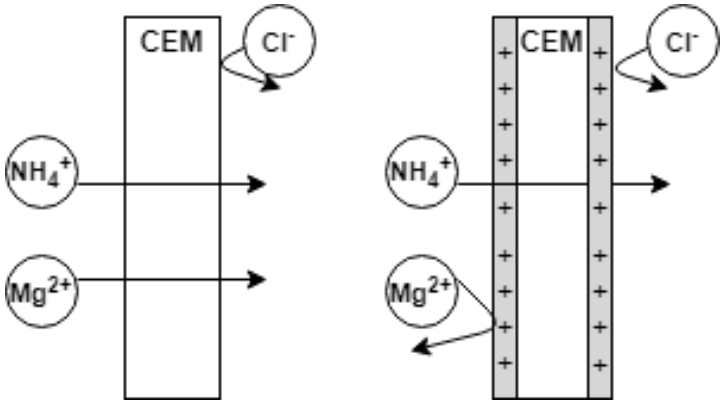

Figure 2.4: Visual representation of the difference between a standard CEM and a monovalent selective CEM. The monovalent selective CEM (right) has an oppositely charged surface layer. This causes electrostatic repulsion, hindering the transport of the divalent ion.

The electrochemical potential is a function of two additive terms. Namely the chemical potential and electrical potential The formula for calculating the electrochemical potential is given by equation 2.1

$$\mu_i = RT \ln(\gamma_i c_i) + F z_i \phi \tag{2.1}$$

Here μ_i is the electrochemical potential (J/mol), R the universal gas constant ($J/(K \cdot mol)$), T the temperature (K), γ_i the activity coefficient for species i (-), c_i the concentration of species i (mol/L), F the Faraday constant (C/mol), z_i the valence of species i and ϕ the potential (V).

2.3.2. Ion transport in electrodialysis

One of the most common approaches of describing ion transport in an electrolyte solution is given by the Nernst-Planck flux equation [75]. The Nernst-Planck equation introduces the electrochemical potential (eq. 2.1) as a driving force for ion transport [52]. This equation is given by equation 2.2.

$$J_i = -D_i \left[\frac{\delta c_i(x)}{\delta x} + \frac{c_i z_i F}{RT} \frac{\delta \phi}{\delta x} \right] \tag{2.2}$$

Here J_i is the mass flux of species i (mol) and D_i the diffusion coefficient of species i (m^2/s). The Nernst-Planck equation describes two different driving mechanisms which both contribute to the ionic flux in ED. The first term of eq. 2.2 is the diffusion term. Ionic flux is caused by diffusion when ions move from a higher ionic concentration to a lower ionic concentration over a certain length interval. The second term of eq. 2.2 is the electromigration term. Ionic flux is caused by electromigration when an electrical potential difference is present over a certain length interval.

Arguably, a third term can be introduced. This term is convection. However, this term is neglected since convective transport perpendicular towards IEM while running ED is negligible compared to diffusion and electromigration [75, 86, 87].

2.3.3. Uphill transport

In conventional ED, ions are preferably transported from the diluate solution to the concentrate solution. A chemical potential difference is present between both solutions which are separated by the adjacent IEM. When a mixture is present on both sides of the membrane that

consist of monovalent and multivalent ions, the system will exchange monovalent and multivalent ions through the membrane between solutions in order to achieve a chemical potential equilibrium. Mono- and multivalent ions differ in valence. What this means is that the electromotive force of monovalent ions is larger with respect to that of multivalent ions which can be seen by equation 2.3. This leads to transport of multivalent ions against the salinity gradient in exchange for monovalent ions. This process is called uphill transport and is illustrated in figure 2.5 [78, 79, 88, 89].

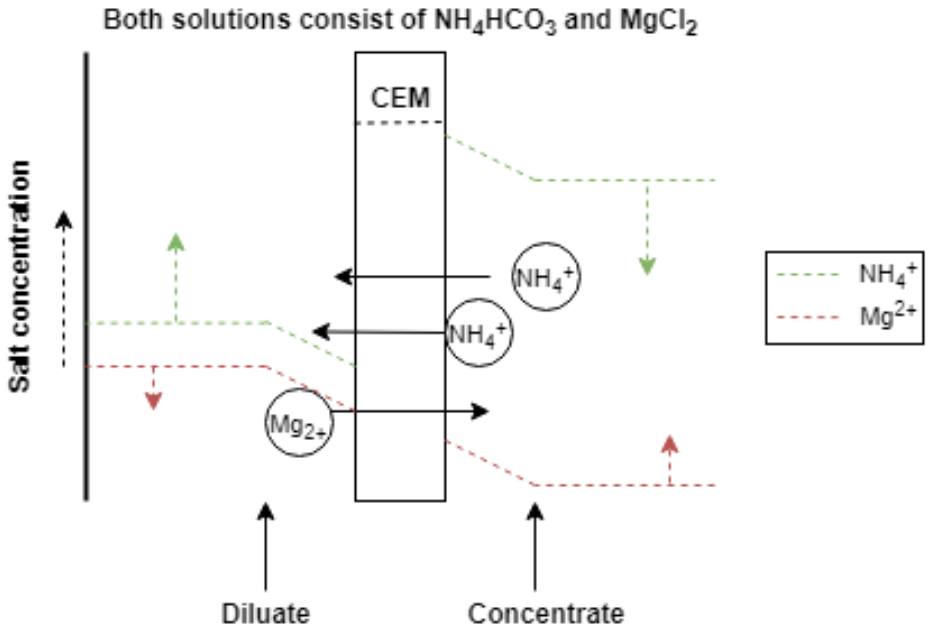

Figure 2.5: Graphical visualisation of uphill transport of Mg^{2+} against the salinity gradient in exchange for 2 NH_4^+ ions. The green dotted lines represent the NH_4^+ concentration and the red dotted line represent the Mg^{2+} concentration. The arrows represent an increase/decrease in concentration of the ionic species.

$$E = \alpha \frac{RT}{z_i F} \ln \frac{a_{i,dil}}{a_{i,con}} \tag{2.3}$$

Equation 2.3 shows the electromotive force of species i over a membrane. Here α is the membrane permselectivity and a is the activity of species i. This equation can be expanded for multiple ions within both diluate and concentrate assuming a steady state system with constant feed concentrations. From there the flux of mono- and multivalent ions can be calculated for the system to reach equal electromotive force in both bulk solutions. This equation for flux calculation is given by equation 2.4 [79]. In this formula NH_4^+ and Mg^{2+} are chosen as the cations as they are representable for this report.

$$\left(\frac{\gamma_{NH_{4,dil}^+}(c_{NH_{4,dil}^+} - 2J/V_{dil})}{\gamma_{NH_{4,con}^+}(c_{NH_{4,con}^+} + 2J/V_{con})} \right) = \left(\frac{\gamma_{Mg_{dil}^{2+}}(c_{Mg_{dil}^{2+}} + J/V_{dil})}{\gamma_{Mg_{con}^{2+}}(c_{Mg_{con}^{2+}} - J/V_{con})} \right)^{1/2} \tag{2.4}$$

Here γ represents the ion activity (-), C the concentration (mol/L), J the total molar transport of Mg^{2+} towards the concentrate compartment (mol) and V the volume of the solution (L). Uphill transport is considered undesirable when trying to achieve a high recovery of NH_4^+ while keeping recovery of Mg^{2+} at a minimum.

2.3.4. Back-diffusion

As stated in section 2.3.3 a chemical potential difference is present between both solutions which are separated by the adjacent IEM. Such a gradient can drive ions to diffuse through the membrane from the solution with higher salinity to the solution with lower salinity. This process is called back-diffusion and is visualised in figure 2.6 [80]. For each charge that diffuses back through the membrane an opposite charge has to be transported back as well because of electroneutrality within the system. The quantity of this flux depends on the actual salinity gradient between the solutions and the diffusive quantities of the membrane separating the liquid [90, 91]. Back-diffusion in ED is undesirable, because it requires ions to be re-transported against the salinity gradient. This lowers current efficiency for the recovery of the according ionic species [62, 91].

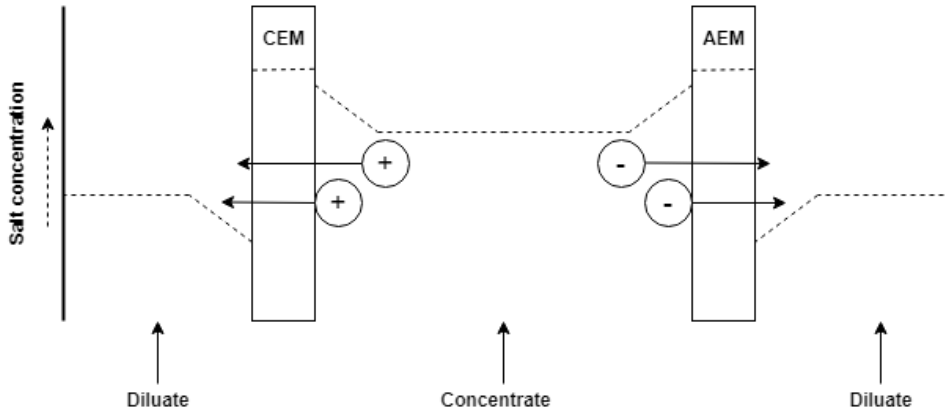

Figure 2.6: Graphical visualisation of back-diffusion. Ions are transported from the solution with higher salinity (concentrate) through the membrane towards the concentration with lower salinity (diluate). For this example both diluate and concentrate solutions consist of a mixture containing NH_4^+, Mg^{2+}, HCO_3^- and Cl^-. The relative concentration is assumed to be the same for both concentrate and diluate solution, but they vary in total concentrations.

2.3.5. Electro-osmosis and osmosis

IEMs are specifically engineered to be selective towards charged species only. This means that water transport or i.e. the solvent solution through the IEM is limited as much as possible [53]. However, when operating ED, water transport does take place via processes called electro-osmosis and osmosis [52, 91].

Transport of bound water molecules is called electro-osmosis. Ions in solution are surrounded by a hydration shell. These bound water molecules are transported alongside the ion through the membrane, hence causing water transport [91, 92]. The actual quantity of this water transport is directly proportional to the ions transported and the amount of water molecules bound to the primary hydration sphere of the ionic species [92, 93]. Different ionic species, hold different quantities of water molecules in their primary hydration sphere. NH_4^+ ions transport $\sim$ 4 moles of water, Mg^{2+} and Cl^- $\sim$ 6 moles of water and HCO_3^- $\sim$ 7 moles of water per transported mole of according ionic species [94–97].

Osmosis occurs when there is a chemical potential difference present between solutions and the adjacent IEM combined with the absence of a hydrostatic pressure difference between those solutions and where the membrane is permeable for the solvent [52]. In order to obtain a chemical potential equilibrium, solvent solution (water) is transported through the membrane to dilute the concentrated solution and vice versa [91, 92]. The amount of osmosis taking place can be significantly reduced by changing mesh open area, material and surface

properties [98]. This means that the amount of osmosis that takes place during ED operation is also membrane dependent.

Both types of transport are undesired in ED since they lower the final product quality that is produced in the concentrate solution by diluting it. Figure 2.7 illustrates both electro-osmosis and osmosis.

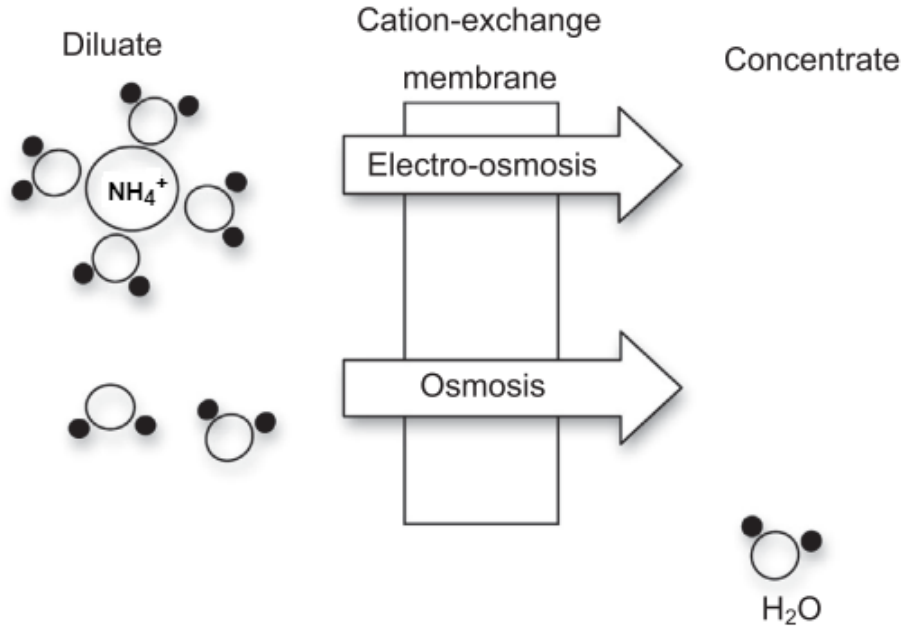

Figure 2.7: Graphical visualisation of electro-osmosis and osmosis. 4 water molecules are transported per NH_4^+ ion (electro-osmosis). Water molecules are transported from a lower salinity to a higher salinity (osmosis). Figure retrieved from *Rottiers* and adapted [91].

2.4. Chemical and electrical potential distribution

As discussed in previous sections, mass transport between solutions and the adjacent membranes is the result of gradients in the electrical and chemical potential. However, the distribution of these potentials vary at different positions within the cell pairs. How these potentials are distributed are key in understanding the functioning and limitations of an ED system.

2.4.1. Chemical potential distribution

Figure 2.8 shows a graphical visualisation of the salt concentration profiles across the diluate and concentrate solutions and the cation exchange membrane as well as the main transport mechanisms. Three main phases can be distinguished:

- Diluate and concentrate bulk: These phases are regarded as completely stirred continuously flowing solutions. The concentration of these solutions change over time when operating the ED system [75].
- Diluate and concentrate boundary layer: The boundary layer between the diluate bulk solution and the IEM. The flow in this phase is assumed to be stagnant and unstirred. The ionic flux perpendicular to the membrane surface is governed by diffusion and migration [87]. The adjacent IEM have a high membrane selectivity towards counter ions.

Flux of counter ions is higher in the membrane phase than it is in the boundary layers. This means that the concentration of ions in the DBL of the diluate decreases towards the membrane while the concentration of the concentrate DBL increases towards the membrane. This process is known as concentration polarization [52, 75, 99].

- Ion exchange membrane: The salt concentration within ion exchange membranes is high compared to that of the bulk concentrations, because of the high amount of fixed ions attached to the membrane matrix [52].

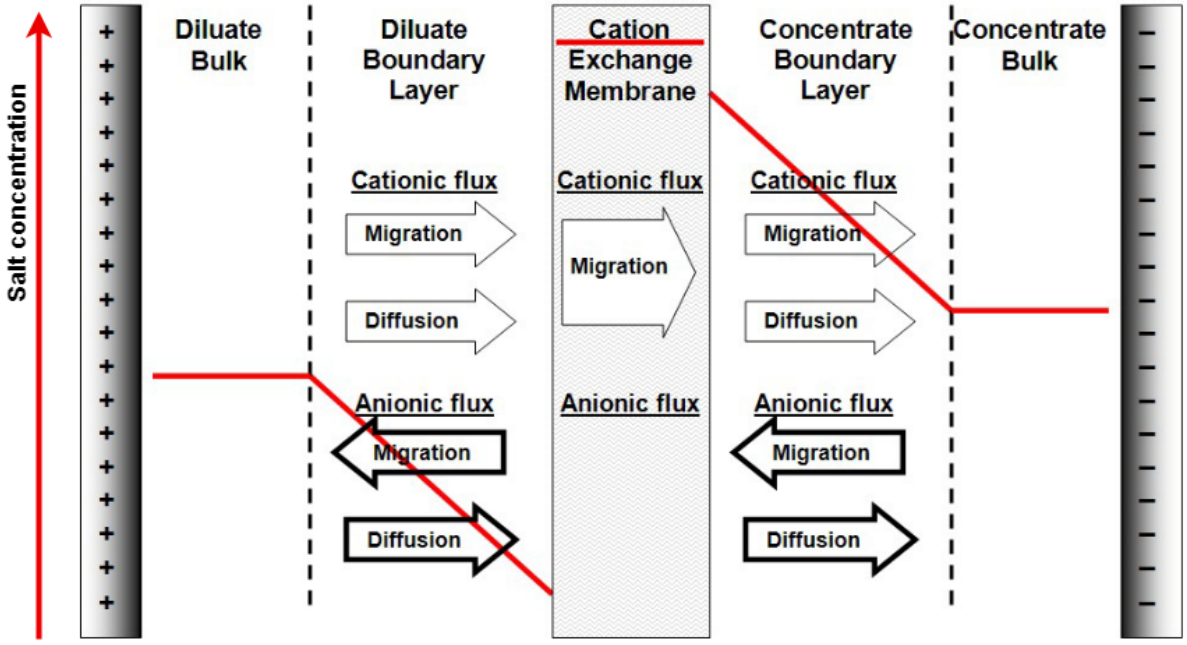

Figure 2.8: Graphical visualisation of the chemical potential differences across the bulk solutions, dilute boundary layers and the IEM. Image retrieved from *Kim* and adapted [87]. Note that this image is not to scale as the actual thickness of the DBL is lower than that of the diluate bulk and IEM. For this example both diluate and concentrate solutions consist of a mixture containing NH_4^+, Mg^{2+}, HCO_3^- and Cl^-. The relative concentration is assumed to be the same for both concentrate and diluate solution, but they vary in absolute concentrations.

Concentration polarization can be reduced by changing numerous fixed and operational parameters such as:

- Increasing linear flow velocity: This decreases the diffusive boundary layer thickness, hence decreasing the limitations by transport in the diffusive boundary layer [87].
- Spacer geometry: The geometry of the spacer has influence on the Reynolds number. Concentration polarization is lowered with increased Reynolds number. A high Reynolds number means turbulent flow in the bulk solutions [100].
- Operating at lower current density: A lower current density decreases the gradient in the diffusive boundary layer, therefore less concentration polarization is present.

2.4.2. Electrical potential distribution

Figure 2.9 shows the electric potential gradients across a cell pair. The electrical potential drops consist of resistances which are present in the bulk solutions, diffusion boundary layers and membrane phases as well as the Donnan potentials at the membrane interfaces. The

Donnan potential is the electrical potential difference between the membrane and the adjacent solution [52, 85].

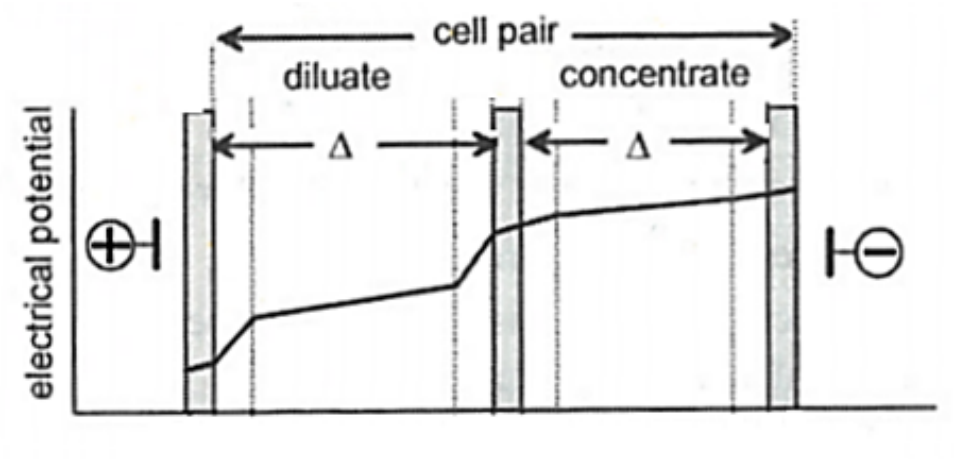

Figure 2.9: Graphical visualisation of the electrical potential differences across the bulk solutions, dilute boundary layers and the IEM. Retrieved from *Strathmann* and adapted [52].

2.5. Limiting current density

Due to concentration polarization, the ion concentration in the diluate cell near the membrane surface decreases as shown in figure 2.8. At increasing current density, the ionic gradient in the diffusion boundary layer becomes steeper towards the membrane because of the increase in ionic flux. Therefore the ion concentration at the membrane will eventually approach zero [54, 87]. The current density involving the zero concentration at the membrane surface is called the limiting current density (LCD) [87].

Figure 2.10 shows that when operating at a current density below the limiting current density, the current density linearly increases when the applied voltage increases. According to Ohm's law this means that the resistance of the stack remains constant [54]. Once the limiting current density is reached, the cell resistance drastically increases because of the depletion of ions between the membrane interface and the diffusive boundary layer [87]. The increase of applied voltage now only marginally increases the current density. This is referred to as the limiting current plateau [87]. When the applied voltage keeps being increased, a certain overlimiting current density is reached. After reaching the overlimiting current density, there is once again a linear increase in current density with increasing applied voltage, thus a decreased resistance at the membrane interface. Although not fully understood yet, it is hypothesized that this is due to (uncontrolled) water splitting and electro-convection. Water is being split in hydroxide and hydrogen ions, carrying charges across the membranes [52, 54, 87].

In conventional ED operation, it is highly preferred to operate below the limiting current density. Water splitting occurring at overlimiting current density leads to unnecessary transport of hydrogen and hydroxide ions instead of concentrating targeted ions. Also, water splitting can lead to rapid increases/decreases of the pH within areas in the ED cell.

2.6. Scaling in Electrodialysis

Figure 2.8 shows that due to concentration polarization, there is an accumulation of ions in the diffusive boundary layer in the concentrate compartments during ED operation. When ED

is used for treating waters that contain ionic species that have a tendency to form ionic complexes with relatively low solubility, scaling can occur. Scaling is unwanted precipitation of salts and can cause membrane and/or spacer fouling [54, 101]. Especially due to concentration polarization, scaling can occur much quicker than it normally would in the bulk solution due to the much higher local concentration of ions in the concentrate DBL. Therefore, it is highly favored to operate an ED system in such a way that concentration polarization is limited or by retaining ions that cause scaling in the diluate solution.

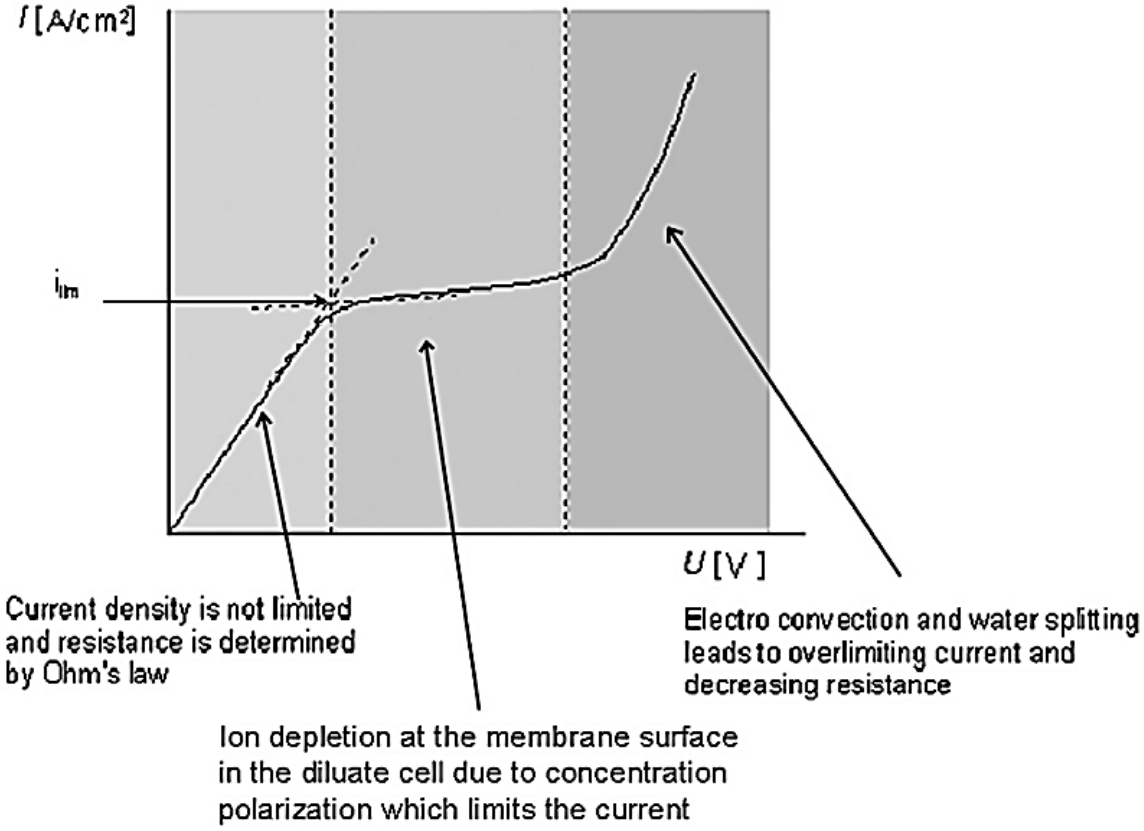

Figure 2.10: Current-voltage curve explaining Ohmic behaviour, limiting current density and overlimiting current density. Retrieved from *Strathmann* and adapted [54].

2.7. Current density, current efficiency and permselectivity

Ions carry the current through the IEMs. In literature the amount of charge per unit time that flows through a unit area of a chosen cross section is generally referred to as the current density [102]. The current density can be derived from Faraday's law as given by equation 2.5.

$$i = \frac{I}{A} = F \sum_{i}^{n} |z_i| J_i \tag{2.5}$$

Here i is the current density (A/m^2), I the current (A) and A the effective membrane surface area for ion transport [72].

When multiple ionic species are being transported through an IEM simultaneously, the current is carried by all involved species that move through the IEM. The fraction of the total current used for the transport of that species relative to the sum of current used by all ionic species is referred to as the current efficiency (or transport number) η_i [72, 75]. This is given by equation 2.6 For consistency with previous research, the term current efficiency is preferred over transport number.

$$\eta_i = \frac{|z_i|J_i}{\sum_i^n |z_i|J_i} \cdot 100\% \tag{2.6}$$

Equation 2.7 gives the exact formula used for the calculation of the current efficiency of the species during the experiments.

$$\eta_{NH_4^+} = \frac{z \cdot F \cdot \Delta M_{NH_4^+}}{N \cdot \sum_{t=0}^{t} I_t \cdot \Delta t} \cdot 100\% \tag{2.7}$$

Here $\eta_{NH_4^+}$ is the current efficiency (%), z the valence of species i, N the number of cell pairs, M the mass of the transported species species (mol), I the current (A) and t the time (min). The current efficiency is negatively impacted by non-electro-migration related transport such as ion back diffusion from the concentrate to the diluate [60, 62, 63].

The current efficiency of each species is an indication of the relative ion permselectivity between different counter-ions. The permselectivity (or relative permeability) between counter-ions and the IEM can be defined by the ratio of their respective current efficiencies over the ratio of their respective concentrations adjacent to the membrane in the diluate compartment [53]. This is given by equation 2.8. Mg^{2+} and NH_4^+ are chosen for this equation as they are the primary set of counter-ions this research focuses on.

$$P_{NH_4^+}^{Mg^{2+}} = \frac{\eta_{Mg^{2+}}/\eta_{NH_4^+}}{C_{Mg^{2+}}^{Dil,t=n}/C_{NH_4^+}^{Dil,t=n}} \tag{2.8}$$

Here $P_{NH_4^+}^{Mg^{2+}}$ is the permselectivity between Mg^{2+} and NH_4^+ $(-)$, η the current efficiency of species i (%) and $C^{Dil,t=n}$ the equivalent concentration of the counter-ion in the diluate solution at time interval n (mol/L). What should be taken into account is that equation 2.8 suggest to use the counter-ion concentration on the membrane surface adjacent to the diluate side [53, 72]. However for this research it is assumed that the concentrations at the membrane surface adjacent are comparable to that of the bulk solution, because concentration polarization is mostly negligible throughout the experiments. This is because the system is operated below the limiting current density for the majority of the experiments' duration [76].

2.8. Energy consumption and resistance

One of the primary objectives of using ED for this research was to recover NH_4^+. The corresponding energy consumption that is required to recover NH_4^+ is an important parameter for comparing different performed experiments in this report. Energy consumption is also often used as a parameter for comparing other competitive techniques that focus on NH_4^+ removal. A good way of expressing energy consumption is energy consumed per kilogram of nitrogen removed ($MJ/kg_{N_{removed}}$) [60]. Equation 2.9 shows how the energy consumption is calculated.

$$E_{N_{removed}} = \frac{\sum_{t=0}^{t} U_t \cdot I_t \cdot \Delta t \cdot 3.6}{\Delta M_{NH_4^+}} \cdot \frac{18}{14} \tag{2.9}$$

Here ΔU is the electrical potential (V), ΔI the electrical current (A) and t the time. These three together form the energy consumption in kWh. $\Delta M_{NH_4^+}$ is the mass of NH_4^+ removed from the diluate (kg). The factor of 3.6 is to convert the value from $kWh/kg_{N_{removed}}$ to $MJ/kg_{N_{removed}}$. The $\frac{18}{14}$ term converts the mass from NH_4^+ to molecular N [62].

The energy consumption when operating ED at given current density is largely determined by the overall resistance of the system. The resistance of the overall system is determined by the resistance of the components of the ED system including IEMs, spacers, electrolyte solutions and electrodes. The total resistance is the sum of these components. This is given by equation 2.10 [60].

$$R_{Tot}^{ED} = n \cdot R_{Dil} + n \cdot R_{Con} + n \cdot R_{CEM} + (n-1) \cdot R_{AEM} + 2 \cdot R_{AEEM} + 2n \cdot R_{sp} + R_{elec} \quad (2.10)$$

Here R_{Tot}^{ED} is the total resistance of the ED stack (Ω), R_{Dil} the resistance of the diluate electrolyte solution, R_{Con} the resistance of the concentrate electrolyte solution, R_{CEM} the resistance of the cation exchange membrane, R_{AEM} the resistance of the anion exchange membrane, R_{AEEM} the resistance of the anion exchange end membranes, R_{sp} the resistance of the spacers and R_{elec} the resistance of the electrolyte rinse solution and the electrodes. n is the number of cell-pairs of the IEM stack.

2.9. Removal efficiency

The removal efficiency is used to calculate how much of the total mass of a specific ionic species is removed from the diluate. This is given by formula 2.11.

$$R.E._i = \left(1 - \frac{M_i^{dil,t=end}}{M_i^{dil,t=0}}\right) \cdot 100\% \quad (2.11)$$

Here $R.E._i$ is the removal efficiency of species i (%), $M_i^{dil,t=0}$ the initial mass of species i in the diluate and $M_i^{dil,t=end}$ the final mass of species i in the diluate.

3

Materials and Methods

This chapter describes the materials, setup and analytical equipment used for the experiments done for this research. Detailed explanations are given on how the different experiments are conducted and how data was analysed as well. It is also discussed why different operational parameters were used and why different make-up waters were used.

3.1. Material

For all experiments, a standard electrodialysis unit was used. This section describes the specification of the components and analytical equipment of the ED system.

3.1.1. Electrodialysis setup

The ED setup used for this research was a '*PCCell standard ED cell model ED 64002*' supplied by '*PCCell GmbH*'. The cell consisted of a polypropylene housing with both electrodes embedded in the structure. The anode was made from Pt/Ir- coated Titanium and the cathode from V4A Steel. Two different membrane stacks were supplied by PCCell as well. A standard cell package '*MP-010-1101*' and a monovalent selective cell package '*MP-010-NG01*'. Both sets were pre-assembled and consisted of:

- 9 standard/monovalent cation exchange membranes (PVSK/PCMVK)
- 10 standard/monovalent anion exchange membranes (PCSA/PCMVA)
- 2 standard cation exchange end membranes (PCCEEM)
- 20 Flow-dispensers/spacers
- 2 electrode flow-dispensers/spacers

In order to reduce the possibility of NH_4^+ and Mg^{2+} accumulation in the electrode rinse solution, the pre-assembled membrane stacks were adjusted by swapping out the CEEMs and interchanging them with AEEMs. This also required that two AEMs were taken from the stack. This modification was done for both the standard and monovalent stack in order to avoid flow channels where no ion exchange would be possible. The modification meant that there was a total number of 9 cell pairs present for both stacks. Each membrane had a size of 110x110 mm with an active membrane area of 80x80 mm. The membranes had a thickness of $\sim$ 100 μm and the spacers a thickness of $\sim$ 500 μm [103].

3.1.2. Analytical equipment

The analytical equipment used for logging experiment data and analysing sampled data is itemized below.

- Electrical conductivity (EC) and pH probes: During experiments the electrical conductivity and pH of the diluate, concentrate and electrode rinse were measured with use of two '*WTW IDS digital conductivity cells TetraCon® 925*' and one '*WTW universal IDS pH-electrodes SenTix® 940*'. Both sensor types simultaneously measured the temperature of the solutions as well. The data was stored on a '*WTM MultiLine® Multi 3630 IDS multimeter*'. The data storage interval was set to 5 seconds per measurement. After each experiment the data was exported to Microsoft Excel via USB cable.

- Electrical data: For the supply of an external potential to the ED system, a programmable DC power '*TENMA 72-2535*' was used. While functioning as the power supply during the experiments, the current and voltage data was simultaneously logged on a laptop with use of the supplied operational software for the TENMA. The data storage interval was set to 1 second per measurement.

- Sample analysis IC: The bulk of the samples taken were analysed via ion chromatography (IC). The IC setup consisted of a *Metrohm 919 autosampler, IC 818 anion system and 883 IC cation system*. Samples were prepared for the IC by a 200x dilution. The dilution was done by using pipets. The IC was used to measure the ion concentrations of NH_4^+, Mg^{2+} and Cl^-.

- Sample analysis photometry: Some samples were analysed by a '*Macherey-Nagel Spectrophotometer NANOCOLOR*'. For NH_4^+ measurements the '*NANOCOLOR Ammonium 2000 and 200*' test kits were used. For Mg^{2+} the '*NANOCOLOR Hardness Ca/Mg*' kits were used.

3.2. Experimental methodology

This section describes the different experiments that were conducted for this research. While each experiment served its own purpose, the operational methods were kept as closely related as possible. Figure 3.1 gives a visual representation of the used ED setup for this research. Three continuously stirred solutions were continuously recirculated through the ED membrane stack by a peristaltic pump (*Watson & Marlow 520s)*. These solutions were the diluate, concentrate and electrode rinse. The current was regulated via a current regulator which was connected to the ED cell via copper cables. The laptop was used to control the current regulator and to directly log the electrical data on the laptop. The conductivity, pH and temperature of the solutions were measured with EC and pH probes. The data was collected by a multimeter and directly logged on the laptop. The colored lines in figure 3.1 indicate the flow directions for each solution.

All experiments were carried out in batch mode, meaning that there is no external supply of solutions during experiments. The initial diluate and concentrate solutions always had an initial volume of 1 liter. The electrode rinse always had an initial volume of 0.5 liter and consisted of a 1 molar $NaHCO_3$ concentration. The weight of all solutions was measured before and after each experiment. The cross-flow velocity of the diluate and the concentrate solutions through the membrane stack were kept constant at $\sim 2\ cm/s$ (90 RPM) as advised [52, 61].

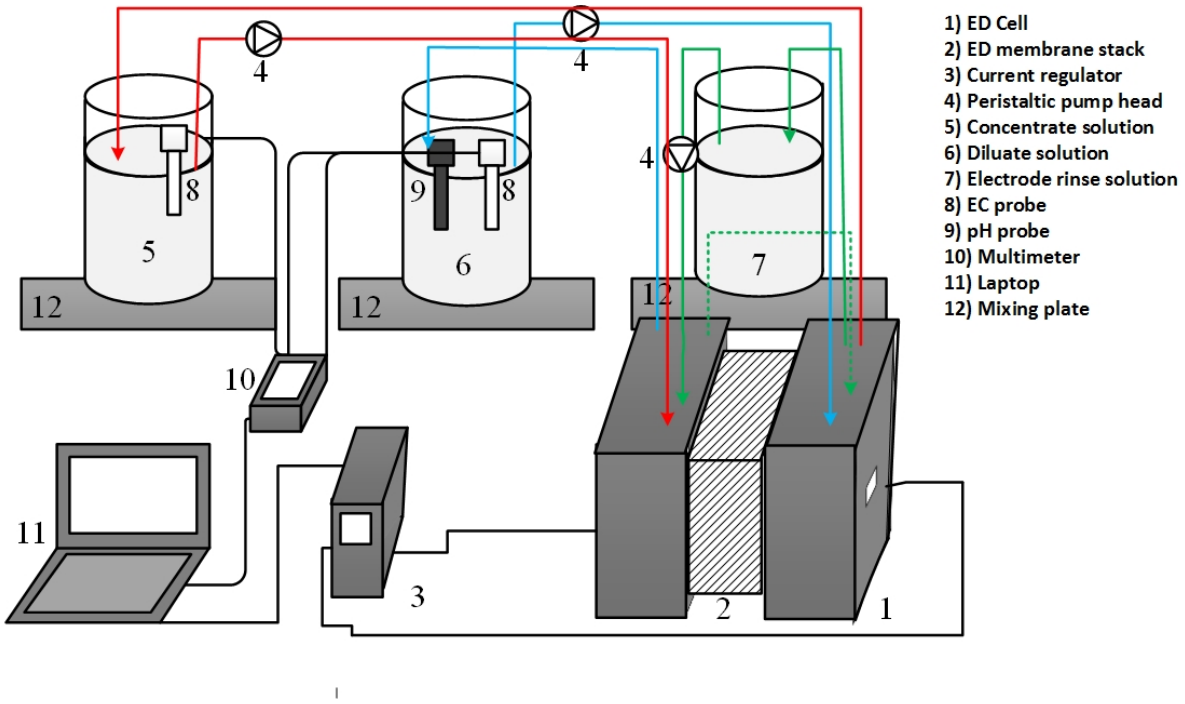

Figure 3.1: Visual representation of the used experimental setup for this research. Partially retrieved and modified [62].

3.2.1. Constant current selectivity experiments

The bulk of the conducted experiments consisted of operating ED at a constant current to determine the selective transport between NH_4^+ and Mg^{2+}. Four different make-up waters were used for the experiments. These make-up waters were based on representative real life situations (as mentioned in section 1.5.2). Therefore the molar ratios of Mg^{2+} to NH_4^+ were chosen to be 1:20, 1:10 and 1:4. The fourth make-up water consisted only of NH_4^+ as cation. The initial NH_4^+ concentration was always kept at 1.5g in both the diluate and concentrate. The initial concentrate solution always consisted of 1.5 g NH_4^+. The salts used for making the synthetic water were NH_4HCO_3 and $MgCl_2$. Table 3.1 summarizes the different make-up waters.

Table 3.1: Composition of the diluate make-up waters used for the constant current selectivity experiments.

Ratio Mg^{2+}/NH_4^+ [mol/mol]	added NH_4HCO_3 [g]	added $MgCl_2$ [g]
1:20	6.57	0.39
1:10	6.57	0.73
1:4	6.57	1.96
Only NH_4^+	6.57	-

Three different current densities were used. The used current densities were derived from the limiting current density of the diluate make-up water that consisted only of NH_4HCO_3. For both standard and monovalent selective membranes, the LCD of this solution was 160 A/m^2. How the limiting current density was determined is explained in section 3.2.3. For this experiments, fixed current densities were set at 20, 40 and 60% of the initial LCD. These correspond to a current density of 32, 64 and 96 A/m^2. Two different membrane stacks were used as described in section 3.1.1. These stacks were interchanged between experiments. All runs were

duplicated, resulting in a total of 48 experiments.

Each experiment initially consisted of an 1 L diluate, 1 L concentrate and 0.5 L electrode rinse solution. The diluate and concentrate solutions were prepared by solving 6.57 g of NH_4HCO_3 in 1L of demineralized water. Depending on what experiment, $MgCl_2$ was also solved in the diluate (according to table 3.1). The electrode rinse was prepared by adding 42 g of $NaHCO_3$ in 0.5 L of demineralized water. The electrode rinse was renewed after $\sim$ 8 runs.

The solutions were continuously recirculated through the ED stack. Once a current was applied to the system, the conductivity of the diluate solution started to decrease and the conductivity of the concentrate solution started to increase due to ionic transport through the IEX membranes from the diluate to concentrate solution. Figure 3.2a shows a representative example of the EC values of an experiment. A current was applied until the diluate concentration reached a value corresponding to 1000 $\mu S/cm$ or if the maximum voltage of 30 V was reached by the current regulator. Figure 3.2b shows a representative example of the electrical data of an experiment. 2 mL samples were taken from the diluate every 5 minutes until 30 minutes. After 30 minutes a sample of the diluate was taken every 10 minutes. At the start and end of the experiment, samples were also taken of the concentrate and electrode rinse.

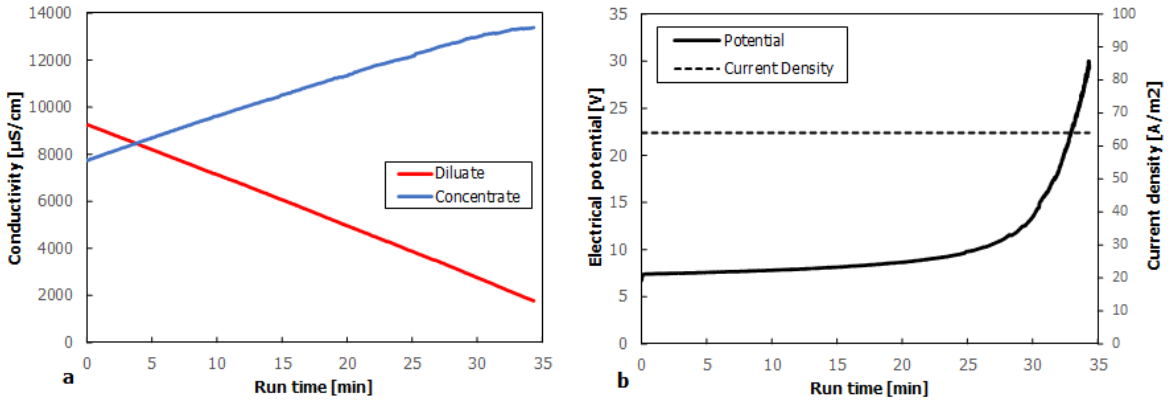

Figure 3.2: EC (a) and electrical (b) data of constant current experiment with a molar ratio Mg^{2+}/NH_4^+ of 1:10 at a constant current density of 64 A/m^2 and with standard IEX membranes. The conductivity of the diluate increased linearly over time. The conductivity of the concentrate increased linearly over time. The current density was constant over time, and the voltage increased exponentially over time. The experiment was stopped when the voltage reached 30 V. These trends were representative for all constant current selectivity experiments.

3.2.2. Constant voltage selectivity experiments

In order to determine if the applied voltage had an influence on the selective transport of NH_4^+ and Mg^{2+}, constant voltage selectivity experiments were conducted. These were conducted in the same fashion as the experiments described in section 3.2.1, but at a constant voltage of 10 V. These experiments were done with make-up diluate water with molar ratios of Mg^{2+}/NH_4^+ of 1:20 and 1:4. Experiments were done with both the standard and monovalent selective IEM stacks. The added salt quantities were the same as shown in table 3.1. 2 mL samples were taken from the diluate every 10 minutes. At the start and end of the experiment, samples were also taken of the concentrate and electrode rinse. Figure 3.3 shows representative EC and electrical data of these experiments.

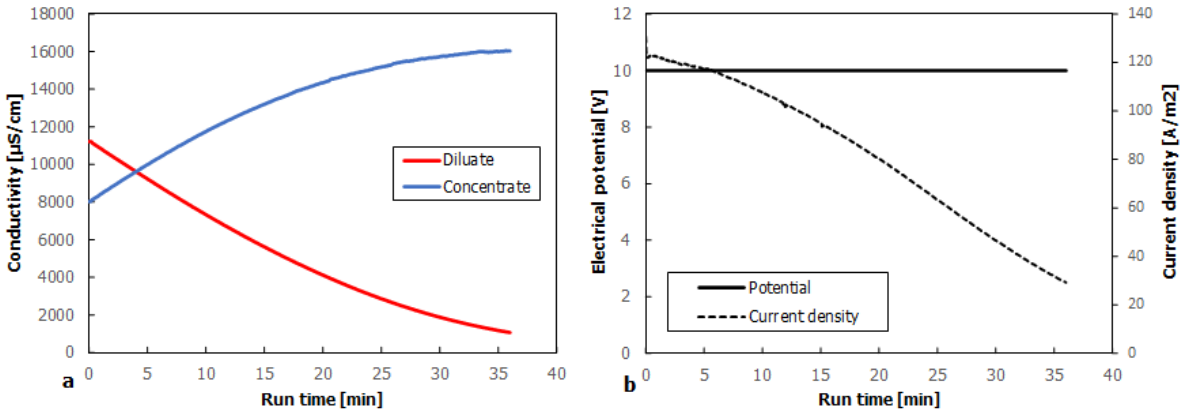

Figure 3.3: EC (a) and electrical (b) data of constant voltage experiment with a molar ratio Mg^{2+}/NH_4^+ of 1:4 at a constant voltage of 10 V and with standard IEX membranes. The conductivity of the diluate increased over time at exponentially decreasing rates. The conductivity of the concentrate increased over time at exponentially decreasing rates. The voltage remained constant over and the current density decreased over time. These trends were representative for all constant voltage selectivity experiments.

3.2.3. Limiting current density determination

The LCD was determined for the different initial diluate make-up waters given by table 3.1. It was later decided that an extra solution needed to be tested with a molar ratio of 1:7 Mg^{2+}/NH_4^+. The respective water was recirculated through the diluate and concentrate compartment simultaneously by recombining the flows in the same bottle. A step wise increasing current was applied to the solution. No net transport of ions took place during this experiment, therefore the electrolyte solution composition stayed the same for the entire duration of the experiment. The system was shut down once a current of 3 A or voltage of 30 V was reached (current regulator limitations). The LCD was found by taking the current density corresponding to the lowest electrical resistance found during the experiment. This is graphically illustrated by figure 3.4. Solutions were tested only once before being disposed, because of the increasing temperature of the solution during the experiments. Therefore it could potentially influence the results if a solution was tested multiple times.

3.2.4. Uphill transport experiments (1/2)

Tests were conducted to determine the magnitude of uphill transport of Mg^{2+} from the diluate solution to the concentrate solution. The initial diluate solution had a molar ratios of Mg^{2+}/NH_4^+ of 1:4 by adding 6.57 g of NH_4HCO_3 and 1.96 g of $MgCl_2$ to the diluate solution(see table 3.1). 6.57 g of NH_4HCO_3 was also added to the initial concentrate solution. The solutions were continuously recirculated through the ED system for 60 minutes without supply of an external electrical potential. Samples of the diluate and concentrate were taken at 0, 3, 10, 30 and 60 minutes. It was determined that a single pass of the diluate and concentrate solution took 3 minutes. Therefore a sample was taken after 3 minutes. The tests were done with both standard and monovalent selective IEM stacks.

3.2.5. Uphill transport and back-diffusion experiments (2/2)

Uphill transport/back-diffusion experiments were conducted to estimate how much uphill transport and back-diffusion took place between the diluate and concentrate solutions during experiments. The constant current selectivity experiments had varying operational parameters, diluate concentrations and membrane types, making it difficult to quantify the uphill and diffusive fluxes for all experiments. Therefore a comprehensive test was done to quantify these

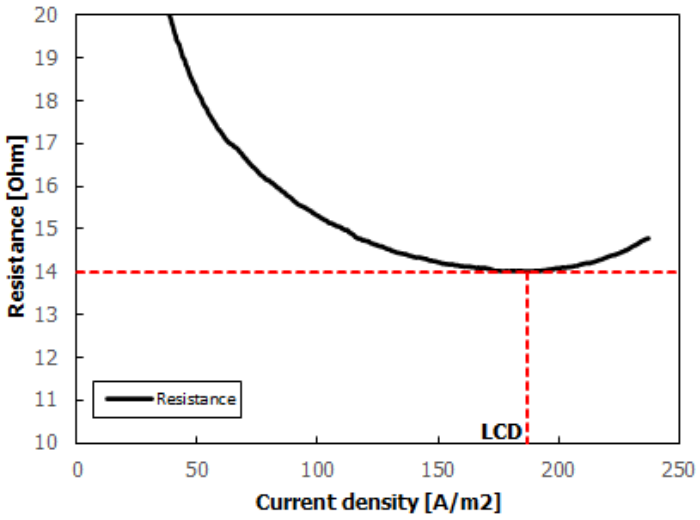

Figure 3.4: Current density versus resistance for LCD experiment with molar ratio Mg^{2+}/NH_4^+ of 1:4 and standard IEX membranes. The LCD is the current density where the electrical resistance is at a minimum. This trend is representative for all LCD determination experiments.

fluxes in a representative way for all experiments. According to section 2.3.3 and 2.3.4, uphill transport and diffusion are driven by the chemical potential difference between the diluate and concentrate solution. Since this chemical potential difference increased during the experiments, it was estimated that the potential for diffusive transfer would also increase over time. Therefore diffusion was estimated to be the most significant towards the end of each experiment when the concentration differences between diluate and concentrate were the largest. Potential for uphill transport also changed during the experiments because of the changes in diluate/concentrate composition and concentration.

For the standard IEM stack, 2.30 g NH_4HCO_3 and 0.6 g $MgCl_2$ were dissolved to form the diluate. 10.90 g NH_4HCO_3 and 1.43 g $MgCl_2$ were dissolved to form the concentrate. For the monovalent selective IEM stack, 2.40 g NH_4HCO_3 and 1.62 g $MgCl_2$ were dissolved to form the diluate. 10.85 g NH_4HCO_3 and 0.34 g $MgCl_2$ were dissolved to form the concentrate. These values were chosen because they represent the NH_4^+ and Mg^{2+} concentration at $\sim 80\%$ run time of constant current selectivity experiments ran at 64 A/m^2 with an initial molar Mg^{2+}/NH_4^+ ratio of 1:4. This data was acquired by analysing samples of the earlier conducted constant current selectivity experiments described in section 3.2.1. The solutions were continuously recirculated through the ED system for 60 minutes without supply of an external electrical potential. Samples of the diluate and concentrate were taken at 0, 30 and 60 minutes.

4

Results and discussion

This chapter describes the results from the different conducted experiments. The results are used for answering the research questions as described in section 1.6.2. The results are thoroughly discussed and compared with literature.

4.1. Limiting current density for different IEMs

The limiting current densities for the different initial diluate solutions for the two different membrane types were determined by the experiments described in section 3.2.3. Figure 4.1 shows the limiting current densities for the different diluate solutions at their corresponding conductivity. The points with the lowest conductivity represent 6.57 g of NH_4HCO_3 without any added $MgCl_2$. The conductivity was raised by adding $MgCl_2$ only.

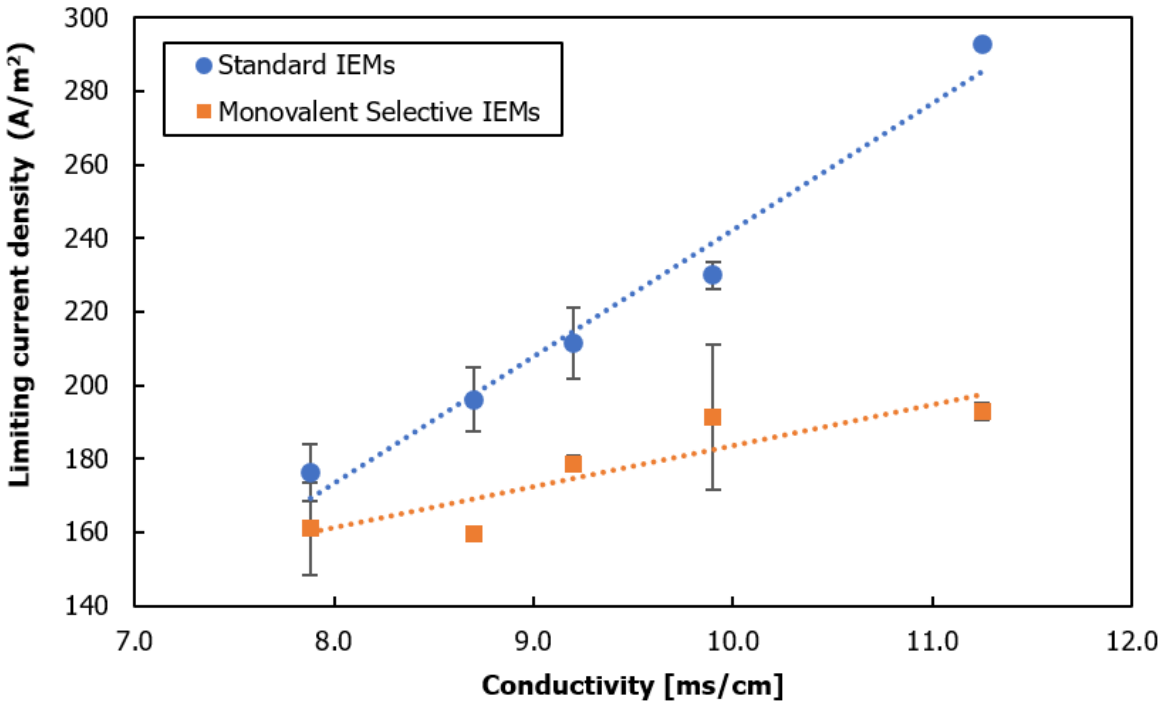

Figure 4.1: Limiting current densities for the different initial diluate solutions for standard and monovalent selective IEMs. The points with the lowest conductivity represent 6.57g NH_4HCO_3. The conductivity was raised by adding $MgCl_2$ only.

It can be seen that the LCD for standard IEMs and monovalent selective IEMs was roughly the same when only monovalent ions were in the solution. For standard IEMs it can be seen that when $MgCl_2$ was added, the LCD linearly increased as the conductivity of the solution increased. This linear increase in the LCD at increasing conductivity was as expected, as this trend has been demonstrated in previous research [60, 61]. This relation held for standard IEMs even though a salt containing divalent cations was added to increase the conductivity.

For monovalent selective IEMs there was also an overall increase in LCD present when $MgCl_2$ was added. However, the increase in LCD is substantially lower when compared to the standard IEMs. Since divalent cations were added to the solution it was expected that the monovalent selective membranes would have a repulsive effect on these divalent ions. Because of this repulsive effect, Mg^{2+} flux through the membranes was likely lower than for standard IEMs. Therefore concentration polarization was more prevalent at increasing current densities. This was clearly visible as the LCD for monovalent selective IEMs only marginally increased when the conductivity was increased by adding divalent ions. The increase in LCD was accounted for by assuming that the monovalent selective IEMs are not perfectly selective between mono- and divalent ions. Therefore divalent ion transport, although reduced, was still taking place.

Another explanation for the varying LCD could be that there was a difference in resistance between the different membrane stacks. The standard AEM and CEM had an area resistance of 1.8 and 2.5 $\Omega \cdot cm^2$, respectively. The monovalent selective AEM and CEM had an area resistance of 5 and 6 $\Omega \cdot cm^2$, respectively. When only NH_4HCO_3 was present the average LCD for monovalent selective IEMs was found to be lower than for standard IEMs. A higher area resistance could have lowered the LCD for monovalent selective IEMs. However, the data points for both IEM types were within each others error margin. Therefore, the theory that a higher area resistance of the IEMs decreases the LCD was unsubstantial. It could not be excluded that the membrane resistance had a lowering effect on the LCD, but it could be excluded as sole contributor to the visible trend difference between the IEM types.

Because 160 A/m^2 was found to be the lowest limiting current density, the constant currents for the selectivity experiments were set at 20, 40 and 60% of 160 A/m^2 as explained in section 3.2.1.

4.2. Overall performance

This section describes the overall performance of the standard IEMs and monovalent selective IEMs for the constant current selectivity experiments. Performance is described in terms of removal and transport efficiencies as well as energy usage.

4.2.1. Removal efficiencies

The removal efficiencies of NH_4^+ and Mg^{2+} were calculated for the different operational parameters and for different IEM types. A high removal efficiency of NH_4^+ and a low removal efficiency of Mg^{2+} was preferred. Figure 4.2 and 4.3 show the NH_4^+ and Mg^{2+} removal efficiencies for both IEM types for the different Mg^{2+}/NH_4^+ ratio and applied current densities.

It can be seen from figure 4.2 that the removal efficiencies for NH_4^+ ranged from 68-92%. The difference in removal efficiency of NH_4^+ between the different current densities was mainly due to the fact that the experiments with a constant current density of 32 A/m^2 were able to achieve a lower final diluate conductivity. At the higher current densities, the maximum volt-

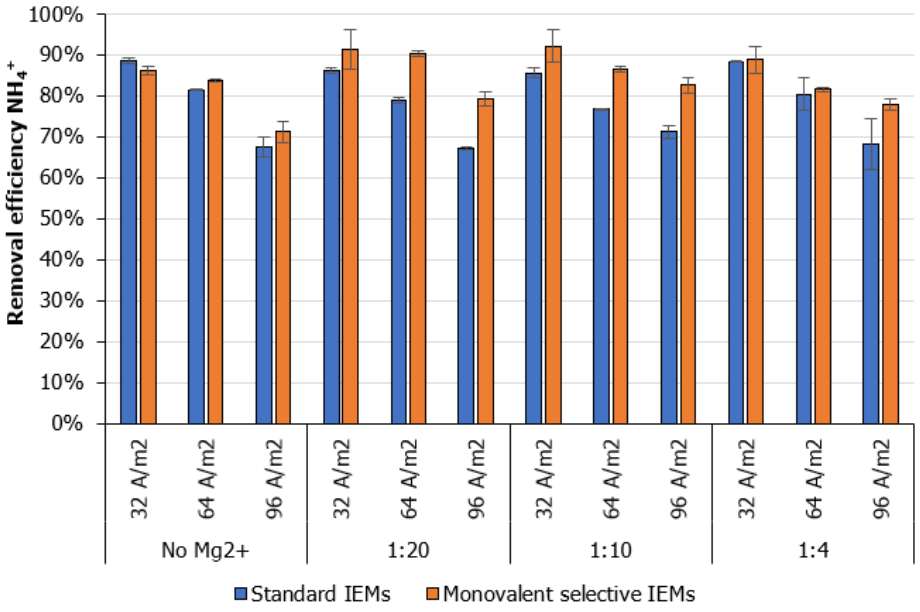

Figure 4.2: NH_4^+ removal efficiency for all conducted selectivity experiments operated at constant current density.

age of 30V was often reached before reaching a diluate conductivity of 1000 $\mu S/cm$. This prevented a higher NH_4^+ removal efficiency. The NH_4^+ removal efficiencies did compare to previously conducted research and were in line with expected results [61, 62]. Overall, the monovalent selective IEMs showed a slightly higher NH_4^+ removal efficiency for the comparable experiments.

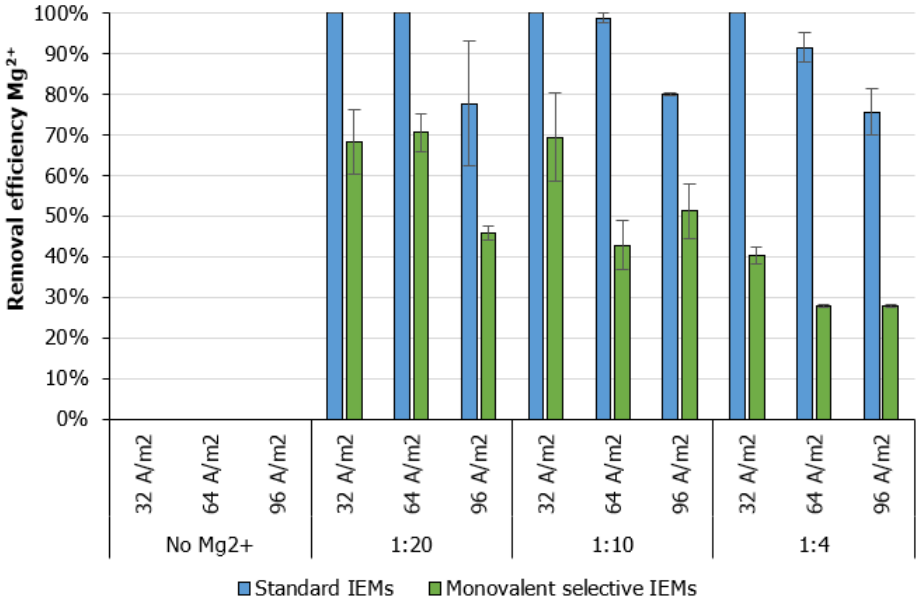

Figure 4.3: Mg^{2+} removal efficiency for all conducted selectivity experiments operated at constant current density.

Figure 4.3 depicts a difference in Mg^{2+} removal efficiency when comparing standard IEMs and monovalent selective IEMs. It can be seen that standard IEMs showed a higher Mg^{2+} removal efficiency compared to the monovalent selective IEMs. The Mg^{2+} removal efficien-

cies for standard IEMs ranged from 78-100% and for monovalent selective IEMs from 28-71%. This was a noticeable performance difference. Especially at a molar Mg^{2+}/NH_4^+ ratio of 1:4, the monovalent selective IEMs showed only 28-40% Mg^{2+} removal efficiency versus 75-100% Mg^{2+} removal efficiency with standard IEMs.

It was concluded that monovalent selective membranes showed comparable, if not better, NH_4^+ removal efficiencies while showing a 30-60% lower Mg^{2+} removal efficiency.

4.2.2. Transport efficiencies

Table 4.1 shows how much Mg^{2+} was transported per mol of NH_4^+ transported from the diluate for the different initial concentration ratios and current densities. For each mol of NH_4^+ that was transported, between 0.06-0.28 mol of Mg^{2+} was transported for standard IEMs and 0.03-0.10 mol Mg^{2+} was transported for monovalent selective IEMs depending on the diluate water composition. At a 1:20 Mg^{2+}/NH_4^+ ratio, the net Mg^{2+} transport varied a factor $\sim$ 1.5-2 between membrane types. At a 1:4 Mg^{2+}/NH_4^+ ratio, the net Mg^{2+} transport varied a factor $\sim$ 2-2.5. While monovalent selective membranes did remove less Mg^{2+}, they were by no means considered perfectly selective towards monovalent ions only according to the data from these experiments.

An increasing ratio between Mg^{2+}/NH_4^+ in the diluate, increased the Mg^{2+} that was removed alongside NH_4^+. This was the case for both IEM types. However, the relative increase in Mg^{2+} transport alongside NH_4^+ transport increased more for standard IEMs at increasing Mg^{2+}/NH_4^+ ratio than for monovalent selective IEMs. It can be seen in table 4.1 that there was a factor $\sim$ 4 difference for standard IEMs and a factor $\sim$ 3 difference for monovalent selective IEMs in Mg^{2+} transport going from a Mg^{2+}/NH_4^+ ratio of 1:20 to 1:4. This is an indication that the permselectivity between Mg^{2+} and NH_4^+ decreased at increased Mg^{2+}/NH_4^+ ratio. This means that monovalent selective IEMs could be increasingly effective when compared to standard IEMs at increasing Mg^{2+} in feed-waters. Though, based on this data such a conclusion would have been premature.

Table 4.1: The molar transport of Mg^{2+} per mol of NH_4^+ transported at different Mg^{2+}/NH_4^+ ratios and current densities.

Ratio Mg^{2+}/NH_4^+	Current density	Transport Mg^{2+}/NH_4^+ Standard IEMs	Transport Mg^{2+}/NH_4^+ Monovalent sel. IEMs
	[A/m^2]	[mol/mol]	[mol/mol]
1:20	32	0.065	0.041
	64	0.069	0.041
	96	0.067	0.032
1:10	32	0.118	0.072
	64	0.119	0.046
	96	0.109	0.063
1:4	32	0.253	0.120
	64	0.278	0.093
	96	0.277	0.097

4.2.3. Energy consumption

The energy consumption of the different constant current experiments are shown in figure 4.4. What can be seen is that when the current density was increased, the energy consumption per kg-N removed increased. According to the current-voltage curve shown in figure 2.10, the voltage increases when the current density increases [52, 104]. This same trend was visible for the conducted experiments. If both the applied current and voltage increased, the power also increased. There was a factor ~ 3 difference in power between operating at 32 and 64 A/m^2 and a factor ~ 7 difference in power between operating at 32 and 96 A/m^2. At higher current densities, the run times of the experiments were lower. However, the lowering in energy consumption by having a decreased run time was outweighed by the increased power. Therefore, there was a net increase in energy consumption per kg-N removed at increasing current densities as can be seen in equation 2.9.

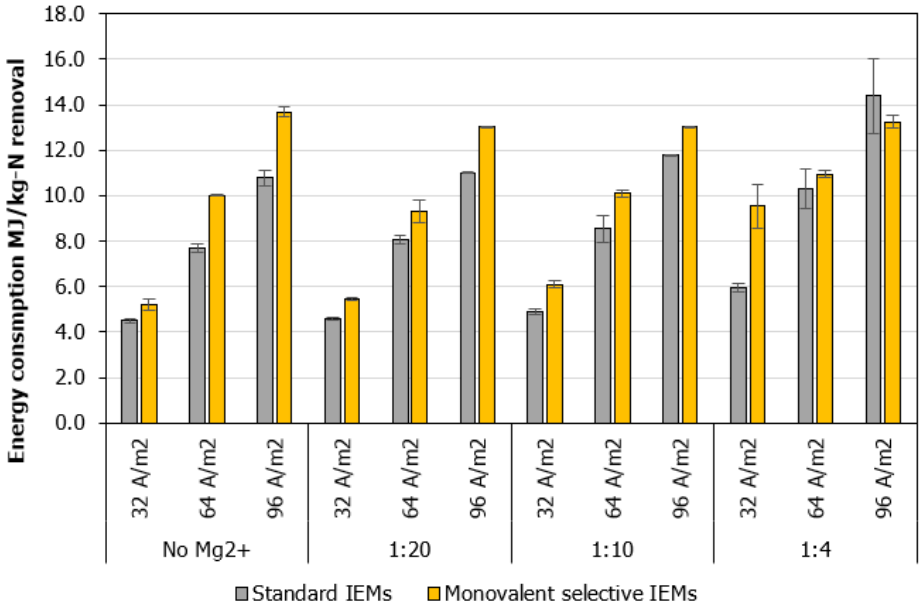

Figure 4.4: Mg^{2+} Energy consumption for all conducted selectivity experiments operated at constant current density.

Figure 4.4 also shows that the energy consumption per kg-N removed was higher for monovalent selective IEMs than for standard IEMs. As previously mentioned, the area resistance of the monovalent AEMs and CEMs were higher than of the standard AEMs and CEMs. The standard AEMs and CEMs had an area resistance of 1.8 and 2.5 $\Omega \cdot cm^2$, respectively. The monovalent selective AEMs and CEMs had an area resistance of 5 and 6 $\Omega \cdot cm^2$, respectively. As given by equation 2.10 the total resistance of the ED system was given by the resistance of the IEMs, spacers, electrolyte solutions and electrodes. With a higher IEM resistance, the total resistance of the ED system also increased. When the current stays constant, according to Ohm's law, an increase in resistance should increase the voltage. This was the case for operating the ED system with monovalent selective IEMs as the applied voltage during experiments averaged $\sim$ 13% higher than for standard IEMs. Again, according to equation 2.9 this increased the energy consumption per kg-N removed.

4.3. Selective transport for standard ion exchange membranes

This section describes the selective ion transport between NH_4^+ and Mg^{2+} for standard IEMs by analysing the differences in current efficiency and ion transport during the experiments. As described in section 3.2.1, samples of the diluate were taken at set intervals. These samples were analysed to determine the ionic concentration of NH_4^+ and Mg^{2+}. The analysed ionic concentrations were corrected for the (electro)-osmosis that took place during the experiments. The net mass changes of the ionic species in the diluate over time, combined with the electrical data were used to calculate the current efficiency of NH_4^+ and Mg^{2+}. This calculation is given in equation 2.7.

4.3.1. Ion transport and current efficiency for standard IEMs

Figure 4.5 shows the NH_4^+ and Mg^{2+} concentrations and current efficiencies during the constant current experiment with an initial molar Mg^{2+}/NH_4^+ of 1:4 and a current density of 32 A/m^2. The concentrations are displayed on the right y-axis. The corresponding species current efficiencies are displayed on the left y-axis. For clarity and simplicity, only a single experimental data set is analysed. Note that in this section, the trends discussed and represented by figure 4.5 were representative for all other conducted constant current experiments with standard IEMs. The results of all other constant current experiments with standard IEMs are given in appendix A.

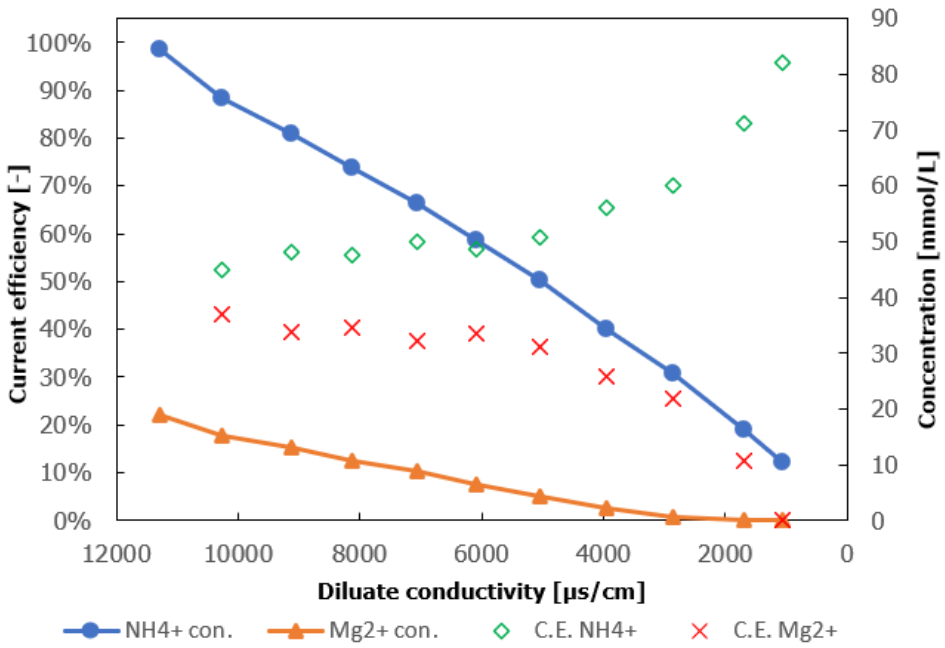

Figure 4.5: NH_4^+ and Mg^{2+} concentration (right y-axis) and current efficiency (left y-axis) as a function of the diluate conductivity. Initial molar Mg^{2+}/NH_4^+ ratio of 1:4 operated at 32 A/m^2 with standard IEMs.

According to figure 4.5, NH_4^+ and Mg^{2+} were transported from the diluate at a constant rate. The current efficiency was higher for NH_4^+ than for Mg^{2+}, meaning that the transport rate of NH_4^+ was higher than for Mg^{2+}. When comparing current efficiencies of both species at the different initial Mg^{2+}/NH_4^+ ratios, it can be seen that a higher initial Mg^{2+}/NH_4^+ ratio resulted in a higher current efficiency for Mg^{2+} and a lower current efficiency for NH_4^+. The current efficiencies of both species stayed more or less constant for the duration of the experiment until the Mg^{2+} concentration in the diluate started to approach zero. Once it approached zero,

the current efficiency for Mg^{2+} subsequently decreased exponentially until the Mg^{2+} concentration reached zero. Vice versa, The current efficiency for NH_4^+ increased, as no more Mg^{2+} was left to be transported.

Figure 4.5 shows that from the start and for a large duration of the experiment, the current efficiency for Mg^{2+} was $\sim$ 40% and for NH_4^+ $\sim$ 55-60% . Knowing that the initial Mg^{2+}/NH_4^+ ratio was 1:4, this current efficiency distribution across both species was disproportionate. This indicates that there was selective transport present between NH_4^+ and Mg^{2+} that favored Mg^{2+} transport over NH_4^+ transport. At the other initial ratios of 1:20 and 1:10, the current efficiencies of Mg^{2+} and NH_4^+ were also disproportional to the respectable Mg^{2+}/NH_4^+ ratio as can be seen in appendix A. This difference in current efficiencies was caused by a difference in preferential transport through IEMs. The ion transport is related to size and the valence of the ions. Ions with a higher valance are preferably transported into the IEM [105]. Divalent ions exhibit a stronger coulombic force than monovalent ions because of the higher charge [72]. According to equation 2.1, a higher valence increases the electrical potential of the ionic species, thus subsequently increasing the electrochemical potential of that species. This explained why Mg^{2+} was preferentially removed over NH_4^+. These findings were in close agreement with the cation exchange order described by *Strathmann* [52] and the '*Hofmeister cation series*' [72, 106].

At equal valence, the difference in stokes radii of the ions dominate the selectivity. However, not relevant to this study, this should be taken into account for more complex water matrices containing multiple multivalent ions [52, 106].

4.3.2. Influence of ion ratio on current efficiency for standard IEMs

Section 4.3.1 discussed that the current efficiencies of NH_4^+ and Mg^{2+} were varying during the experiments and dependent on the ratio between Mg^{2+}/NH_4^+. For each sample taken over time during the experiment, the ratio between Mg^{2+}/NH_4^+ and the respective current efficiencies of NH_4^+ and Mg^{2+} were calculated. These are plotted in figure 4.6 for the 3 different applied current densities.

Figure 4.6 shows the current efficiency of NH_4^+ and Mg^{2+} plotted against the ion ratio. There was a clear trend visible between the amount of Mg^{2+} present relative to NH_4^+ in the diluate and the corresponding current efficiencies. A higher Mg^{2+}/NH_4^+ ratio equaled a higher current efficiency for Mg^{2+} and a lower current efficiency for NH_4^+. According to the Nernst-Planck equation given by equation 2.2, a difference in ion concentration determines a difference in ion flux. Since there was selective transport between Mg^{2+} and NH_4^+ taking place, there was a difference in ion flux between NH_4^+ and Mg^{2+}. Because of this difference in flux, the ratio between Mg^{2+}/NH_4^+ changed continuously during ED operation. This change in relative concentration, functioned as a feedback mechanism as it, according to the Nernst-Planck equation, continuously changed the flux of the corresponding species. Therefore, at increasing Mg^{2+}/NH_4^+ ratio, the current efficiency of Mg^{2+} increased and the current efficiency of NH_4^+ decreased. On average, a two times higher Mg^{2+}/NH_4^+ ratio decreased the NH_4^+ current efficiency and increased the Mg^{2+} by $\sim$ 10%. A three times higher Mg^{2+}/NH_4^+ ratio decreased the NH_4^+ current efficiency and increased the Mg^{2+} by $\sim$ 15-16%

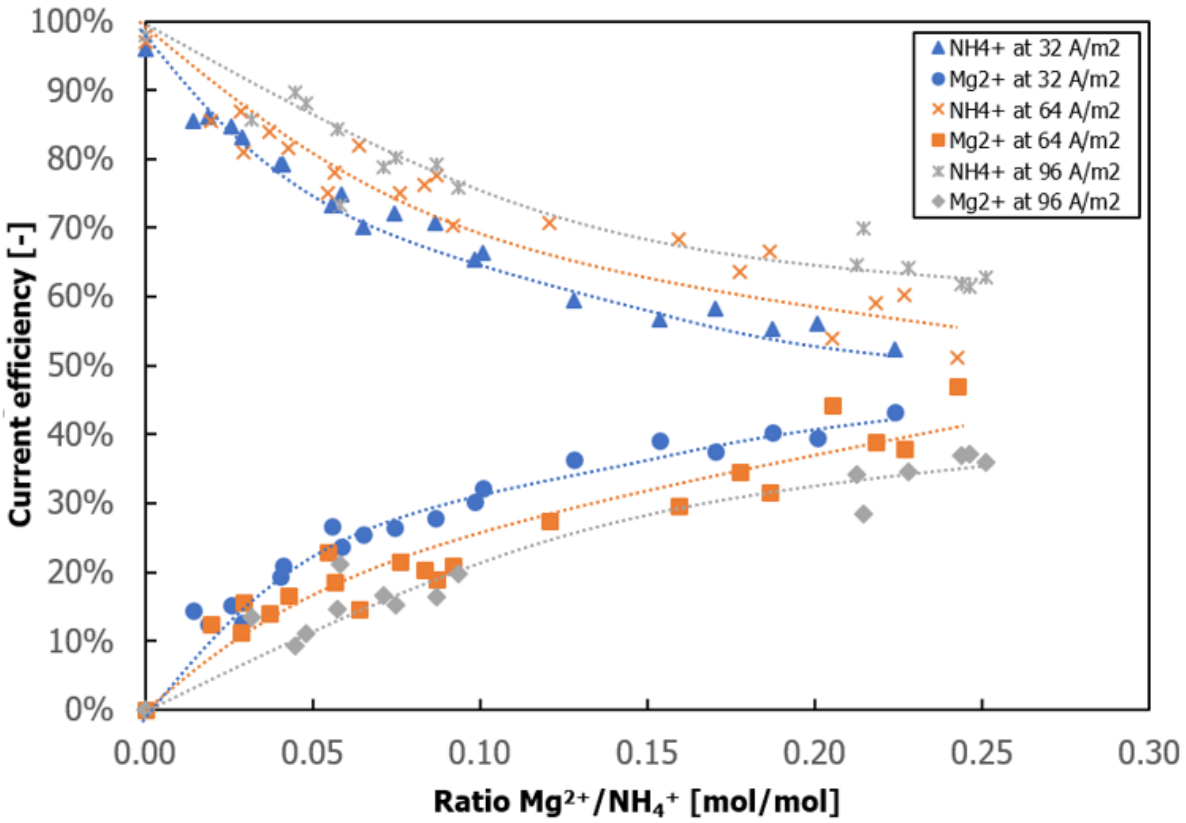

Figure 4.6: Current efficiency of NH_4^+ and Mg^{2+} against the molar Mg^{2+}/NH_4^+ ratio. Each data point is an averaged sample taken during the experiments. The trend lines are manually drawn across the median of the data points with the corresponding current densities.

When the Mg^{2+}/NH_4^+ ratios were equal but, the total concentrations of NH_4^+ and Mg^{2+} in the diluate varied, no difference was found in the current efficiency for both NH_4^+ and Mg^{2+}. This strongly indicated that the total concentration of both species had no effect on the species current efficiency.

4.3.3. Influence of current density on current efficiency for standard IEMs

Figure 4.6 also shows that the applied current density had an effect on the current efficiencies of NH_4^+ and Mg^{2+}. It can be seen that a higher current density resulted in a higher current efficiency for NH_4^+ and a lower current efficiency for Mg^{2+}. When operating at an intermediate current density below limiting current density values, the mass transfer in the diluate compartment is mainly governed by the diffusive boundary layer (DBL) conditions [76, 107]. The DBL is considered stagnant and dominated by diffusive transport of ions [75, 76]. At the current densities applied in these experiments, concentration polarization was considerable. An increase in current density, resulted in a steeper concentration gradient in the DBL. NH_4^+ has a higher self-diffusion coefficient than Mg^{2+} ($D_{NH_4^+}$ = 1.98× 10^{-9} m^2/s and $D_{Mg^{2+}}$ = 0.705× 10^{-9} m^2/s) [72, 76]. Therefore, concentration polarization in the DBL was less predominant for NH_4^+ than for Mg^{2+}. At higher applied current densities, the concentration of NH_4^+ adjacent to the membranes in the DBL remained higher than the Mg^{2+} concentration during the ED operation. This increased the current efficiency for NH_4^+ while subsequently decreasing the current efficiency for Mg^{2+}, thus increasing selective transport in favor of NH_4^+.

On average, operating at 64 A/m^2 increased the current efficiency of NH_4^+ and decreased the current efficiency of Mg^{2+} by $\sim$ 4-5% compared to operating at 32 A/m^2. When operating at 96 A/m^2 the current efficiency of NH_4^+ increased and the current efficiency of Mg^{2+} decreases by $\sim$ 10% compared to operating at 32 A/m^2. It was concluded that for standard IEMs, increasing the current density, increased selective transport of NH_4^+ over Mg^{2+}. This was agreement with literature [75–77].

The current density had a large influence on the current efficiencies of the ionic species. However, the Mg^{2+}/NH_4^+ ratio had an even larger effect on the ratio. Therefore, it was concluded that the increase in ratio had a larger contribution to the change in current efficiency than the applied current density. This is in agreement with literature [75].

4.4. Selective transport for monovalent selective IEMs

This section describes the selective ion transport between NH_4^+ and Mg^{2+} for monovalent selective IEMs by analysing the differences in current efficiency and permselectivity during the experiments.

4.4.1. Ion transport and current efficiency for monovalent selective IEMs

Figure 4.7 shows the NH_4^+ and Mg^{2+} concentration during the constant current experiment with an initial molar Mg^{2+}/NH_4^+ of 1:4 and a current density of 32 A/m^2. For clarity and simplicity, again only a single experimental data set is analysed. Note that in this section, the trends discussed and represented by figure 4.7 are representative for all other conducted constant current experiments with monovalent selective IEMs. The results of all other constant current experiments with monovalent selective IEMs are given in appendix B.

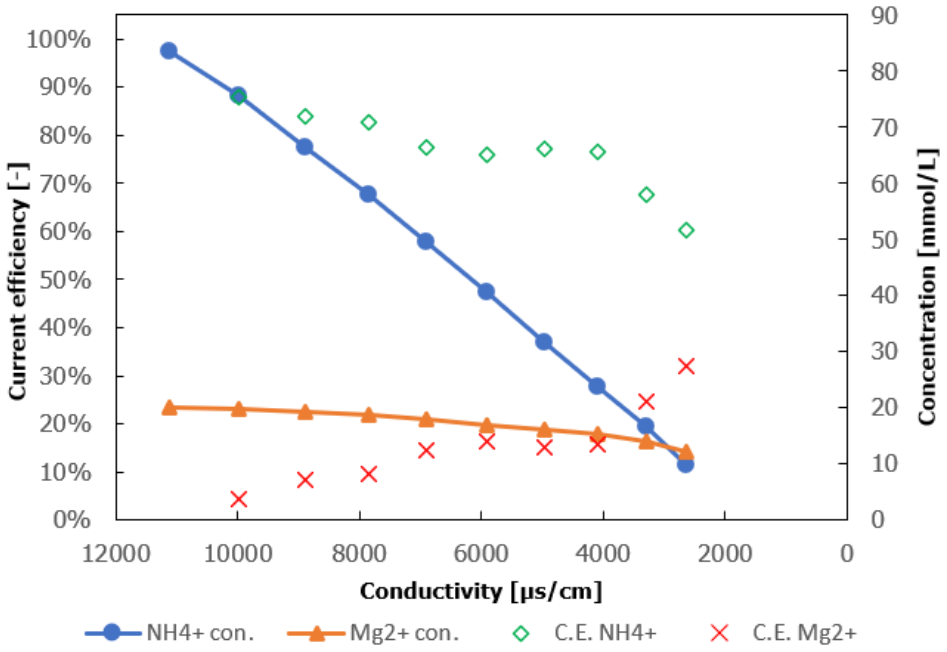

Figure 4.7: NH_4^+ and Mg^{2+} concentration (right y-axis) and current efficiency (left y-axis) as a function of the diluate conductivity. Initial molar Mg^{2+}/NH_4^+ ratio of 1:4 operated at 32 A/m^2 with monovalent selective IEMs.

According to figure 4.7, NH_4^+ was transported from the diluate at a constant rate. The Mg^{2+} transport was initially very low but exponentially increased at decreasing diluate conductivity. There was a clear transport order present, where firstly a large amount of NH_4^+ was transported before the Mg^{2+} transport started to significantly increase. This order of cation transport (NH_4^+ > Mg^{2+}) was consistent with literature [72, 73]. The current efficiency of NH_4^+ was much higher than of Mg^{2+} for the duration of the experiment, meaning that the transport rate of NH_4^+ was much higher than for Mg^{2+}. By comparing all the current efficiencies from the conducted experiments with monovalent IEMs from Appendix B, an overall trend was visible where the current efficiency of Mg^{2+} linearly increased as the conductivity decreases. This linear trend was visible until ~ 70% NH_4^+ was removed from the diluate. When ~ 70% of the NH_4^+ in the diluate was removed (diluate conductivity of ~ 4000 $\mu s/cm$ in figure 4.7) the current efficiency of Mg^{2+} started to increase exponentially at decreasing conductivity. For all other conducted experiments with monovalent selective IEMs, the current efficiency of Mg^{2+} also started to increase exponentially when ~ 60-80% of the NH_4^+ in the diluate was removed. The same trend was visible for the current efficiency of NH_4^+, although be the opposite manner. It was found that a higher Mg^{2+}/NH_4^+ ratio resulted in a higher current efficiency for Mg^{2+} and a lower current efficiency for NH_4^+ throughout the entire experiment.

4.4.2. Influence of ion ratio on current efficiency for monovalent selective IEMs

Figure 4.7 and the figures in Appendix B showed that NH_4^+ is transported from the diluate at a much higher rate compared to Mg^{2+}. Just as with standard IEMs, this resulted in an continuous increase of the Mg^{2+}/NH_4^+ ratio during ED operation. This increase in ratio again functioned as a feedback mechanism allowing an increase in Mg^{2+} transport, as described by section 4.3.2. This continuous increase in Mg^{2+}/NH_4^+ ratio throughout ED operation is one explanation why the current efficiency of Mg^{2+} increased at decreasing diluate conductivity.

However, the difference in ion ratio did not explain why the current efficiency of Mg^{2+} exponentially increased when ~ 70% NH_4^+ was removed from the diluate. Figure 4.8 shows the current efficiencies and the calculated total resistance of the ED system as a function of the diluate conductivity. What can be seen is that when the resistance exponentially increased, the current efficiency of Mg^{2+} also exponentially increased. Because the conductivity of the diluate decreased during operation, the resistance of the system increased. Concentration polarization in the diluate DBL started to become significant once ~ 70% NH_4^+ was removed from the diluate. This caused the resistance to exponentially increase. This instant increase in resistance also meant that the LCD was reached and the system was operating at an overlimiting current density from there on. Because only a limited amount of Mg^{2+} was initially removed during operation compared to NH_4^+, the concentration polarization of Mg^{2+} in the DBL was limited. Therefore, concentration polarization in the DBL was mainly governed by the transport of NH_4^+ between the diluate bulk solution, through the DBL towards the IEMs. A decrease of the NH_4^+ concentration in the diluate bulk solution resulted in a decreased presence of NH_4^+ in the DBL. With less NH_4^+ being present in the DBL, less NH_4^+ was present at the membrane interface. The moment the LCD was reached, the membrane interface reached such a level of NH_4^+ depletion that not all charge could be transported by NH_4^+. Because ions still needed to be transported across the IEM, the Mg^{2+} flux increased when NH_4^+ became increasingly depleted at the IEM interface. This caused the current efficiency of Mg^{2+} to exponentially increase and the current efficiency of NH_4^+ to exponentially decrease. It was therefore concluded that the total NH_4^+ concentration in the diluate bulk solution is a variable that steers selective transport between NH_4^+ and Mg^{2+}.

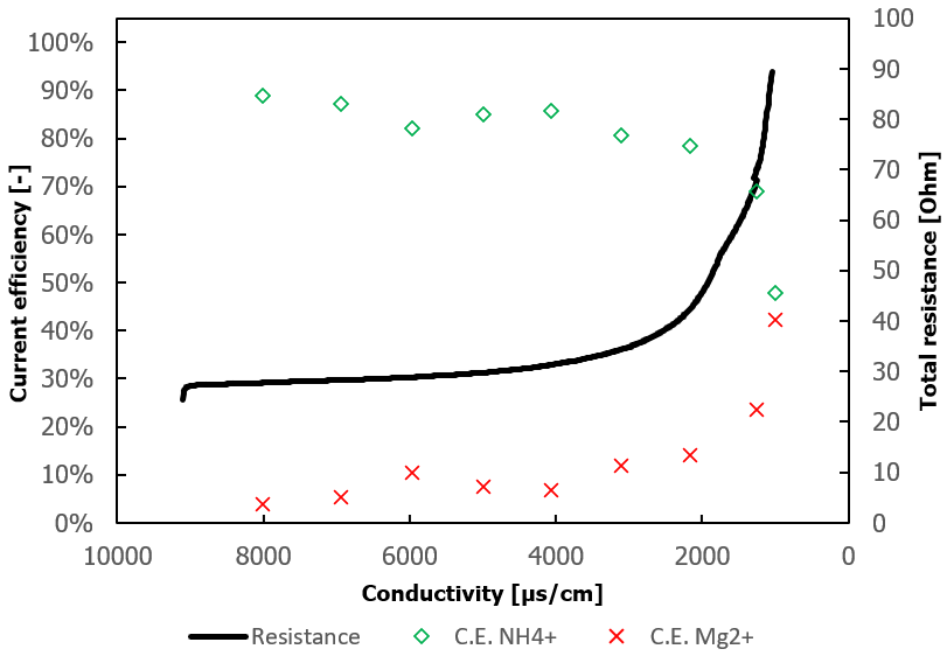

Figure 4.8: Current efficiencies of NH_4^+ and Mg^{2+} (left y-axis) and the total resistance of the ED stack + membranes as a function of the diluate conductivity. Initial molar Mg^{2+}/NH_4^+ ratio of 1:10 operated at 32 A/m^2 with monovalent selective IEMs.

It was found that when operating ED with monovalent selective IEMs, the selective transport between di/monovalent ions was not only influenced by the di/monovalent ion ratio, but also the monovalent counter ion concentration in the diluate. Figure 4.9 shows the relationship between the concentration of NH_4^+ in the diluate, the Mg^{2+}/NH_4^+ ratio and the current efficiency of Mg^{2+}.

The red dots in figure 4.9 represent the averaged sampled data points taken during the constant current experiments. Each data point consists of 3 variables:

- NH_4^+ concentration $[mmol/L]$ as x-axis value
- Ratio of Mg^{2+}/NH_4^+ $[mol/mol]$ as y-axis value
- Current efficiency of Mg^{2+} [%] as z-axis value

In order to visualize the current efficiency of Mg^{2+} as a function of both the NH_4^+ concentration and the Mg^{2+}/NH_4^+ ratio, the current efficiency of Mg^{2+} was interpolated over a grit between the sampled experimental data points. The color represents the current efficiency of Mg^{2+} at given NH_4^+ concentration and ion ratio. The plots for the other current densities are given in appendix C.

According to figure 4.9 the current efficiency of Mg^{2+} was the lowest at low Mg^{2+}/NH_4^+ ratio and at large NH_4^+ concentration in the diluate. This indicated that the monovalent selective IEMs show a very high selectivity in NH_4^+ transport over Mg^{2+} when there is limited di/monovalent counter-ion competition and concentration polarization at the IEM interface. As previously mentioned, an increase in di/monovalent ion ratio and a decrease in total monovalent counter-ion quantity, increased the current efficiency of the divalent ion fraction. This is

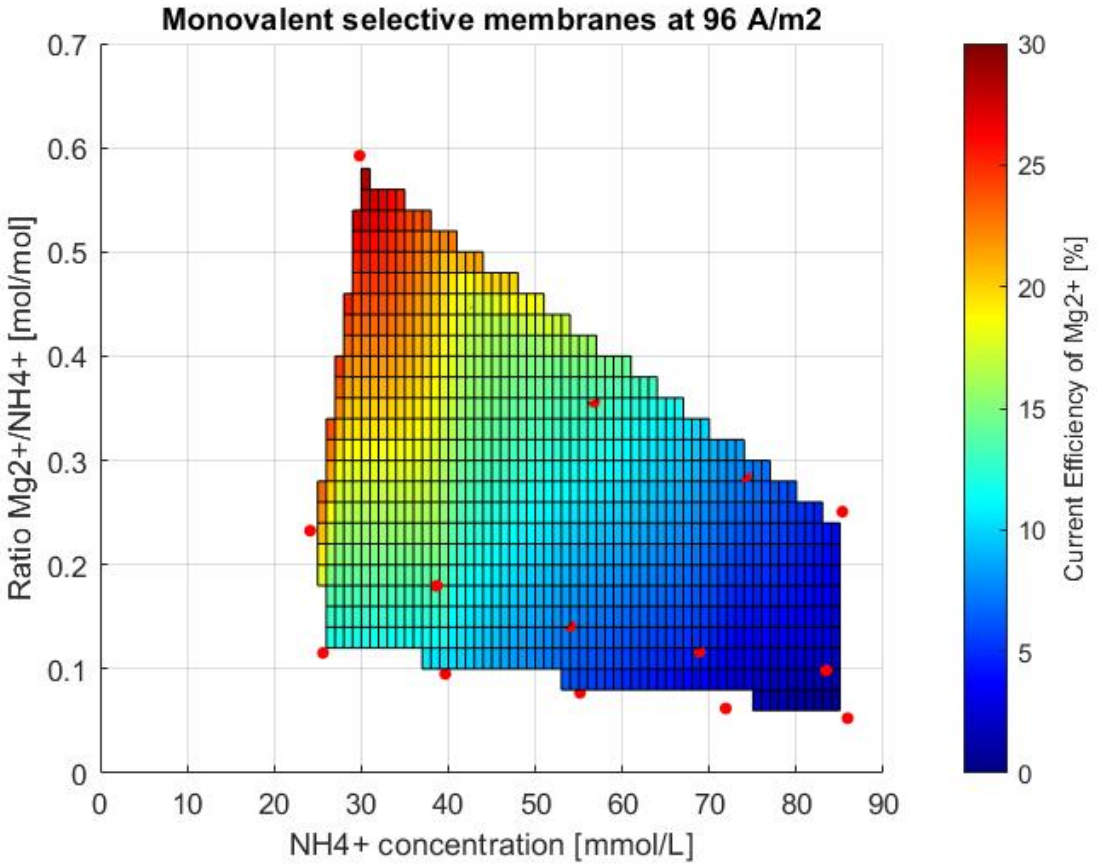

Figure 4.9: Concentration of NH_4^+ in the diluate (x-axis), the Mg^{2+}/NH_4^+ ratio (y-axis) and the current efficiency of Mg^{2+} (z-axis). Red dots are average sampled data points collected during experiments.

exactly shown by figure 4.9. A diagonal color progression is visible, representing the increase in current efficiency of Mg^{2+}. Here, both the decrease of NH_4^+ concentration and an increase in Mg^{2+}/NH_4^+ attributed to the increase of current efficiency of Mg^{2+}. The attribution of both factors were the reason why Mg^{2+} is transported at an exponentially increasing rate during ED operation.

It can be concluded that the use of monovalent selective IEMs gave a noticeable increase in NH_4^+ transport over Mg^{2+} compared to standard IEMs. However, the effectiveness in which NH_4^+ is removed over Mg^{2+} decreases exponentially at increasing NH_4^+ removal.

4.4.3. Influence of current density on current efficiency for monovalent selective IEMs

The effect of the current density on the current efficiencies of NH_4^+ and Mg^{2+} was analysed by comparing the current efficiencies for the different applied current densities. When operating at a lower current density, a lower conductivity was reached when operating at a higher current density because of the $30V$ limit of the current regulator. As discussed in the previous section, the current efficiency of Mg^{2+} increased exponentially at decreasing diluate conductivity. Because a lower conductivity was reached when operating at 32 A/m^2, taking the average current efficiencies of all experiments at the different current densities would have given an overestimation of the current efficiency of Mg^{2+} when operating at 32 A/m^2 compared to 64 and 96 A/m^2.

Instead of taking the averages, the grid data from figure 4.9 and the other figures in appendix C were compared. In order to find a value for the current efficiencies, only the values were compared where all three of the figures from appendix C overlapped. This ensures that only the current efficiencies were compared where the NH_4^+ concentration and Mg^{2+}/NH_4^+ ratio match. This leaves the current density to be the only dependent variable and made it possible to compare the the average current efficiency of Mg^{2+}. It was also ensured that only the values were compared where the system was operating below the LCD. The averages of these analysed current efficiencies shown in table 4.2.

Table 4.2: The average current efficiencies of NH_4^+ and Mg^{2+} for the analysed model data at different current densities.

Current density [A/m^2]	Current efficiency Mg^{2+}	Current efficiency NH_4^+	Total current efficiency
32	10.4%	82.1%	92.5%
64	10.8%	84.8%	95.6%
96	11.7%	85.3%	97%

Table 4.2 shows that there was only a marginal difference in the current efficiency of Mg^{2+} at the different current densities when operating below LCD. Higher current densities slightly increased the current efficiency of Mg^{2+}. This could have been due to the slightly higher concentration polarization of NH_4^+ at higher current densities. *Xu et al.* documented that the current efficiency of divalent ion transport increases at increasing current density [74]. Therefore, this theory could be plausible. However, the differences in current efficiency of Mg^{2+} at different current densities were so small, that such a conclusion is premature. However, it could be concluded that the current density had a negligible impact on the current efficiency of Mg^{2+}.

The current efficiency of NH_4^+ and the total current efficiency also increased at increasing current densities below the LCD. Operating at a higher current density increased the total current efficiency, because it reduces the run times of the ED operation. Because the chemical potential of the concentrate was higher than of the diluate for the entirety of the experiment, ion back-diffusion occurred. The longer the experiment lasts, the more back-diffusion takes place [60, 61]. This caused ions to be re-transported, which lowered the total current efficiency. This is in agreement with previously conducted research [60, 62].

When operating at higher current densities, concentration polarization in the DBL is larger [75, 76]. Operating at a lower current density increased the NH_4^+ removal before the LCD was reached. Because the exponential increase in Mg^{2+} transport was linked to operating at overlimiting current density, it could be highly beneficial to lower the current density once the LCD is reached to achieve maximum NH_4^+ transport over Mg^{2+}.

4.5. Constant voltage

When operating at a constant current, the diluate conductivity decreased as ions were transported to the concentrate. This caused the resistance in the diluate to increase as previously mentioned. In order to keep operating at a constant current, the voltage subsequently increased as well. There was a strong correlation found between the increase in voltage and the increase in current efficiency of Mg^{2+} for the constant current experiments. To analyse the influence of the voltage on the selective transport between Mg^{2+} and NH_4^+, the current

efficiencies were compared when operating ED with a constant voltage.

The ED cell was set to operate at a constant voltage of $10V$. By operating at $10V$ it was ensured that the applied current density remained below the limiting current density for the entirety of the experiments. Also, at $10V$, the run times of the experiments were comparable with the other selectivity experiments.

4.5.1. Current efficiency for standard IEMs at constant voltage

Figure 4.10 shows the NH_4^+ and Mg^{2+} concentrations and current efficiencies during the constant voltage experiment with an initial molar Mg^{2+}/NH_4^+ ratio of 1:4 operated at $10V$ with standard IEMs. The same constant decrease in NH_4^+ and Mg^{2+} concentrations was observed as for the constant current experiments. It was calculated that when operating at $10V$, the current density remained $\sim$ 55% of the LCD for the entire duration of the experiment. Operating at constant voltage, limited concentration polarization in the DBL by remaining below LCD values. The ratio between Mg^{2+}/NH_4^+ increased only slightly, the more ions were removed. Because of these two factors, the current efficiencies of NH_4^+ and Mg^{2+} remained constant for the entire duration of the experiment. Overall, the trends found for the constant voltage experiments with standard IEMs were in good agreement between the constant current experiments. No major differences were observed.

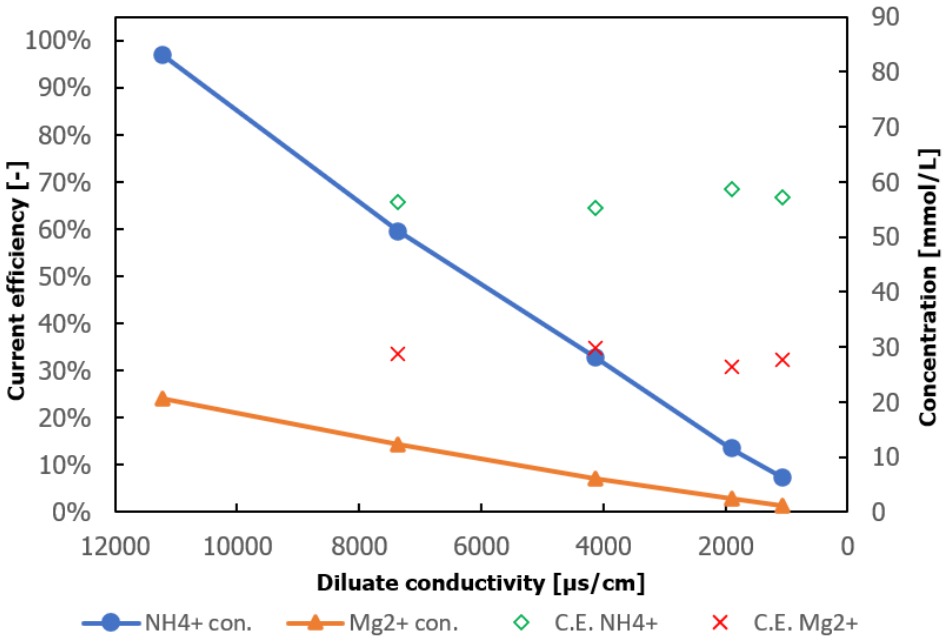

Figure 4.10: NH_4^+ and Mg^{2+} concentration (right y-axis) and current efficiency (left y-axis) as a function of the diluate conductivity. Initial molar Mg^{2+}/NH_4^+ ratio of 1:4 operated at 10 V with standard IEMs.

4.5.2. Current efficiency for monovalent selective IEMs at constant voltage

Figure 4.11 shows the NH_4^+ and Mg^{2+} concentrations and current efficiencies during the constant voltage experiment with an initial molar Mg^{2+}/NH_4^+ ratio of 1:4 operated at $10V$ with monovalent selective IEMs. The NH_4^+ concentration decreased constantly over time. The Mg^{2+} concentration decreased only slightly for the most part of the experiment and decreased more exponentially at decreasing diluate conductivity. The current efficiency of Mg^{2+} only slightly increased as the conductivity decreases. When ~ 80% of the NH_4^+ concentration was removed the current efficiency of Mg^{2+} started to increase exponentially. These exact same trends were also visible when operating at a constant current.

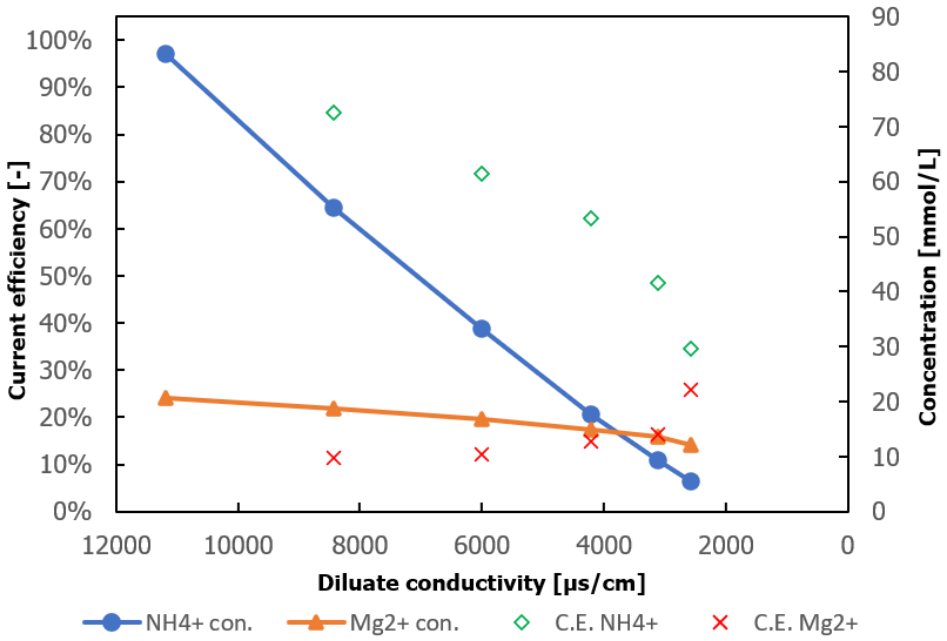

Figure 4.11: NH_4^+ and Mg^{2+} concentration (right y-axis) and current efficiency (left y-axis) as a function of the diluate conductivity. Initial molar Mg^{2+}/NH_4^+ ratio of 1:4 operated at 10 V with monovalent selective IEMs.

Two differences were found when comparing operating at a constant voltage and constant current. Operating at a constant voltage (below LCD values) ensured that more NH_4^+ was removed before the Mg^{2+} transport started to exponentially increase. This was because the system stayed below LCD values during operation at all time. This limited the amount of concentration polarization of NH_4^+ in the DBL. Therefore, operating at constant voltage below LCD leads to a slight increase in selective transport of NH_4^+ over Mg^{2+} compared to operating at a constant current. The removal efficiency of NH_4^+ was 95% at only 40% Mg^{2+} removal. This outperformed the constant current experiments.

The downside of operating at a constant voltage was that the current efficiency of NH_4^+ was lower than when operating at a constant current as can be seen by comparing figure 4.11 to the figures in appendix B. The current efficiency of NH_4^+ decreased linearly at decreasing conductivity. Operating at constant voltage meant that the current was constantly lowered at decreasing conductivity. Simultaneously, the chemical potential difference between the diluate and concentrate increased. This increased the amount of back-diffusion that took place. This lowered the current efficiency of NH_4^+. Even with an overall lower current efficiency, the energy consumption was still competitive with the constant current experiments at 10 $MJ/kg-N$ removed.

It was concluded from the constant voltage experiments with monovalent selective IEMs that it was beneficial to operate below LCD values at all time to increase the selective transport of NH_4^+ over Mg^{2+}. Operating at constant voltage was a viable solution to achieve that.

4.6. Uphill transport and back-diffusion

Electrodialysis is a highly dynamic system. During ED operation, the concentration ratios and absolute quantities between the ionic species and solutions continuously change. Transport mechanisms such as uphill transport and back-diffusion are quantitatively coupled to this dynamic system. Therefore, the fluxes related to uphill transport and back-diffusion contributing fluxes vary continuously throughout the experiment. This section shows how much Mg^{2+} can theoretically be transported by uphill transport. This section also quantifies the actual measured fluxes related to uphill transport and back-diffusion.

4.6.1. Theoretical uphill transport

Equation 2.4 was used to calculate the theoretical Mg^{2+} flux caused by uphill transport throughout one of the constant current experiments for both standard and monovalent selective membranes. These results are given by figure 4.12.

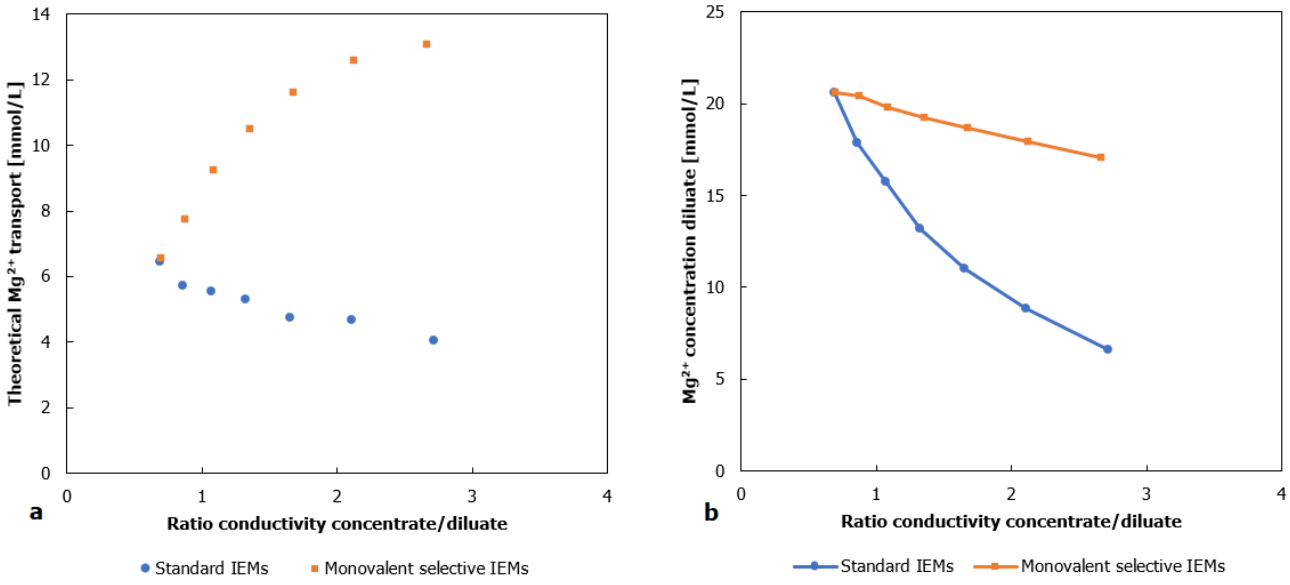

Figure 4.12: Theoretical Mg^{2+} flux from the diluate to the concentrate solution by uphill transport at different concentrate/diluate conductivity ratios (a). Mg^{2+} concentration in the diluate at different concentrate/diluate conductivity ratios. Data taken from constant current experiments operated at 64A/m2 with a Mg^{2+}/NH_4^+ ratio of 1:4 (b).

Figure 4.12a shows the theoretical uphill transport of Mg^{2+} that could take place at the different stages during ED operation. The theoretical flux was calculated with the analysed sampled data from one of the constant current experiments and by numerically solving equation 2.4. The fluxes given in figure 4.12 are not the actual Mg^{2+} fluxes that took place due to uphill transport, but the fluxes that would've taken place when no external potential difference was applied and the solutions were recirculated until chemical equilibrium.

During ED operation, ions are transported from the diluate to the concentrate solution. This decreases the conductivity of the diluate and increases the conductivity of the concentrate. This means that the concentrate/diluate conductivity increases ratio over time. Equation 2.4 shows that an increase in gradient between diluate and concentrate as well as an increase of Mg^{2+} in the diluate results in a higher Mg^{2+} flux. Figure 4.12a shows that at increasing concentrate/diluate ratio, the theoretical Mg^{2+} flux from diluate to concentrate decreased for standard IEMs. This was because the Mg^{2+} concentration in the diluate also decreased during ED operation. This is shown in figure 4.12b. At an increasing concentrate/diluate ratio, the theoretical Mg^{2+} flux from diluate to concentrate increased for monovalent selective IEMs. This is also shown in figure 4.12b.

The most important conclusion drawn from figure 4.12 are that at an initial Mg^{2+}/NH_4^+ ratio of 1:4, $\sim$ 6.5 mmol/L of Mg^{2+} could theoretically have been transported from the diluate to the concentrate solution via uphill transport. This represents $\sim$ 30% of the total initial Mg^{2+} present in the diluate. The potential for uphill transport was continuously present during ED operation as long as Mg^{2+} was present in the diluate. Also, the potential for uphill transport became increasingly larger during operation for ED with monovalent selective IEMs.

4.6.2. Uphill transport and back-diffusion for standard IEMs

Figure 4.13 represents the results for the experiments described by section 3.2.4 for standard IEMs. Figure 4.13 shows the concentrations of NH_4^+ and Mg^{2+} in the diluate (a) and the flux by uphill transport from the diluate (b) as a function of time. Exact experimental conditions are given in section 3.2.4. The diluate and concentrate conductivity remained constant at 11.3 and 8 ms/cm throughout the experiment.

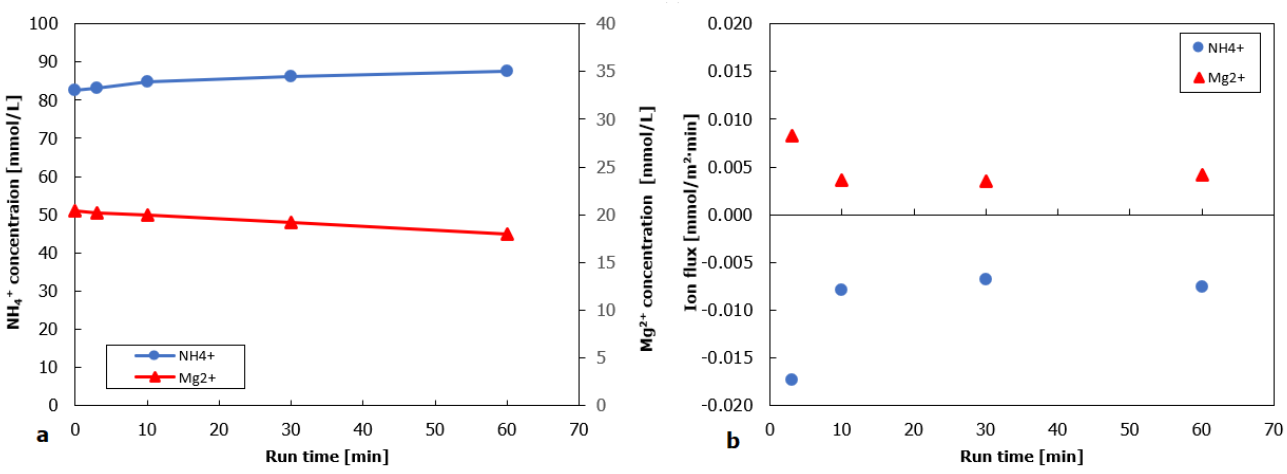

Figure 4.13: NH_4^+ and Mg^{2+} concentration in the diluate (a) and the flux by uphill transport from the diluate (b) as a function of time. Initial molar Mg^{2+}/NH_4^+ ratio of 1:4 with standard IEMs.

Figure 4.13a shows that the diluate NH_4^+ concentration slightly increased and the Mg^{2+} concentration slightly decreased over time. Figure 4.13b shows that after a single pass (3 minutes) Mg^{2+} flux of 0.0082 $mmol/m^2 \cdot min$ was found. From 3 to 60 minutes the Mg^{2+} flux averaged 0.0038 $mmol/m^2 \cdot min$. The NH_4^+ fluxes were twice as large. This is because 1 ion of Mg^{2+} being transported requires 2 NH_4^+ ions to be transported as well to maintain electro neutrality (see eq. 2.4). The NH_4^+ flux is negative, meaning that NH_4^+ was transported to the diluate. No back-diffusion took place at these concentrations.

Figure 4.14 represents the results for the experiments described by section 3.2.5 for standard IEMs. Figure 4.13 shows the concentrations of NH_4^+ and Mg^{2+} in the diluate (a) and the flux by uphill transport from the diluate and the flux by back-diffusion (b) as a function of time. Exact experimental conditions are given in section 3.2.5. The conductivity of the diluate increased from 4.2 to 4.5 ms/cm and the conductivity of the concentrate decrease from 15 to 14.4 ms/cm throughout the experiment.

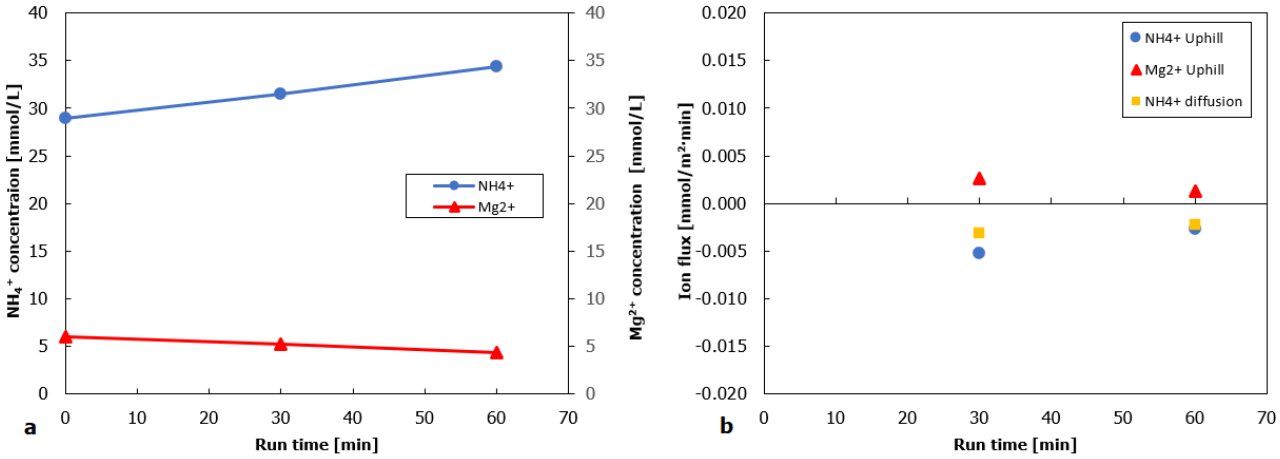

Figure 4.14: NH_4^+ and Mg^{2+} concentration in the diluate (a) and the flux by uphill transport from the diluate (b) as a function of time.

Figure 4.14a shows that the diluate NH_4^+ concentration increased and the Mg^{2+} concentration decreased over time. Mg^{2+} was transported from the diluate to the concentrate against the concentration gradient via uphill transport at an average flux of 0.0026 $mmol/m^2 \cdot min$ from 0 to 30 minutes and 0.0013 $mmol/m^2 \cdot min$ from 30 to 60 minutes. By knowing that the fluxes by uphill transport were twice that of Mg^{2+}, NH_4^+ was transported from the concentrate to the diluate via uphill transport at an average flux of 0.0052 $mmol/m^2 \cdot min$ from 0 to 30 minutes and $mmol/m^2 \cdot min$ from 30 to 60 minutes. These fluxes were lower than the ones found in figure 4.13. This was in agreement with the theoretically calculated fluxes from figure 4.12, where the Mg^{2+} flux via uphill transport decreases throughout ED operation with standard IEMs.

The total NH_4^+ flux from concentrate to diluate was higher than the flux required for just the uphill transport. Because of the high concentration gradient between concentrate and diluate (con/dil ratio ~ 3.5) NH_4^+ diffused back from the concentrate to the diluate. NH_4^+ back-diffusion took place at an average flux of 0.0031 $mmol/m^2 \cdot min$ from 0 to 30 minutes and 0.0022 $mmol/m^2 \cdot min$ from 30 to 60 minutes.

At lower current densities, the run time of the ED operation increased. Because a large concentration gradient is present between the solutions for the majority of the experiment, the net flux of back-diffusion of NH_4^+ was higher and had a larger impact on the current efficiency of NH_4^+ transport. This was already concluded in table 4.2 and again in this section.

For the conducted constant current experiments with standard IEMs it was found that longer operational run times resulted in more Mg^{2+} transport via uphill transport. At 32, 64 and 96 A/m^2 uphill transport was calculated to be responsible for ~ 15, 8 and 4 % of the total transported Mg^{2+}, respectively . These values are lower than the theoretical 30%, but not insignificant.

4.6.3. Uphill transport and back-diffusion for monovalent selective IEMs

Figure 4.15 represents the results for the experiments described in section 3.2.4 for monovalent selective IEMs. Figure 4.15 shows the concentrations of NH_4^+ and Mg^{2+} in the diluate. Exact experimental conditions are given in section 3.2.4. The diluate and concentrate conductivity remained constant at 11.3 and 8 ms/cm throughout the experiment.

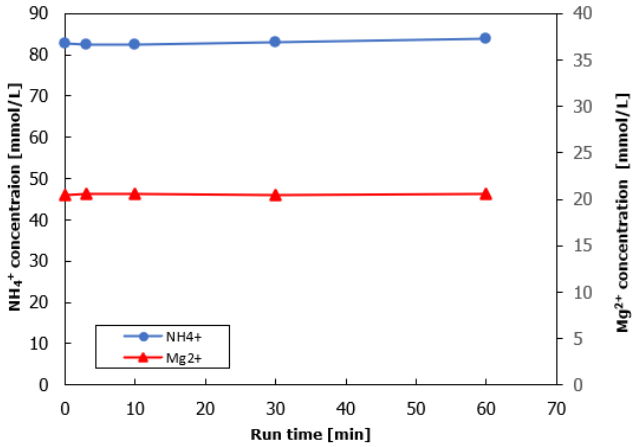

Figure 4.15: NH_4^+ and Mg^{2+} concentration in the diluate (a) and the flux by uphill transport from the diluate (b) as a function of time. Initial molar Mg^{2+}/NH_4^+ ratio of 1:4 with monovalent selective IEMs.

What can be seen from figure 4.15 is that the concentration of NH_4^+ and Mg^{2+} remained constant for the duration of the run. There was zero ion flux of NH_4^+ and Mg^{2+} taking place between the diluate and concentrate solution. According to figure 4.12, the Mg^{2+} flux related to uphill transport should be equally as large as for standard IEMs. This was clearly not the case. It could have been that the electrostatic repulsion of the oppositely charged surface layer on the monovalent IEMs, hampered Mg^{2+} uphill transport at given concentrations. What also could be is that the monovalent IEMs have a higher fixed charge density. A higher fixed charge density of the IEMs decrease uphill transport [79]. Unfortunately, the fixed charge densities of both IEMs are unknown.

It was concluded that at these diluate and concentrate concentrations, no uphill transport took place for monovalent selective IEMs. This indicated that unwanted Mg^{2+} transport caused by uphill transport is potentially less prevalent when operating with monovalent IEMs over standard IEMs. This is in agreement with literature [78, 79].

Figure 4.16 represents the results for the experiments described by section 3.2.5 for standard IEMs. Figure 4.16 shows the concentrations of NH_4^+ and Mg^{2+} in the diluate (a) and the flux related to uphill transport from the diluate and the flux by back-diffusion (b) as a function of time. Exact experimental conditions are given by section 3.2.5. The diluate and concentrate conductivity remained constant at 6.3 and 13.1 ms/cm throughout the experiment.

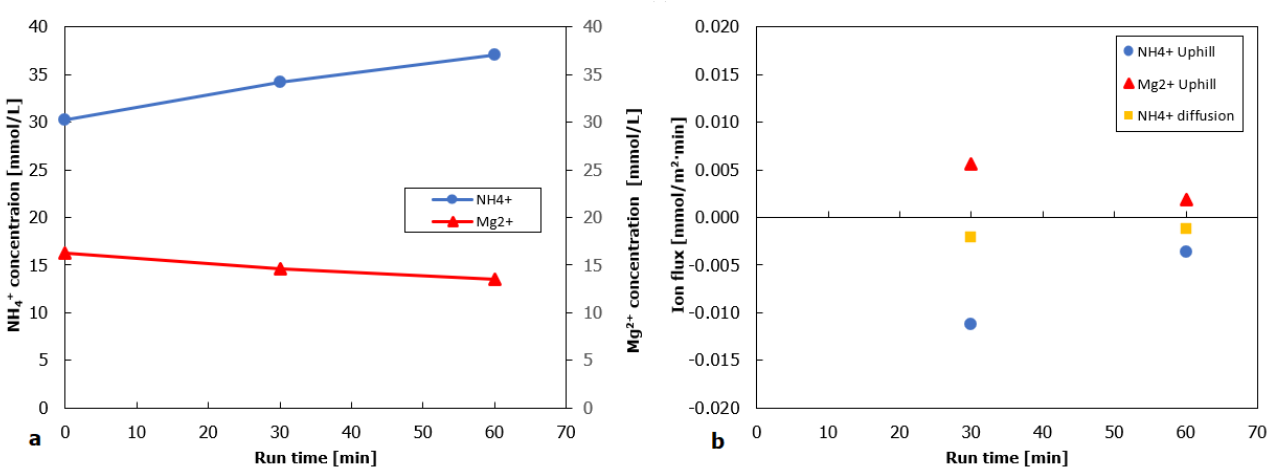

Figure 4.16: NH_4^+ and Mg^{2+} concentration in the diluate (a) and the flux by uphill transport from the diluate (b) as a function of time.

Contrary to the findings in figure 4.15, figure 4.16a does show that the diluate NH_4^+ concentration increased and the Mg^{2+} concentration decreased over time. Mg^{2+} was transported from the diluate to the concentrate against the concentration gradient via uphill transport at an average flux of 0.0056 $mmol/m^2 \cdot min$ from 0 to 30 minutes and 0.0018 $mmol/m^2 \cdot min$ from 30 to 60 minutes. The NH_4^+ flux related to uphill transport was found to be 0.011 $mmol/m^2 \cdot min$ from 0 to 30 minutes and 0.0036 $mmol/m^2 \cdot min$ from 30 to 60 minutes.

These experiments confirmed that the Mg^{2+} transport caused by uphill transport increased as more NH_4^+ was removed from the diluate during ED operation. As mentioned in section 4.4, the Mg^{2+} transport from the diluate starts to exponentially increase as the gradients between concentrate and diluate increase. By comparing the averaged found Mg^{2+} uphill transport flux and the actual measured flux for the constant current experiments it was found that when operating ED with monovalent selective IEMs at 32, 64 and 96 A/m^2, uphill transport was calculated to be responsible for $\sim$ 24, 14 and 8 % of the total transported Mg^{2+}, respectively.

5

Conclusions

The main objective of this research was to analyse how selective transport of NH_4^+ and Mg^{2+} takes place when recovering NH_4^+ from synthetic waste waters. ED was operated at different current densities and with different synthetic make-up waters. Both standard IEMs and monovalent selective IEMs were used. By analysing sampled data from lab experiments, literature research and MATLAB programming, the sub-research questions from section 1.6.2 were answered.

1. *How do standard IEMs and monovalent selective IEMs compare in terms of removal efficiency and energy consumption.*

   When ED was operated at constant current, both standard and monovalent IEMs reached a NH_4^+ removal efficiency of 68-92%. When ED was operated at a lower current density, a lower final diluate conductivity was reached. This explained why there is a difference in the NH_4^+ removal efficiencies. At equal operational conditions, the monovalent selective IEMs showed a slightly higher NH_4^+ removal efficiency compared to standard IEMs. Monovalent selective IEMs showed a 30-60 % lower Mg^{2+} removal efficiency compared to standard IEMs. The use of monovalent selective IEMs decreased the Mg^{2+} transport by a factor of $\sim$ 1.5-2.5 compared to standard IEMs depending on the operational conditions.

   The monovalent selective IEMs had a higher area resistance compared to standard IEMS. Therefore, the voltage during ED operation was higher for monovalent selective IEMs. This resulted in a higher energy consumption for monovalent selective IEMs compared to standard IEMs.

2. *What is the influence of the molar Mg^{2+}/NH_4^+ ratio and total NH_4^+ and Mg^{2+} concentration in the diluate solution on the selective transport of NH_4^+ and Mg^{2+}.*

   Standard IEMs:

   - It was found that the current efficiencies of Mg^{2+} and NH_4^+ were disproportional to the ion ratio. Ions with higher valence were preferably transported into the IEMs. Therefore, Mg^{2+} was preferentially transported over NH_4^+. At constant current both NH_4^+ and Mg^{2+} were transported from the diluate at constant rates.

- The Mg^{2+}/NH_4^+ ratio had a direct influence on the current efficiency of NH_4^+ and Mg^{2+}. A higher Mg^{2+}/NH_4^+ ratio increased the current efficiency of Mg^{2+} and decreased the current efficiency of NH_4^+. It was concluded that an increase in Mg^{2+}/NH_4^+ ratio decreased the selective transport of NH_4^+ over Mg^{2+}. On average, a doubling the Mg^{2+}/NH_4^+ ratio, increased the current efficiency of Mg^{2+} by $\sim$ 10%. Tripling the Mg^{2+}/NH_4^+ ratio increased the current efficiency of Mg^{2+} by $\sim$ 15-16% (and vice versa for NH_4^+)
- If the Mg^{2+}/NH_4^+ ratio remained the same, variations in the total concentrations of NH_4^+ and Mg^{2+} in the diluate had no effect on the current efficiency of both species. It was concluded that the total concentrations of NH_4^+ and Mg^{2+} had no effect on the selective transport of NH_4^+ over Mg^{2+}.

Monovalent selective IEMs:

- NH_4^+ was transported from the diluate at a constant transport rate. Mg^{2+} transport was initially low. At decreasing diluate conductivity the Mg^{2+} transport exponentially increased . A clear transport order was present where firstly, a large part of the NH_4^+ was transported before the Mg^{2+} transport significantly increased.
- The Mg^{2+}/NH_4^+ ratio had a direct influence on the current efficiency of NH_4^+ and Mg^{2+}. A higher Mg^{2+}/NH_4^+ ratio increased the current efficiency of Mg^{2+} and decreased the current efficiency of NH_4^+. It was concluded that an increase in Mg^{2+}/NH_4^+ ratio decreased the selective transport of NH_4^+ over Mg^{2+}.
- The NH_4^+ concentration in the diluate had an influence on the current efficiency of both NH_4^+ and Mg^{2+}. When more NH_4^+ was transported from the diluate, concentration polarization of NH_4^+ became more predominant in the DBL. This decreased the current efficiency of NH_4^+ and increased the current efficiency of Mg^{2+} roughly linear at decreasing diluate NH_4^+ concentration . When the LCD was reached, the current efficiency of NH_4^+ decreased exponentially and the current efficiency of Mg^{2+} increased exponentially. It was concluded that a decrease in NH_4^+ concentration in the diluate decreased the selective transport of NH_4^+ over Mg^{2+}.

3. *What is the influence of the applied current density on the selective transport of NH_4^+ and Mg^{2+}*

Standard IEMs:

- It was found that operating at a higher current density, resulted in steeper concentration gradients in the DBL. Mg^{2+} has a lower diffusion rate than NH_4^+. Therefore, at increasing current densities, concentration polarization in the DBL became more predominant for Mg^{2+} compared to NH_4^+. On average, operating at 64 A/m^2 increased the current efficiency of NH_4^+ and decreased the current efficiency of Mg^{2+} by $\sim$ 4-5% compared to operating at 32 A/m^2. When operating at 96 A/m^2 the current efficiency of NH_4^+ increased and the current efficiency of Mg^{2+} decreases by $\sim$ 10% compared to operating at 32 A/m^2. It was concluded that increasing the current density, increased selective transport of NH_4^+ over Mg^{2+}.

Monovalent selective IEMs:

- It was found that at increasing current density, the current efficiency of Mg^{2+} only marginally increased. However, the differences in the current efficiency of Mg^{2+}

were so little, that it was concluded that the current density had a negligible impact on the current efficiency of Mg^{2+}.

- At increasing current density, the current efficiency of NH_4^+ increased. Increasing the current density resulted in lower experimental run times. Therefore, less back-diffusion of NH_4^+ took place.

4. *What is the influence of the applied voltage on selective transport of NH_4^+ and Mg^{2+}*

   Standard IEMs:

   - For standard IEMs the trends found in transport rates and current efficiencies were in good agreement with the constant current experiments. No differences were observed while operating at a constant voltage compared to a constant current.

   Monovalent selective IEMs:

   - For monovalent selective IEMs the trends found in transport rates and current efficiencies were in good agreement with the constant current experiments. The differences were that more back-diffusion took place compared to constant current experiments. This decreased the current efficiency of NH_4^+ when the current was lowered at decreasing diluate conductivity. Operating at a constant voltage also allowed the system to operate below LCD at all times. This resulted in a slightly higher selective transport of NH_4^+ over Mg^{2+} at NH_4^+ removal rates of over 70%.

5. *How much Mg^{2+} is transported by uphill transport*

   Theoretically, $\sim$ 30% of the Mg^{2+} concentration in the diluate could be transported to the concentrate solution via uphill transport at infinite run time without an externally applied potential difference. For standard membranes operated at 32, 64 and 96 A/m^2, uphill transport was calculated to be responsible for 11, 8 and 4 % of the total transported Mg^{2+}, respectively. For monovalent selective IEMs operated at 32, 64 and 96 A/m^2 uphill transport was calculated to be responsible for 24, 14 and 8 % of the total transported Mg^{2+} respectively. These values are lower than the theoretical flux, but not insignificant. At equal operational conditions, less uphill transport took place for monovalent selective IEMs. It was therefore concluded that monovalent selective IEMs reduced uphill transport compared to standard IEMs.

6

Recommendations

The following chapter gives recommendations for follow up studies regarding further research, extension of the framework and process optimisation.

Real waste water

For this research, synthetic waters consisting of only one mono and one divalent cation species were used. The next step would be to introduce more mono- and multivalent cat/anion species to analyse selective transport with monovalent selective IEMs. The goal is to eventually apply ED with monovalent selective IEMs on real wastewaters as described in the introduction. This introduces an even more complex water matrix which potentially contain non ion species such as suspended solids and fatty acids.

Further research

This research concluded that Mg^{2+} transport increased as the NH_4^+ concentration in the diluate decreased and concentration polarization increased. It would be interesting to see how the found trends compare to synthetic water types with the same Mg^{2+}/NH_4^+ ratio, but at higher total concentrations of both species. Such concentrations would still be realistic, as for example digested cow manure can have a NH_4^+ concentration of $\sim$ 2.5-3 g/L and a combined Mg^{2+}, Ca^{2+} concentration of $\sim$ 0.2-0.3 g/L [48, 108].

It would be interesting to see how much the gradients between concentrate and diluate influence the selective transport. Doing the same experiments as done for this research, but in sequencing batch mode, significantly increases the NH_4^+ concentration in the concentrate solution as more batches are run. It has already been concluded that sequencing batch operating increases back-diffusion by *Bandinu* [60], but only monovalent ions were used in that research. According to theory and the found Mg^{2+} transport caused by uphill transport in this research, it is expected that Mg^{2+} transport by uphill transport increases at increasing concentrate/diluate concentration ratio. This can potentially limit the effectiveness of ED operation with monovalent IEMs as Mg^{2+} will potentially be increasingly transported via uphill transport.

Concentration polarization in the DBL is decreased at increasing cross-flow velocities. This is because the thickness of the diffusive boundary layer decreases at increasing cross-flow velocities [109]. It would be interesting to know what the influence of the cross-flow velocity is on the selective transport between mono- and divalent ions.

Process optimisation

When operating with monovalent selective IEMs, it became increasingly difficult to transport NH_4^+ from the diluate without transporting Mg^{2+} at NH_4^+ removal efficiencies exceeding $\sim$ 70%. It is therefore advised to lower the aimed removal efficiency from 90% to 70% as this drastically limits the net Mg^{2+} removal from the diluate. If the aim is to remove as little Mg^{2+} as possible it is more beneficial to quantitatively treat larger volumes of wastewater than to qualitatively treat smaller volumes.

ED staging with monovalent selective IEMs could be an effective double boundary for Mg^{2+} transport. The concentrate solution of the first ED system is used as the diluate solution for a follow up (bipolar) ED system. However, it is expected that this could also result in double opex and capex.

Continuous development on monovalent selective membranes and spacer composition will enable membranes to be developed that achieve higher mono/divalent cation selectivity. *Irfan et al.* [110] have reported a Na^+/Mg^{2+} permselectivity of 25.26. Although, not discussed in this research, the average NH_4^+/Mg^{2+} permselectivity found for the monovalent selective IEMs in this research averaged 1.42. These value for permselectivity was influenced by operational parameters so this comparison is not very valid. However, it shows that monovalent selective IEMs with an even higher monovalent over divalent selectivity will inevitably make an entree into the commercial IEM market.

Monovalent selective IEMs show less uphill transport compared to standard IEMs. Because there are multiple ways of designing/modifying membranes to get a monovalent selective IEM, membrane properties will vary. Just as with membrane permselectivity between ions, the transport related to uphill transport will also vary per membrane manufacturer/modification. Uphill transport can be measured for the different membranes and a substantiated decision can be made on which membrane serves the purpose of limiting uphill transport and is more suited.

Bibliography

[1] S. Salm, D. Allen, and E. Nester. *Nester's Microbiology: A Human Perspective*. McGraw-Hill Higher Education, 2015. ISBN: 9780077730932. URL: https://books.google.nl/books?id=VqhZCgAAQBAJ.

[2] M. Kuypers, H. K. Marchant, and B. Kartal. "The microbial nitrogen-cycling network". In: *Nature Reviews Microbiology* 16 (2018), pp. 263–276.

[3] N Lehnert, H. Dong, and J. Harland. "Reversing nitrogen fixation". In: *Nature Reviews Chemistry* 2.10 (2018), pp. 278–289. ISSN: 23973358. DOI: 10.1038/s41570-018-0041-7. URL: http://dx.doi.org/10.1038/s41570-018-0041-7.

[4] James N. Galloway et al. "The Nitrogen Cascade". In: *BioScience* 53.4 (Apr. 2003), pp. 341–356. ISSN: 0006-3568. DOI: 10.1641/0006-3568(2003)053[0341:TNC]2.0.CO;2. URL: https://doi.org/10.1641/0006-3568(2003)053[0341:TNC]2.0.CO;2.

[5] Phys.org. *NOx gases in diesel car fumes Why are they so dangerous?* [Online; accessed 17 January 2021]. URL: https://phys.org/news/2015-09-nox-gases-diesel-car-fumes.html.

[6] United States Environmental Protection Agency. *Greenhouse Gas Reporting Program*. Tech. rep. United States Environmental Protection Agency, 2019. URL: https://www.epa.gov/ghgreporting.

[7] Milkha S. Aulakh. "Nitrogen Losses and Fertilizer N use efficiency in irrigated porous soils". In: *Nutrient cycling in agroecosystems* 47 (1996), pp. 197–212. DOI: 10.1007/BF01986275.

[8] Charles T. Driscoll and Gregory B. Lawrence. "Acidic deposition in the northeastern United States: Sources and inputs, ecosystem effects, and management strategies". In: *BioScience* 51.3 (2001), pp. 180–198. ISSN: 00063568. DOI: 10.1641/0006-3568(2001)051[0180:ADITNU]2.0.CO;2.

[9] Nancy N. Rabalais. "Nitrogen in Aquatic Ecosystems". In: *AMBIO: A Journal of the Human Environment* 31.2 (2002), pp. 102–112. DOI: 10.1579/0044-7447-31.2.102. URL: https://doi.org/10.1579/0044-7447-31.2.102.

[10] Churchill B. Grimes. "Fishery Production and the Mississippi River Discharge". In: *Fisheries* 26.8 (2001), pp. 17–26. DOI: https://doi.org/10.1577/1548-8446(2001)026<0017:FPATMR>2.0.CO;2. URL: https://afspubs.onlinelibrary.wiley.com/doi/abs/10.1577/1548-8446%282001%29026%3C0017%3AFPATMR%3E2.0.CO%3B2.

[11] J F M Huijsmans. *Manure application and ammonia volatilization*. ISBN: 9058089371.

[12] Scott D. Wilson and David Tilman. "QUADRATIC VARIATION IN OLD-FIELD SPECIES RICHNESS ALONG GRADIENTS OF DISTURBANCE AND NITROGEN". In: *Ecology* 83.2 (2002), pp. 492–504. DOI: https://doi.org/10.1890/0012-9658(2002)083[0492:QVIOFS]2.0.CO;2. URL: https://esajournals.onlinelibrary.wiley.com/doi/abs/10.1890/0012-9658%282002%29083%5B0492%3AQVIOFS%5D2.0.CO%3B2.

[13] United States Geological Survey. *Mineral Commodity Summaries 2020*. Tech. rep. 703. United States Department of the Interior, 2020. URL: https://pubs.usgs.gov/periodicals/mcs2020/mcs2020.pdf.

[14] Noah Tech Blog. *5 Most Common Industrial Chemicals*. [Online; accessed 24 March 2020]. URL: https://info.noahtech.com/blog/5-most-common-industrial-chemicals.

[15] Common Science. *The Highest Volume Chemical Produced in the World is*. [Online; accessed 24 March 2020]. URL: https://chapelboro.com/town-square/columns/common-science/the-highest-volume-chemical-produced-in-the-world-is.

[16] J. C. Copplestone. *Ammonia and urea production*. 1998, pp. 1–10. URL: www.nzic.org.nz/ChemProcesses/production/index.html.

[17] J. Clark. *The Haber Process*. [Online; accessed 24 March 2020]. 2002. URL: https://www.chemguide.co.uk/physical/equilibria/haber.html.

[18] M. V. Twigg. *Catalyst handbook*. Manson Publishing, 1996. ISBN: 978-1-874545-36-1.

[19] C. W. Hooper. "Ammonia Synthesis: Commercial Practice". In: 1991, pp. 253–283. DOI: 10.1007/978-1-4757-9592-9_7.

[20] European Commission. "Best Available Techniques for the Manufacture of Large Volume Inorganic Chemicals - Ammonia, Acids and Fertilisers -Integrated Pollution Prevention and Control Large Volume Inorganic Chemicals - Ammonia , Acids and Fertilisers". In: *Technical Report* (2007).

[21] Leigh Krietsch Boerner. "Industrial ammonia production emits more CO2 than any other chemical-making reaction. Chemists want to change that". In: *Chemical Engineering news* 97 (2019).

[22] Fertilizer Statistics. *Raw Material Reserves*. [Online; accessed 25 March 2020]. 2002. URL: https://web.archive.org/web/20080424083111/http://www.fertilizer.org/ifa/statistics/indicators/ind_reserves.asp.

[23] B.E. Smith. "Nitrogenase Reveals Its Inner Secrets". In: *Science* 297 (2002), pp. 1654–1655.

[24] Christos M. Kalamaras and Angelos M. Efstathiou. "Hydrogen Production Technologies: Current State and Future Developments". In: *Conference Papers in Energy* 2013 (2013), pp. 1–9. DOI: 10.1155/2013/690627.

[25] T. Brown. *Comparative studies of ammonia production, combining renewable hydrogen with Haber-Bosch*. [Online; accessed 26 March 2020]. 2017. URL: https://ammoniaindustry.com/comparative-studies-of-ammonia-production-combining-renewable-hydrogen-with-haber-bosch/.

[26] T. Brown. *Renewable ammonia: competitive with SMR technology today (in the right place)*. [Online; accessed 26 March 2020]. 2017. URL: https://ammoniaindustry.com/renewable-ammonia-competitive-with-smr-technology-today-in-the-right-place/.

[27] T. Brown. *Ammonia plant cost comparisons: Natural gas, Coal, or Electrolysis?* [Online; accessed 26 March 2020]. 2017. URL: https://ammoniaindustry.com/ammonia-plant-cost-comparisons-natural-gas-coal-or-electrolysis/.

[28] IHS Markit. "Chemical Economics Handbook". In: 2017.

[29] Easychem. *Industrial Uses of Ammonia*. [Online; accessed 26 March 2020]. 2019. URL: https://easychem.com.au/monitoring-and-management/maximising-production/industrial-uses-of-ammonia/.

[30] The Fertilizer Institute. *Fertilizer Product Fact Sheet Ammonia*. [Online; accessed 28 March 2020]. 2019. URL: https://www.tfi.org/sites/default/files/documents/ammoniafactsheet.pdf.

[31] J.W. Erisman et al. "How a century of ammonia synthesis changed the world". In: *Nature Geoscience* 1.10 (2008), pp. 636–639. DOI: 10.1038/ngeo325.

[32] H. Ritchie. *How many people does synthetic fertilizer feed?* [Online; accessed 29 March 2020]. 2017. URL: https://ourworldindata.org/how-many-people-does-synthetic-fertilizer-feed.

[33] Peter M Vitousek et al. "Vitousek et al. 1997". In: *Ecological Applications* 7.3 (1997), pp. 737–750. ISSN: 1051-0761. DOI: 10.1890/1051-0761(1997)007[0737:HAOTGN]2.0.CO;2.

[34] C. Agapakis. *Nitrogen Fixation*. [Online; accessed 29 March 2020]. 2012. URL: https://blogs.scientificamerican.com/oscillator/nitrogen-fixation/.

[35] Grand View Research. "Ammonia Market Analysis By Product Form (Liquid, Gas, Powder), By Application (Fertilizers, Textile, Pharmaceuticals, Refrigerants), By Region, And Segment Forecasts, 2018 - 2025". In: 2017.

[36] Maximize Market Research. "Global Ammonia Market – Industry Analysis and Forecast 2018-2026, by Product Type, by Application, by Regions". In: 2017.

[37] TNO. *Ten Things You Need To Know About Hydrogen*. [Online; accessed 17 January 2021]. URL: https://www.tno.nl/en/focus-areas/energy-transition/roadmaps/towards-co2-neutral-industry/hydrogen-for-a-sustainable-energy-supply/ten-things-you-need-to-know-about-hydrogen/.

[38] A. Valera-Medina et al. "Ammonia for power". In: *Progress in Energy and Combustion Science* 69 (2018), pp. 63–102. ISSN: 03601285. DOI: 10.1016/j.pecs.2018.07.001. URL: https://doi.org/10.1016/j.pecs.2018.07.001.

[39] Zainab D. Abd Ali, Shrok Allami, and Basheer H. Jwad. "Ammonia as Hydrogen Storage Media, Sustainable Method to Hydrogen Evolution". In: *Journal of Physics: Conference Series* 1032.1 (2018). ISSN: 17426596. DOI: 10.1088/1742-6596/1032/1/012062.

[40] Muhammad Aziz, Takuya Oda, and Takao Kashiwagi. "Comparison of liquid hydrogen, methylcyclohexane and ammonia on energy efficiency and economy". In: *Energy Procedia* 158 (2019), pp. 4086–4091. ISSN: 18766102. DOI: 10.1016/j.egypro.2019.01.827. URL: https://doi.org/10.1016/j.egypro.2019.01.827.

[41] Agung Tri Wijayanta, Takuya Oda, and Chandra Wahyu Purnomo. "Liquid hydrogen, methylcyclohexane, and ammonia as potential hydrogen storage: Comparison review". In: *International Journal of Hydrogen Energy* 44.29 (2019), pp. 15026–15044. ISSN: 03603199. DOI: 10.1016/j.ijhydene.2019.04.112. URL: https://doi.org/10.1016/j.ijhydene.2019.04.112.

[42] Ahmed Afif, Nikdalila Radenahmad, and Quentin Cheok. "Ammonia-fed fuel cells: A comprehensive review". In: *Renewable and Sustainable Energy Reviews* 60.February 2020 (2016), pp. 822–835. ISSN: 18790690. DOI: 10.1016/j.rser.2016.01.120.

[43] Ammonia Energy Association. *Zero emission aircraft: ammonia for aviation*. [Online; accessed 17 January 2021]. URL: https://www.ammoniaenergy.org/articles/zero-emission-aircraft-ammonia-for-aviation/.

[44] Cleantech Group. *Green Ammonia – Potential as an Energy Carrier and Beyond*. [Online; accessed 17 January 2021]. URL: https://www.cleantech.com/green-ammonia-potential-as-an-energy-carrier-and-beyond/#:~:text=As.

[45] Jules van Lier. *Course CIE4703 Water Treatment - Anaerobic Digestion*. [Online; accessed 17 January 2021].

[46] Environmental and Energy Study Intitute. *Fact Sheet - Biogas: Converting Waste to Energy*. [Online; accessed 17 January 2021]. URL: https://www.eesi.org/papers/view/fact-sheet-biogasconverting-waste-to-energy.

[47] Alejandro Gonzalez-Martinez et al. “New concepts in anammox processes for wastewater nitrogen removal: recent advances and future prospects”. In: *FEMS Microbiology Letters* 365.6 (Feb. 2018). fny031. ISSN: 0378-1097. DOI: 10.1093/femsle/fny031. URL: https://doi.org/10.1093/femsle/fny031.

[48] Tobias Opschoor. *Proof of Concept: Ammonia Recovery from Raw/digested cow and Pig Manure*. July 2020.

[49] M Boehler, A Heisele, and A Seyfried. “(NH4)2SO4 recovery from liquid side streams”. In: *Environmental science and pollution research international* 22 (Aug. 2014). DOI: 10.1007/s11356-014-3392-8.

[50] Albert Magrí, Fabrice Béline, and Patrick Dabert. “Feasibility and interest of the anammox process as treatment alternative for anaerobic digester supernatants in manure processing - An overview”. In: *Journal of Environmental Management* 131 (2013), pp. 170–184. ISSN: 03014797. DOI: 10.1016/j.jenvman.2013.09.021. URL: http://dx.doi.org/10.1016/j.jenvman.2013.09.021.

[51] Environmental Dynamics Internationa. *Aeration Efficiency Guide*. 2011.

[52] H. Strathmann. *Ion-Exchange Membrane Separation Processes*. Vol. 9. Elsevier Ltd, 2004.

[53] Toshikatsu Sata. *Ion Exchange Membranes. Preparation, Characterization, Modification and Application*. The Royal Society of Chemistry, 2004, pp. X001–X004. ISBN: 978-0-85404-590-7. DOI: 10.1039/9781847551177. URL: http://dx.doi.org/10.1039/9781847551177.

[54] H. Strathmann. “Electrodialysis, a mature technology with a multitude of new applications”. In: *Desalination* 264.3 (2010), pp. 268–288. ISSN: 00119164. DOI: 10.1016/j.desal.2010.04.069. URL: http://dx.doi.org/10.1016/j.desal.2010.04.069.

[55] Andrew J. Ward, Kimmo Arola, and Emma Thompson Brewster. “Nutrient recovery from wastewater through pilot scale electrodialysis”. In: *Water Research* 135 (2018), pp. 57–65. ISSN: 18792448. DOI: 10.1016/j.watres.2018.02.021. URL: https://doi.org/10.1016/j.watres.2018.02.021.

[56] Tongwen Xu and Chuanhui Huang. “Electrodialysis-based separation technologies: A critical review”. In: *AIChE Journal* 54.12 (2008), pp. 3147–3159. DOI: https://doi.org/10.1002/aic.11643. eprint: https://aiche.onlinelibrary.wiley.com/doi/pdf/10.1002/aic.11643. URL: https://aiche.onlinelibrary.wiley.com/doi/abs/10.1002/aic.11643.

[57] Xiaolin Wang, Xu Zhang, and Yaoming Wang. “Simultaneous recovery of ammonium and phosphorus via the integration of electrodialysis with struvite reactor”. In: *Journal of Membrane Science* 490 (2015), pp. 65–71. ISSN: 18733123. DOI: 10.1016/j.memsci.2015.04.034. URL: http://dx.doi.org/10.1016/j.memsci.2015.04.034.

[58] M. Mondor, L. Masse, and D. Ippersiel. “Use of electrodialysis and reverse osmosis for the recovery and concentration of ammonia from swine manure”. In: *Bioresource Technology* 99.15 (2008), pp. 7363–7368. ISSN: 09608524. DOI: 10.1016/j.biortech.2006.12.039.

[59] D. Ippersiel, M. Mondor, and F. Lamarche. “Nitrogen potential recovery and concentration of ammonia from swine manure using electrodialysis coupled with air stripping”. In: *Journal of Environmental Management* 95.SUPPL. (2012), S165–S169. ISSN: 03014797. DOI: 10.1016/j.jenvman.2011.05.026. URL: http://dx.doi.org/10.1016/j.jenvman.2011.05.026.

[60] Giacomo L Bandinu. “Electrodialysis with bipolar membranes for ammonia recovery in wastewater”. In: *MSc Thesis* (2019).

[61] J Deckers. “Optimizing electrodialysis processes for concentrating ammonium rich streams”. In: *MSc Thesis* (2017).

[62] N. van Linden, H. Spanjers, and Jules B. van Lier. “Application of dynamic current density for increased concentration factors and reduced energy consumption for concentrating ammonium by electrodialysis”. In: *Water Research* 163 (2019), p. 114856. ISSN: 18792448. DOI: 10.1016/j.watres.2019.114856. URL: https://doi.org/10.1016/j.watres.2019.114856.

[63] Niels van Linden, Giacomo L. Bandinu, and David A. Vermaas. “Bipolar membrane electrodialysis for energetically competitive ammonium removal and dissolved ammonia production”. In: *Journal of Cleaner Production* 259 (2020), p. 120788. ISSN: 09596526. DOI: 10.1016/j.jclepro.2020.120788. URL: https://doi.org/10.1016/j.jclepro.2020.120788.

[64] Evelien L J Martens. “Vacuum membrane distillation for the production of ammonia fuel gas for solid oxide fuel cells”. In: *MSc Thesis* (2018).

[65] Christiaan Hordijk. “Concentrating Ammonium”. In: *MSc Thesis* September (2017).

[66] *ED, BPMED, VMS and SOFC sequencing experiments*. [Physically conducted by writer of this thesis under supervision of Niels van Linden and Giacomo Bandinu]. 2020.

[67] Emma Brewster. “Nutrient recovery from wastewater using Electrodialysis”. In: 71 (2015), pp. 1–31.

[68] Yang Zhang, Karel Ghyselbrecht, and Boudewijn Meesschaert. “Electrodialysis on RO concentrate to improve water recovery in wastewater reclamation”. In: *Journal of Membrane Science* 378.1-2 (2011), pp. 101–110. ISSN: 0376-7388. DOI: 10.1016/j.memsci.2010.10.036. URL: http://dx.doi.org/10.1016/j.memsci.2010.10.036.

[69] Emma Thompson Brewster, Andrew J. Ward, and Chirag M. Mehta. “Predicting scale formation during electrodialytic nutrient recovery”. In: *Water Research* 110 (2017), pp. 202–210. ISSN: 18792448. DOI: 10.1016/j.watres.2016.11.063. URL: http://dx.doi.org/10.1016/j.watres.2016.11.063.

[70] Niels van Linden. *Various experimental results*. [Verbal audit on results by writer of this thesis]. 2020.

[71] Christophe Casademont, Gérald Pourcelly, and Laurent Bazinet. “Effect of magnesium / calcium ratio in solutions subjected to electrodialysis : Characterization of cation-exchange membrane fouling”. In: 315 (2007), pp. 544–554. DOI: 10.1016/j.jcis.2007.06.056.

[72] Tao Luo, Said Abdu, and Matthias Wessling. “Selectivity of ion exchange membranes: A review”. In: *Journal of Membrane Science* 555.March (2018), pp. 429–454. ISSN: 18733123. DOI: 10.1016/j.memsci.2018.03.051.

[73] L. Firdaous, J. P. Malériat, and J. P. Schlumpf. “Transfer of monovalent and divalent cations in salt solutions by electrodialysis”. In: *Separation Science and Technology* 42.5 (2007), pp. 931–948. ISSN: 01496395. DOI: 10.1080/01496390701206413.

[74] Xuesong Xu, Qun He, and Guanyu Ma. “Selective separation of mono- and di-valent cations in electrodialysis during brackish water desalination: Bench and pilot-scale studies”. In: *Desalination* 428.November 2017 (2018), pp. 146–160. ISSN: 00119164. DOI: 10.1016/j.desal.2017.11.015. URL: https://doi.org/10.1016/j.desal.2017.11.015.

[75] A. H. Galama, G. Daubaras, and O. S. Burheim. “Seawater electrodialysis with preferential removal of divalent ions”. In: *Journal of Membrane Science* 452 (2014), pp. 219–228. ISSN: 03767388. DOI: 10.1016/j.memsci.2013.10.050.

[76] Ting Dong, Jingmei Yao, and Yi Wang. “On the permselectivity of di- and mono-valent cations: Influence of applied current density and ionic species concentration”. In: *Desalination* 488.May (2020), p. 114521. ISSN: 00119164. DOI: 10.1016/j.desal.2020.114521. URL: https://doi.org/10.1016/j.desal.2020.114521.

[77] Karel Ghyselbrecht, Bert Sansen, and Annick Monballiu. “Cationic selectrodialysis for magnesium recovery from seawater on lab and pilot scale”. In: *Separation and Purification Technology* 221.February (2019), pp. 12–22. ISSN: 18733794. DOI: 10.1016/j.seppur.2019.03.079. URL: https://doi.org/10.1016/j.seppur.2019.03.079.

[78] Jan W. Post, Hubertus V.M. Hamelers, and Cees J.N. Buisman. “Influence of multivalent ions on power production from mixing salt and fresh water with a reverse electrodialysis system”. In: *Journal of Membrane Science* 330.1-2 (2009), pp. 65–72. ISSN: 03767388. DOI: 10.1016/j.memsci.2008.12.042.

[79] David A. Vermaas, Joost Veerman, and Michel Saakes. “Influence of multivalent ions on renewable energy generation in reverse electrodialysis”. In: *Energy and Environmental Science* 7.4 (2014), pp. 1434–1445. ISSN: 17545706. DOI: 10.1039/c3ee43501f.

[80] Marian Turek. “Cost effective electrodialytic seawater desalination”. In: *Desalination* 153.1-3 (2003), pp. 371–376. ISSN: 00119164. DOI: 10.1016/S0011-9164(02)01130-X.

[81] Enver Güler, Willem van Baak, and Michel Saakes. “Monovalent-ion-selective membranes for reverse electrodialysis”. In: *Journal of Membrane Science* 455 (2014), pp. 254–270. ISSN: 03767388. DOI: 10.1016/j.memsci.2013.12.054. URL: http://dx.doi.org/10.1016/j.memsci.2013.12.054.

[82] Liang Ge, Bin Wu, and Dongbo Yu. “Monovalent cation perm-selective membranes (MCPMs): New developments and perspectives”. In: *Chinese Journal of Chemical Engineering* 25.11 (2017), pp. 1606–1615. ISSN: 10049541. DOI: 10.1016/j.cjche.2017.06.002. URL: https://doi.org/10.1016/j.cjche.2017.06.002.

[83] Toshikatsu Sata, Tomoaki Sata, and Wongkang Yang. “Studies on cation-exchange membranes having permselectivity between cations in electrodialysis”. In: *Journal of Membrane Science* 206.1-2 (2002), pp. 31–60. ISSN: 03767388. DOI: 10.1016/S0376-7388(01)00491-4.

[84] R. Femmer, M. C. Martí-Calatayud, and M. Wessling. “Mechanistic modeling of the dielectric impedance of layered membrane architectures”. In: *Journal of Membrane Science* 520 (2016), pp. 29–36. ISSN: 18733123. DOI: 10.1016/j.memsci.2016.07.055. URL: http://dx.doi.org/10.1016/j.memsci.2016.07.055.

[85] S E Aly, M Darwish, and K Fathalah. “Potential Drop & Ionic Flux in Desalting Electrodialysis Units”. In: *Journal of King Abdulaziz University-Engineering Sciences* 1.1 (1989), pp. 31–48. ISSN: 1319-1047. URL: http://prod.kau.edu.sa/centers/spc/jkau/Data/Review%7B%5C_%7DArtical.aspx?No=507.

[86] Paula Moon, Giselle Sandí, and Deborah Stevens. “Computational modeling of ionic transport in continuous and batch electrodialysis”. In: *Separation Science and Technology* 39.11 (2004), pp. 2531–2555. ISSN: 01496395. DOI: 10.1081/SS-200026714.

[87] Younggy Kim. “Ionic Separation in Electrodialysis : Analyses of Boundary Layer, Cationic Partitioning, and Overlimiting Current”. In: (2010).

[88] J. Moreno, V. Díez, and M. Saakes. “Mitigation of the effects of multivalent ion transport in reverse electrodialysis”. In: *Journal of Membrane Science* 550.December 2017 (2018), pp. 155–162. ISSN: 18733123. DOI: 10.1016/j.memsci.2017.12.069. URL: https://doi.org/10.1016/j.memsci.2017.12.069.

[89] A. A. Moya. “Uphill transport in improved reverse electrodialysis by removal of divalent cations in the dilute solution: A Nernst-Planck based study”. In: *Journal of Membrane Science* 598.November 2019 (2020), p. 117784. ISSN: 18733123. DOI: 10.1016/j.memsci.2019.117784. URL: https://doi.org/10.1016/j.memsci.2019.117784.

[90] M. A. Izquierdo-Gil, V. M. Barragán, and J. P.G. Villaluenga. “Water uptake and salt transport through Nafion cation-exchange membranes with different thicknesses”. In: *Chemical Engineering Science* 72 (2012), pp. 1–9. ISSN: 00092509. DOI: 10.1016/j.ces.2011.12.040.

[91] T. Rottiers et al. “Influence of the type of anion membrane on solvent flux and back diffusion in electrodialysis of concentrated NaCl solutions”. In: *Chemical Engineering Science* 113 (2014), pp. 95–100. ISSN: 00092509. DOI: 10.1016/j.ces.2014.04.008. URL: http://dx.doi.org/10.1016/j.ces.2014.04.008.

[92] A. H. Galama, M. Saakes, and H. Bruning. “Seawater predesalination with electrodialysis”. In: *Desalination* 342 (2014), pp. 61–69. ISSN: 00119164. DOI: 10.1016/j.desal.2013.07.012. URL: http://dx.doi.org/10.1016/j.desal.2013.07.012.

[93] V. K. Indusekhar and N. Krishnaswamy. “Water transport studies on interpolymer ion-exchange membranes”. In: *Desalination* 52.3 (1985), pp. 309–316. ISSN: 00119164. DOI: 10.1016/0011-9164(85)80040-0.

[94] Liem X. Dang. “Solvation of ammonium ion. A molecular dynamics simulation with non-additive potentials”. In: *Chemical Physics Letters* 213.5-6 (1993), pp. 541–546. ISSN: 00092614. DOI: 10.1016/0009-2614(93)89157-D.

[95] Takao Oi, Kunihiko Sato, and Kazuki Umemoto. “Oxygen and hydrogen isotopic preference in hydration spheres of magnesium and calcium ions”. In: *Zeitschrift fur Naturforschung - Section C Journal of Biosciences* 68 A.5 (2013), pp. 362–370. ISSN: 09395075. DOI: 10.5560/ZNA.2012-0122.

[96] Takao Oi and Hiroaki Morimoto. “Oxygen and hydrogen isotopic preference in hydration spheres of chloride and sulfate ions”. In: *Zeitschrift fur Physikalische Chemie* 227.6-7 (2013), pp. 807–819. ISSN: 09429352. DOI: 10.1524/zpch.2013.0376.

[97] Kevin Leung, Ida M. B. Nielsen, and Ira Kurtz. “Ab Initio Molecular Dynamics Study of Carbon Dioxide and Bicarbonate Hydration and the Nucleophilic Attack of Hydroxide on CO2”. In: *The Journal of Physical Chemistry B* 111.17 (2007). PMID: 17408252, pp. 4453–4459. DOI: 10.1021/jp068475l. URL: https://doi.org/10.1021/jp068475l.

[98] S. Porada, W. J. van Egmond, and J. W. Post. “Tailoring ion exchange membranes to enable low osmotic water transport and energy efficient electrodialysis”. In: *Journal of Membrane Science* 552.January (2018), pp. 22–30. ISSN: 18733123. DOI: 10.1016/j.memsci.2018.01.050. URL: https://doi.org/10.1016/j.memsci.2018.01.050.

[99] Kyösti Kontturi, Lasse Murtomäki, and Jose A. Manzanares. *Ionic transport processes: in electrochemistry and membrane science*. English. United Kingdom: Oxford University Press, 2008. ISBN: 978-0-19-953381-7.

[100] Ting Chia Huang. “Correlations of Ionic Mass Transfer Rate in Ion Exchange Membrane Electrodialysis”. In: *Journal of Chemical and Engineering Data* 22.4 (1977), pp. 422–426. ISSN: 15205134. DOI: 10.1021/je60075a006.

[101] Niels van linden. *Consult about Electrodialysis*. [In person; accessed 24 March 2020].

[102] D. Halliday, R. Resnick, and J. Walker. *Fundamentals of Physics*. Halliday & Resnick Fundamentals of Physics. John Wiley & Sons Canada, Limited, 2010. ISBN: 9780470547939. URL: http://books.google.co.uk/books?id=49h2cgAACAAJ.

[103] PCCell GmbH. *ED 64002: THE STANDARD ED CELL*. [Online; accessed 10 December 2020]. URL: https://www.pccell.de/en/ED-64002-The-standard-ED-cell_9_content2_Lab-Scale-Electrodialysis-Cells_81_Produktdetail.html.

[104] Jae Hwan Choi, Hong Joo Lee, and Seung Hyeon Moon. “Effects of electrolytes on the transport phenomena in a cation-exchange membrane”. In: *Journal of Colloid and Interface Science* 238.1 (2001), pp. 188–195. ISSN: 00219797. DOI: 10.1006/jcis.2001.7510.

[105] Harold F. Walton. “Ion Exchange. F. G. Helfferich. McGraw-Hill, New York, 1962. ix + 624 pp. Illus. 16”. In: *Science* 138.3537 (1962), pp. 133–133. ISSN: 0036-8075. DOI: 10.1126/science.138.3537.133. URL: https://science.sciencemag.org/content/138/3537/133.1.

[106] Tao Luo. “Porous Ion Exchange Membranes for Vanadium Redox Flow Battery”. PhD thesis. RWTH Aachen University, 2017.

[107] Victor V. Nikonenko, Natalia D. Pismenskaya, and Elena I. Belova. “Intensive current transfer in membrane systems: Modelling, mechanisms and application in electrodialysis”. In: *Advances in Colloid and Interface Science* 160.1-2 (2010), pp. 101–123. ISSN: 00018686. DOI: 10.1016/j.cis.2010.08.001. URL: http://dx.doi.org/10.1016/j.cis.2010.08.001.

[108] A. Normak, J. Suurpere, and K. Orupõld. “Simulation of anaerobic digestion of cattle manure.” In: *Agronomy research* 10 (2012), pp. 167–174.

[109] Younggy Kim, W. Shane Walker, and Desmond F. Lawler. “Competitive separation of di- vs. mono-valent cations in electrodialysis: Effects of the boundary layer properties”. In: *Water Research* 46.7 (2012), pp. 2042–2056. ISSN: 18792448. DOI: 10.1016/j.watres.2012.01.004. URL: http://dx.doi.org/10.1016/j.watres.2012.01.004.

[110] Muhammad Irfan, Yaoming Wang, and Tongwen Xu. “Novel electrodialysis membranes with hydrophobic alkyl spacers and zwitterion structure enable high monovalent/divalent cation selectivity”. In: *Chemical Engineering Journal* 383.October 2019 (2020), p. 123171. ISSN: 13858947. DOI: 10.1016/j.cej.2019.123171. URL: https://doi.org/10.1016/j.cej.2019.123171.

A

Constant current standard IEMs

This appendix displays the averaged results from the duplicate constant current experiments for standard IEMs at 32, 64 and 96 A/m^2. The Mg^{2+}/NH_4^+ ratios are 1:20, 1:10, 1:4 and no Mg^{2+}

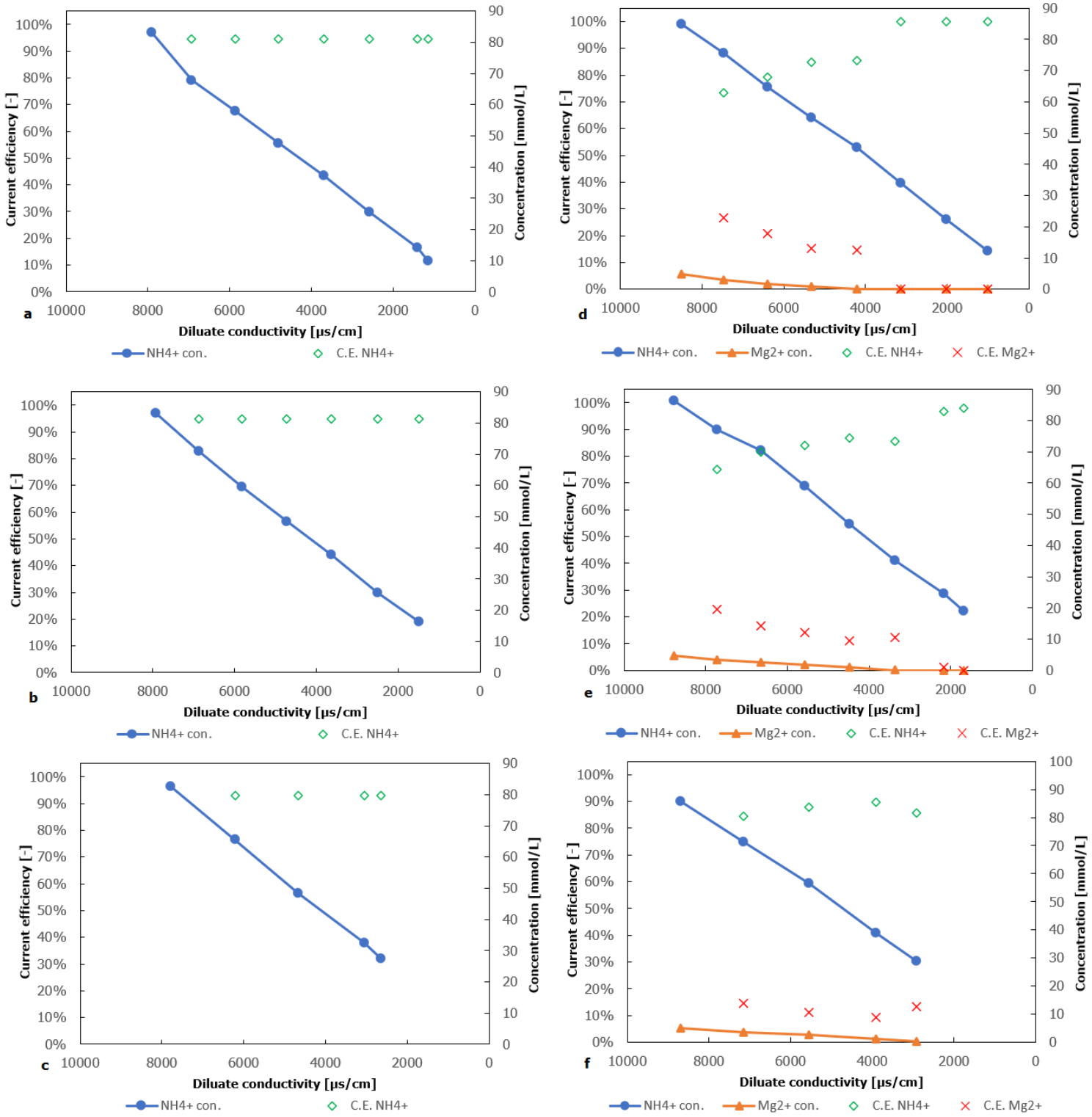

Figure A.1: NH4+ and Mg2+ concentration and current efficiency as a function of the diluate conductivity. Figure a,b and c have no Mg^{2+} and are operated at 32,64 and 96 A/m^2, respectively. Figure d, e and f have an initial molar Mg^{2+}/NH_4^+ ratio of 1:20 and are operated at 32,64 and 96 A/m^2, respectively.

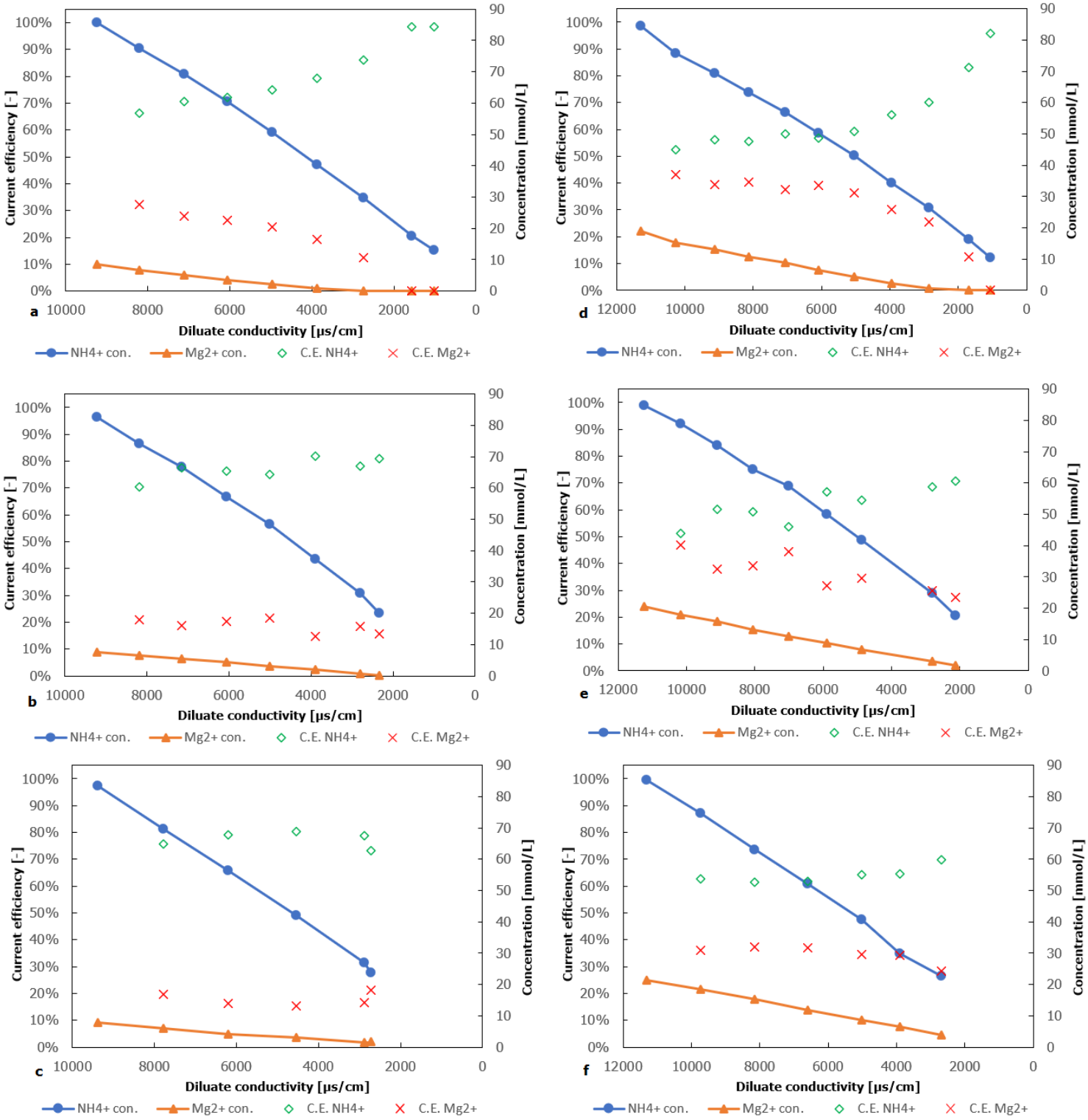

Figure A.2: NH4+ and Mg2+ concentration and current efficiency as a function of the diluate conductivity. Figure a, b and c have an initial molar Mg^{2+}/NH_4^+ ratio of 1:10 and are operated at 32,64 and 96 A/m^2, respectively. Figure d, e and f have an initial molar Mg^{2+}/NH_4^+ ratio of 1:4 and are operated at 32,64 and 96 A/m^2, respectively.

B

Constant current monovalent IEMs

This appendix displays the averaged results from the duplicate constant current experiments for standard IEMs at 32, 64 and 96 A/m^2. The Mg^{2+}/NH_4^+ ratios are 1:20, 1:10, 1:4 and no Mg^{2+}

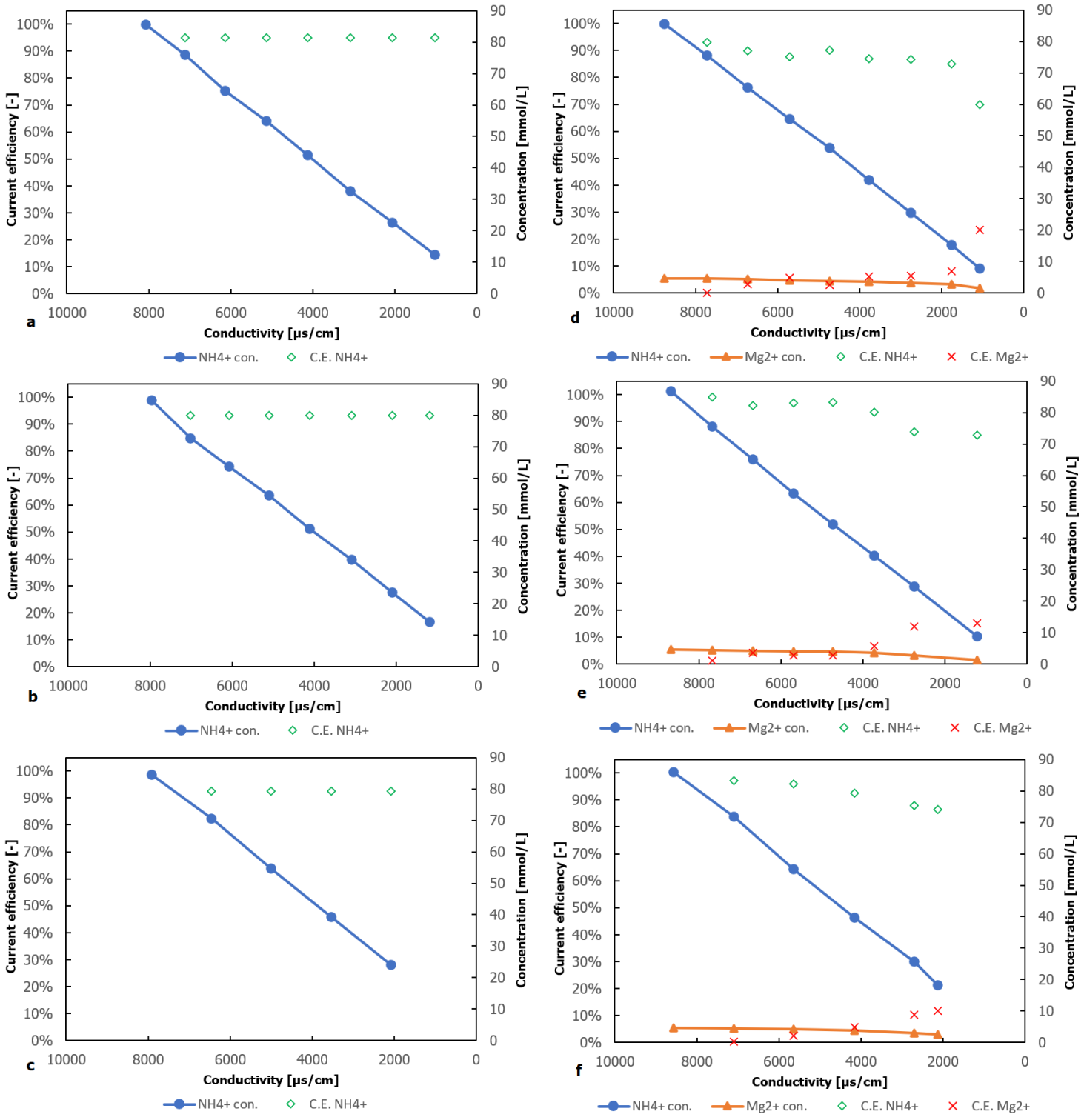

Figure B.1: NH4+ and Mg2+ concentration and current efficiency as a function of the diluate conductivity. Figure a,b and c have no Mg^{2+} and are operated at 32,64 and 96 A/m^2, respectively. Figure d, e and f have an initial molar Mg^{2+}/NH_4^+ ratio of 1:20 and are operated at 32,64 and 96 A/m^2, respectively.

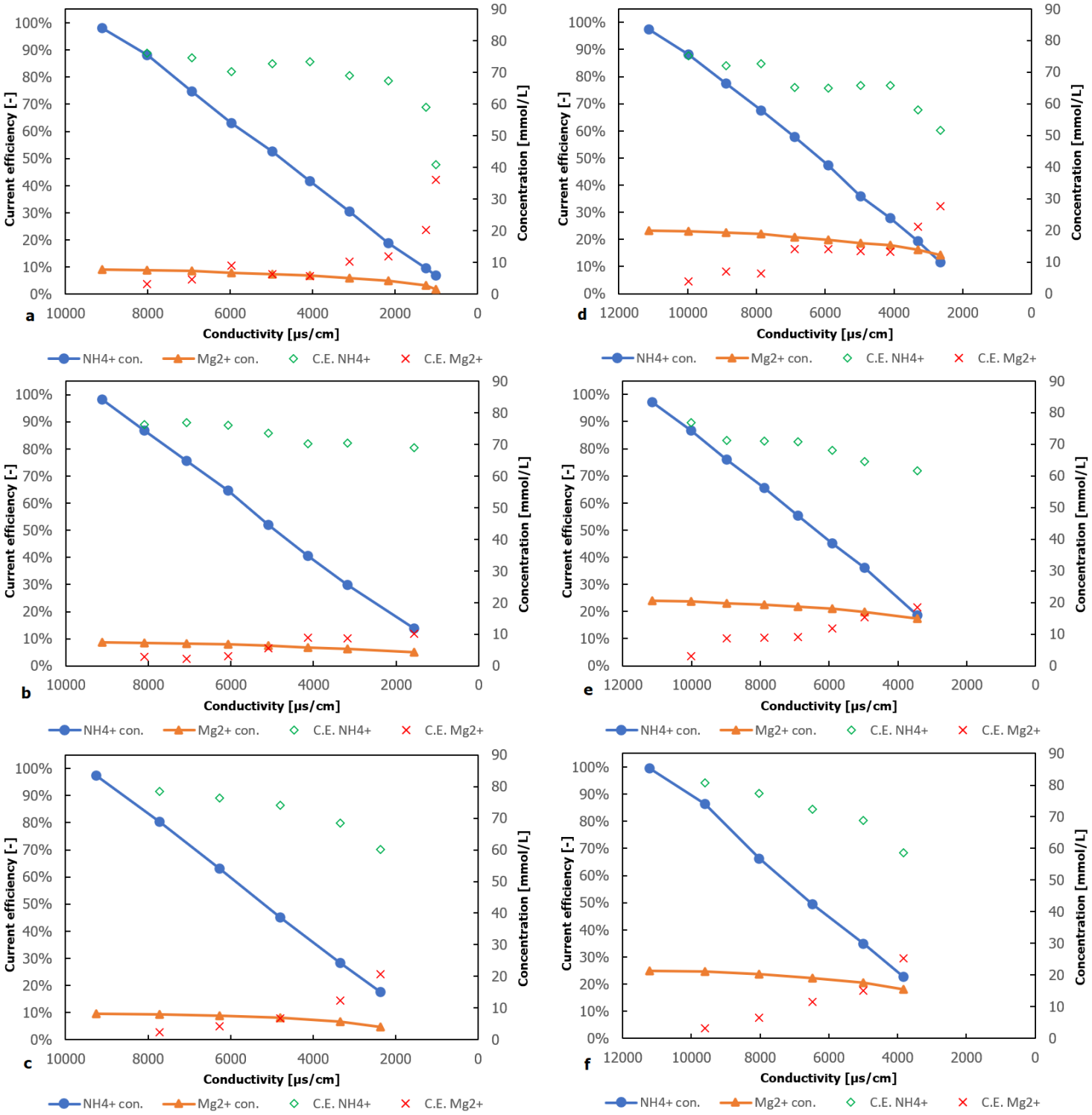

Figure B.2: NH4+ and Mg2+ concentration and current efficiency as a function of the diluate conductivity. Figure a, b and c have an initial molar Mg^{2+}/NH_4^+ ratio of 1:10 and are operated at 32,64 and 96 A/m^2 respectively. Figure d, e and f have an initial molar Mg^{2+}/NH_4^+ ratio of 1:4 and are operated at 32,64 and 96 A/m^2 respectively.

C

Model constant current monovalent IEMs

C.1. Model monovalent selective IEMs 32 A/m^2

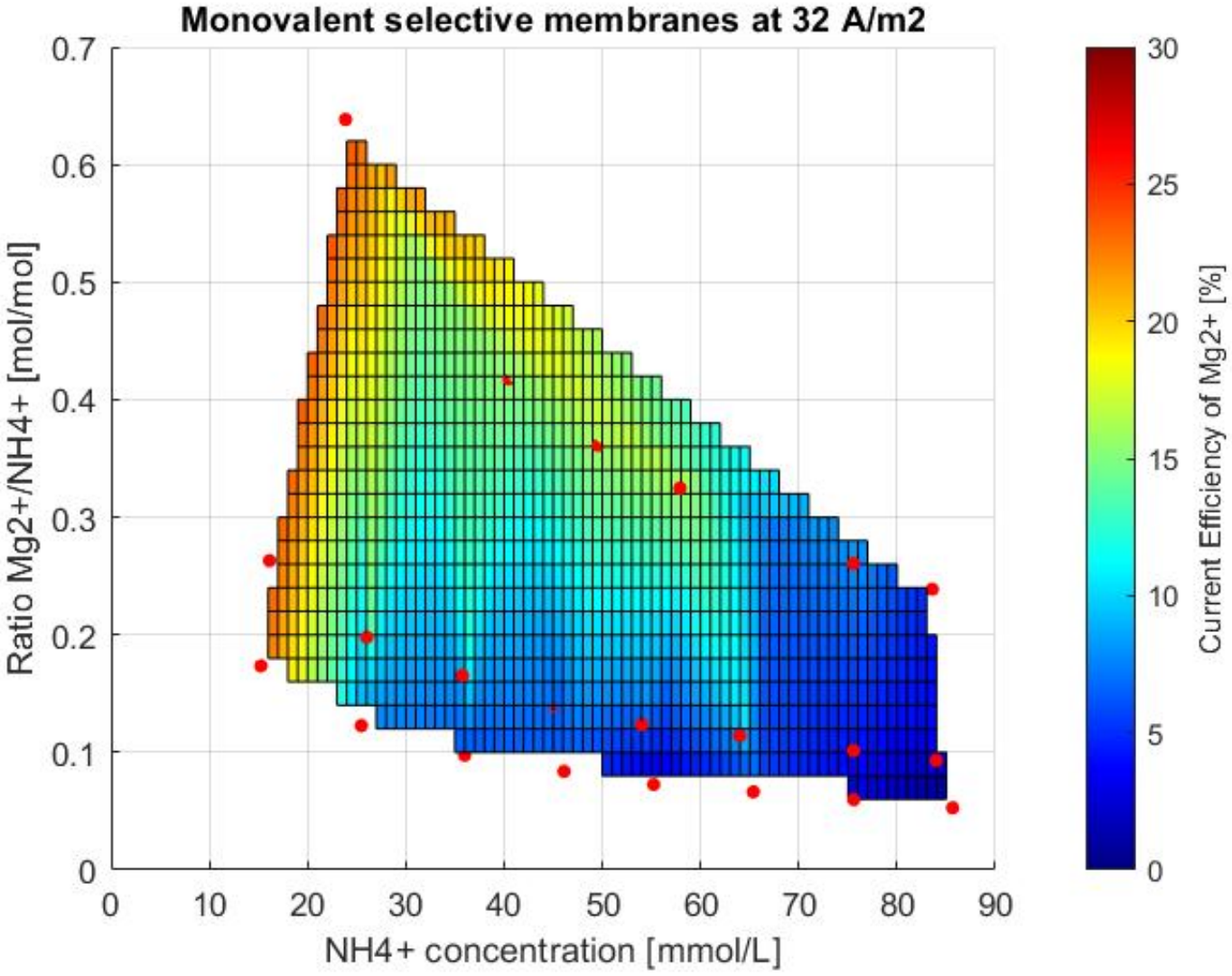

Figure C.1: The current efficiency of Mg^{2+} as a function of both the NH_4^+ concentration and the Mg^{2+}/NH_4^+ ratio, the current efficiency of Mg^{2+} is interpolated over a grit between the sampled data. The color represents the current efficiency of Mg^{2+} at given NH_4^+ concentration and ion ratio. 32 A/m^2.

C.2. Model monovalent selective IEMs 64 A/m^2

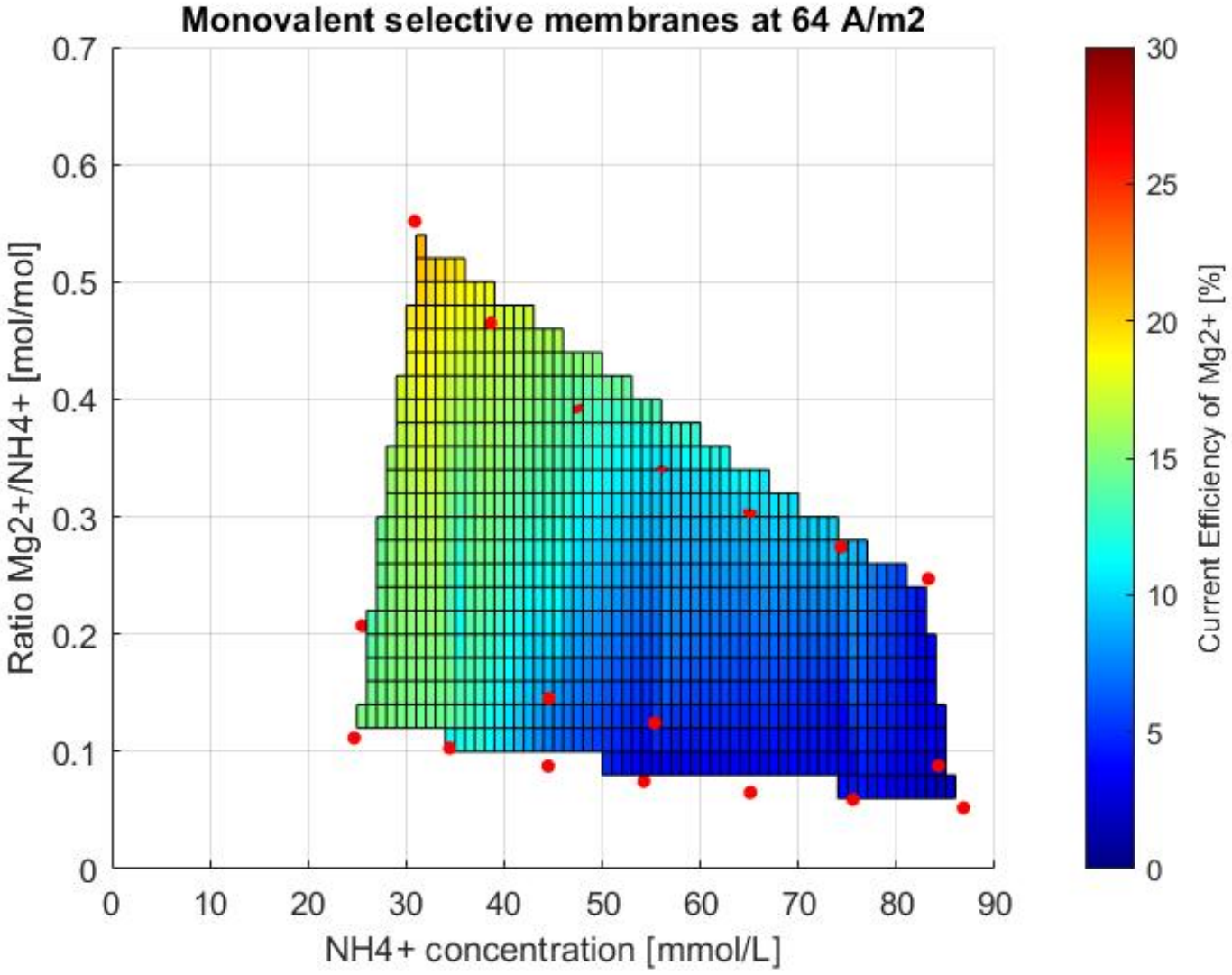

Figure C.2: The current efficiency of Mg^{2+} as a function of both the NH_4^+ concentration and the Mg^{2+}/NH_4^+ ratio, the current efficiency of Mg^{2+} is interpolated over a grit between the sampled data. The color represents the current efficiency of Mg^{2+} at given NH_4^+ concentration and ion ratio. 64 A/m^2.

C.3. Model monovalent selective IEMs 96 A/m^2

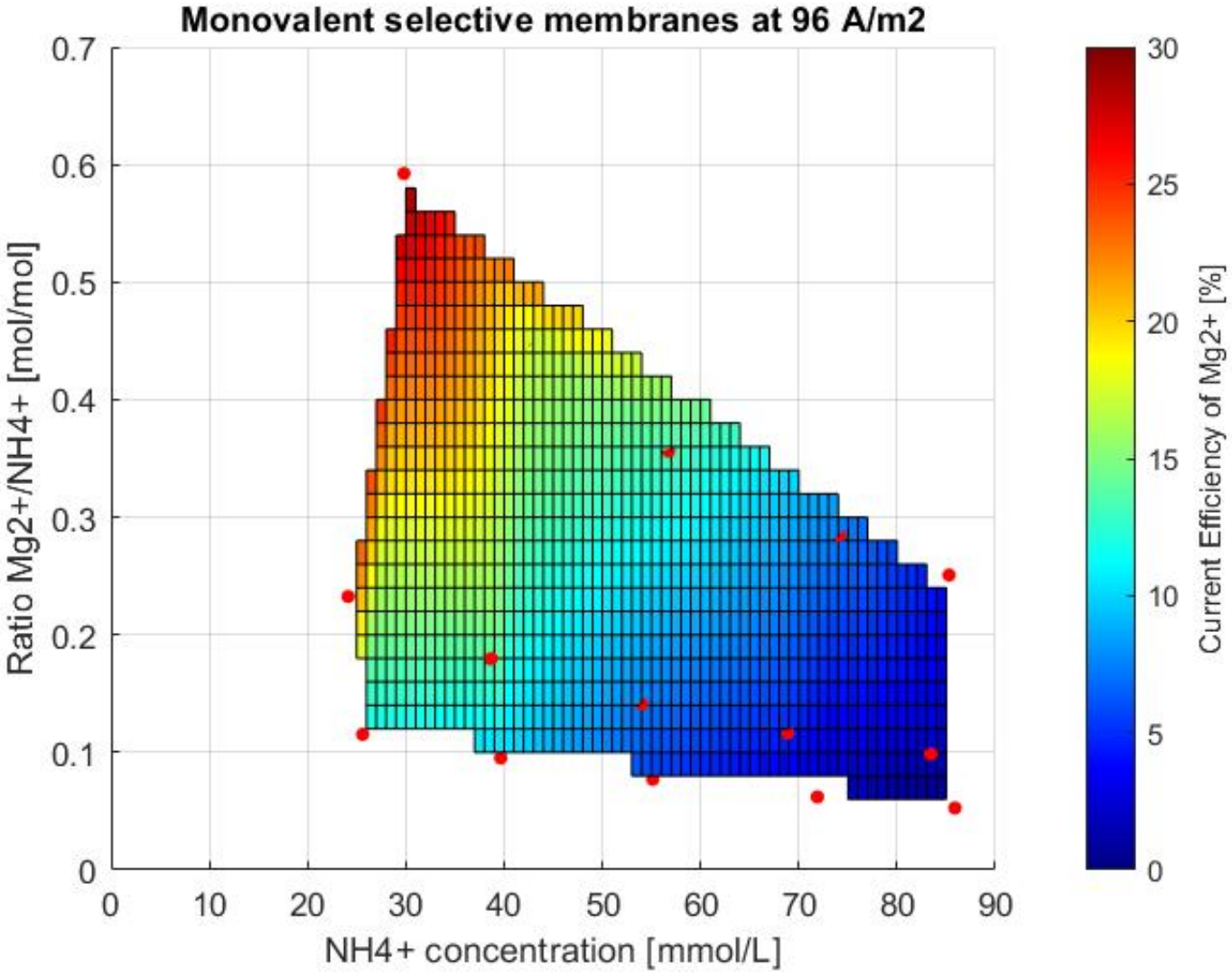

Figure C.3: The current efficiency of Mg^{2+} as a function of both the NH_4^+ concentration and the Mg^{2+}/NH_4^+ ratio, the current efficiency of Mg^{2+} is interpolated over a grit between the sampled data. The color represents the current efficiency of Mg^{2+} at given NH_4^+ concentration and ion ratio. 96 A/m^2.